Optimization of Beam space Design in Frequency Diverse Array Beam forming

Table of Contents

CHAPTER 1

INTRODUCTION

1.1 BACKGROUND OF STUDY

Emitting electromagnetic waves, radar serves as a means of gathering data from a distance. This information may be gleaned from the reflected waves via the radar receiver device. Radar is commonly used to determine a target's distance, speed, and angular position. Target signature analysis, on the other hand, is used to gather information on the target's shape, size, and composition. Weather, terrain avoidance, tracking, early warning systems, track-and-scan-and-fire control are only a few of the numerous commercial applications for which radars are useful. Radar, on the other hand, is widely used in military applications due to its inclusion in practically all aircraft, ships, ground stations, tanks, missiles, and helicopters, among others.

Radar is used to detect the object in terms of range, angle, direction, and velocity. An electromagnetic signal is transmitted in the desired region and the reflected signal contains some useful information. At the initial stage, radar is used for military purposes. Now it is also used for air-traffic control, weather forecasting over speeded vehicle detection by police on the highways.

In order to fulfill the requirement of the modernist eradication, a huge amount of work is done by the researcher for the advancement in radar technology. In result, different kinds of radar developed with time which includes phased-array-radar (PAR), multi-input multi-output radar (MIMO) and frequency-diverse-array radar (FDA). The all of the above types of radar used an array of the antenna element and electronic-beam scanning. PAR has a high gain beam, as an important characteristic of phased-array-radar (PAR), which is useful to detect a weak target.

The other type of radar called the FDA, which use smallest increment in frequency across antenna elements to form an angle-dependent beam pattern. In FDA radar we can improve the signal-noise ratio (SNR), and the maxima of angle repeat in the range at a particular time. Besides this, the beam-pattern has strong coupling in range and angle dimension, which can affect the localization/detection performance. MIMO radar has been proposed for research after rigorous research on MIMO wireless communication, because both have the same objective in terms of using

the antenna for receiving and transmitting electromagnetic-signals. The MIMO-radar sends particular waveform from each antenna element. MIMO radar is divided into two categories, the first one use collocated-antenna to provide waveform diversity, and the second uses a separatedantenna to provide spatial diversity. The advantage of MIMO radar is the cancellation of interference and resolution enhancement; which results in good localization/target tracking and improved parameter-estimation.

1. 2 APPLICATIONS AND TYPES OF RADAR

Radar is an acronym of radio detection and ranging; due to its wide use, the word has a standard noun in English. The first experiment on the radar is conducted by a German physicist named Heinrich Hertz in 1985 and found the reflection of waves. After that Hilsmeyer successfully performs an experiment for detection of ship at a range of over one mile in 1903. After a very slowly progress in radar, the detection of aircraft at a distance of 50 miles was achieved in 1932

Radar is an acronym of radio detection and ranging; due to its wide use, the word has a standard noun in English. The first experiment on the radar is conducted by a German physicist named Heinrich Hertz in 1985 and found the reflection of waves. After that Hilsmeyer successfully performs an experiment for detection of ship at a range of over one mile in 1903. After a very slowly progress in radar, the detection of aircraft at a distance of 50 miles was achieved in 1932,

Radars may be divided into a variety of groups based on a variety of factors, including the waveforms utilised, the antenna type, the frequency band, and the intended function. A radar is classified as either a continuous wave (CW) or pulsed wave (PW) radar by its waveform. While CW radars continually generate electromagnetic waves, PW radars emit a series of pulsed waveforms. When it comes to classification by frequency bands, radars that operate in various bands have a variety of uses. Such as high frequency radars, used to identify targets beyond the horizon, for example. The Early Warning Radars (EWR) typically operate in the VHF and UHF frequency ranges. For long-range applications, the land and maritime systems use the L and S bands (medium range applications). C-band radars are utilised in military fire control and weather detection systems, whereas X-

band radars are used to identify extremely small targets. Ku, Ka, and K band radars are used by traffic enforcement and terrain avoidance radars.

Radars can be classified as monostatic, bistatic, or quasi-monostatic based on the distance between both the transmitter and receiver. In monostatic radars, the transmitter and receiver are placed in close proximity to each other as viewed from the targeted point of view (i.e., transmit and receive antennas are same). For bistatic radars, a reference point is used to position both the transmit and receive antennas (e.g., an airborne receiver and a ground based transmitter). Even when the antennas for transmitting and receiving are positioned in different places, they nonetheless seem to be located in close proximity from a reference point (such as an aeroplane with separate broadcast and receive antennas) [3]. Conventional single-antenna radars and multiple-antenna radars fall into two fundamental categories: In order to cover the complete angular spectrum, single antenna radars spin mechanically. Radar with several antennas, more often known as phased array radars, is the most recent type; it electronically guides the beam. MIMO (multiple input, multiple output) radar is another common type of radar system. Phased array radar (PAR) uses the same waveform for all of its antennas, whereas MIMO radar uses multiple antennas that each produce a separate waveform.

Now, each antenna in the array emits at the same frequency in the two multi-antenna radar systems previously stated. FDA radar, a brand-new idea in radar technology introduced in 2005, is based on the principle of frequency varied arrays. FDA employs an array in which each piece broadcasts at a distinct frequency. Frequency offset refers to the difference in frequency between two elements. The frequency difference might be tiny or significant. It has been used in beamforming applications with a small frequency offset. That's why this particular beampattern formed by this modest inter-element frequency offset has such a distinctive shape, unlike the beampattern of PAR systems, which is just angle-dependent. The higher range resolution and excellent clutter reduction provided by this range-angle dependent beampattern are only two of the many advantages that have emerged from its use. Because unwanted sources are eliminated, the SINR (signal to interference noise ratio) of the system improves. Time and space are modified in the beampattern. Rather of a fixed position, the beampattern's maxima move in and out

of place, both spatially and temporally. The 'auto scanning function' is a result of this drift in time, which allows the radar to scan the whole universe without the need for phase shifters. Independent echoes of the target are possible even with high inter-element frequency offsets. In both circumstances, the FDA provides a wider degree of flexibility and a very effective radar scene information usage.

Wireless communications, satellite navigation, radar, sensor systems, and biomedical engineering all rely heavily on beam formation. Research into radar systems has paid an unusual amount of attention to antenna array design, robust beamforming, and signal processing. As a result, adaptive beamforming concentrates optimum gain at the target spot while minimising the jamming risks or other undesirable interfering [4]. As a result, waves released by array components are combined to form a primary directed beam, with signals coming together constructively at specified angles, while waves coming together destructively at other angles are used to form nulls in the beam pattern [5]. Beamforming is a technique used in communications to direct an antenna toward a specific source of signal while simultaneously lowering the amount of interference. All applications of direction finding make use of beamforming as well [6]. Antenna weights are often modified with phase variation utilising various algorithms and optimization approaches, as well as amplitude and element position control in conventional ABF methods like these.

1.3 PERFORMANCE METRICS OF A RADAR SYSTEM

Range resolution, Doppler resolution, angular resolution, and the likelihood of false alarms are some of the metrics that may be used to assess radar performance. Other parameters include the maximum detection range, received SINR and the chance of false alerts. Radar systems benefit from improvements in antenna array performance since they are the first line of defence in a radar system.

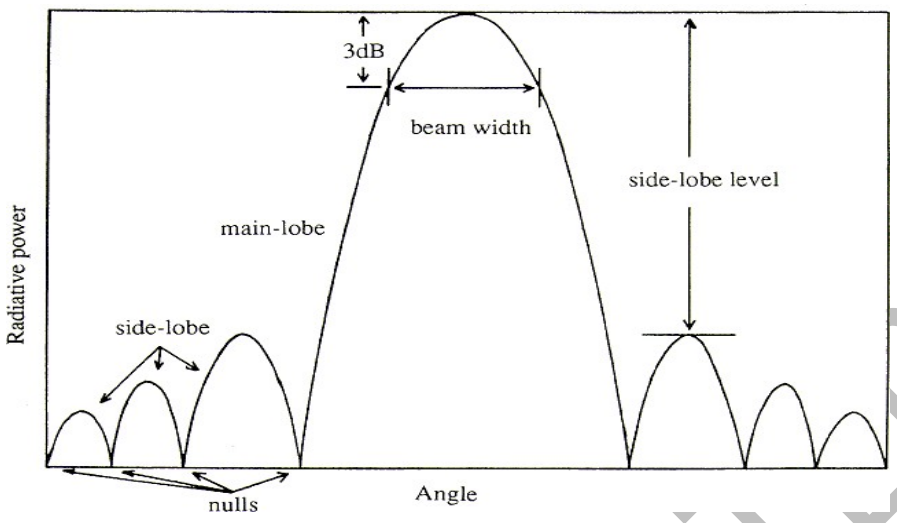

Fig 1.1: Basic antenna beampattern*[115]*

The directional gain, 1/2 beam width, side lobe amplitude, and zero depths of the beams are used to test the efficiency of an array in terms of beam-forming and array radiation trend analysis.

1.4 SIGNIFICANCE OF THE RESEARCH

Beamforming methods and antenna array configurations are not the only factors that contribute to overall system performance [7]. In comparison to other arrangements, linear arrays, for example, offer the maximum directivity. One major shortcoming of linear arrays is that the beam does not scan in all azimuth directions. As a result, rectangular arrays are used in all applications involving 2D radar imaging and the system's requirement for angular information in both azimuth and elevation. Rectangular arrays allow the beam to scan 360 degrees azimuthally, but the additional main lobe of the same intensity on the opposite side is a significant drawback of the rectangular shape [8]. The circular array construction outsmarts the rectangular arrays in this case because of its symmetry. Electronically, the beampattern generated by a circular array may be turned without the need for a main lobe duplicate. A circular array, on either hand, has high side-lobe geometry. Thus, if the inter-element spacing is reduced, the mutual coupling effect becomes stronger in order to diminish the side lobes. Multi-ring topologies and hexagonal arrays are

used to reduce side-lobe levels in smart antenna applications. According on the operational requirements, different array topologies can be used in various radar missions.

Aspects like as directional gain, wide beam width, side lobe level, null depths and SINR are taken into account because the focus of this thesis is on the performance of various geometries in FDA radars. This work will contribute to the existing modern radar technologies. The study will contribute a lot in radar signal processing of radar and its application. Since radar is also used in other areas such as the field of communication and weather forecasting, therefore, the current contribution will also impact those areas. Moreover, it will help in the practical implementation of the modern state of the art systems.

1.5 PROBLEM STATEMENT

FDA received considerable attention of researchers in past years. Most of the published work concentrates only on analyzing the range dependent beam pattern. The beam pattern is coupled in range and angle response. Now the question is how to steer the beam direction in the desired range accurately.

Beam-space design is an active area of research which plays an important role in the improved performance of FDA radar. The main problem is to design a waveform for improved localization and parameter estimation. Moreover, the frequency offset is the most important feature which helps FDA radar to optimize in range as well as angle dimension. Therefore, the design of proper offset for FDA need to be further investigated which will enhance the performance of FDA radar.

1.6 OBJECTIVES OF THE RESEARCH

The main objective of this work is to design a beamspace based algorithm that will improve the performance of FDA radar in terms of improved localization and target tracking. Moreover, a good waveform design with a properly optimized frequency offset will help us to improve the parameter estimation. A state of the art algorithm will be executed to accurately find the optimum solution.

1.7 CONTRIBUTIONS OF THE THESIS

The performance of the suggested beamforming systems in current FDA geometries is the primary focus of this thesis' research. Although alternative array shapes have advantages and are easier to build than linear and rectangular arrays, the FDA is only allowed to use these two. Through its investigation of several antenna array shapes for frequency diversity, the thesis contributes to the development of a single unit 3D radar system. This thesis accomplishes the following goals:

Linear frequency diversity arrays (LFDA) have been used in a non-stationary radar environment to build a cognitive null steering approach. As a consequence, the system is able to sustain the deepest null at the interferer site since the radar system can forecast the next likely location of the signal source. Furthermore, the suggested method of null steering is more effective than other current methods in PAR because it is able to locate the interference not just in angle but also range.

For 3D adaptive beamforming (ABF) in PFDAs, a new and simple solution has been developed employing frequency offset selection scheme (FOSS). Beamforming performance of the suggested technique has also been compared using the MVDR (Minimum Variance Distortionless Response) capabilities of the beamformer in PFDA. It has been determined that the beamforming performance may be measured in terms of SINR and null depth.

Uniform circular frequency diverse arrays (UCFDAs) have been presented as a novel type of circular arrays that have been studied in a frequency varied viewpoint. There includes a presentation of the theory and analysis, adaptive beamforming, fundamental beam steering, and SINR assessment in uniform circular frequency diverse arrays (UCFDA).

Non-uniform frequency offset has been planned for circular frequency diversity arrays (CFDA). Tangent hyperbolic function is the non-uniform function chosen for this purpose. System detection and SINR might be improved by using a 3D single maximum beampattern. An array system that can generate beampatterns of three distinct FDA configurations may be created by modifying a single function parameter using the features of tangent hyperbolic function. Compared to other non-

uniform frequency offset methods, the suggested non-uniform frequency offset technique has lower side lobe levels.

Elliptical frequency diverse array (EFDA) is a novel geometry that has been proposed. With a uniform and non-uniform frequency offset, the geometry of interest has been examined. Analysis indicates beampatterns with diminishing side lobe levels that are very range selective. EFDA has the slimmest beam and deepest side lobe levels beside the range axis when compared to all 2D FDA geometries. Thesis also studies non-uniform frequency offset arrangement tangent hyperbolic function in EFDA and uncovers decreased side-lobe levels and considerable range selective beam patterns.

CHAPTER 2
LITERATURE REVIEW

2.1 INRODUCTION

Phased-array radars, which are the most prevalent form of radar system, are the focus of this chapter's brief history of radar technology. Focuses on frequency varied array radars, which are a relatively new technology. In addition to the principles of the aforementioned radar designs, a detailed assessment of previous and current studies has also been given in this document.

2.2 HISTORY OF RADAR

Counting them fortunate, the bat entrusted the technological development of radar in their care for the 20th century engineers [10]. However, radar technology's roots may be traced back to the year 1900. It was in 1934 that Dr. Kuhnhold created the first radio ranging technology, better known as radar. An anti-aircraft artillery radar with a distinctive 3m parabolic reflector antenna was presented by Telefunken in March 1939.

Radiation research was accelerated in the United States following World War II. There have been several advancements in radar technology since then. Coherent control system and Doppler signal processing, for example, experienced significant progress. The "monopulse tracking system" was advancement in radar tracking technology. Synthetic Aperture Radar (SAR) was invented in June 1951 by C. Wiley of the Goodyear Aircraft Corporation. As a result of his theory, radars now have incredibly high angular resolution. Even while radar technology was developed primarily for military use, it has found several applications in civilian life as well. Air traffic control (ATC) and maritime navigation safety are two of the most critical civilian uses of this technology. The first ATC was created by TELEFUNKEN in 1955. During 1955 and 1957, this ATC radar was renamed the Ground Radar System (GRS).

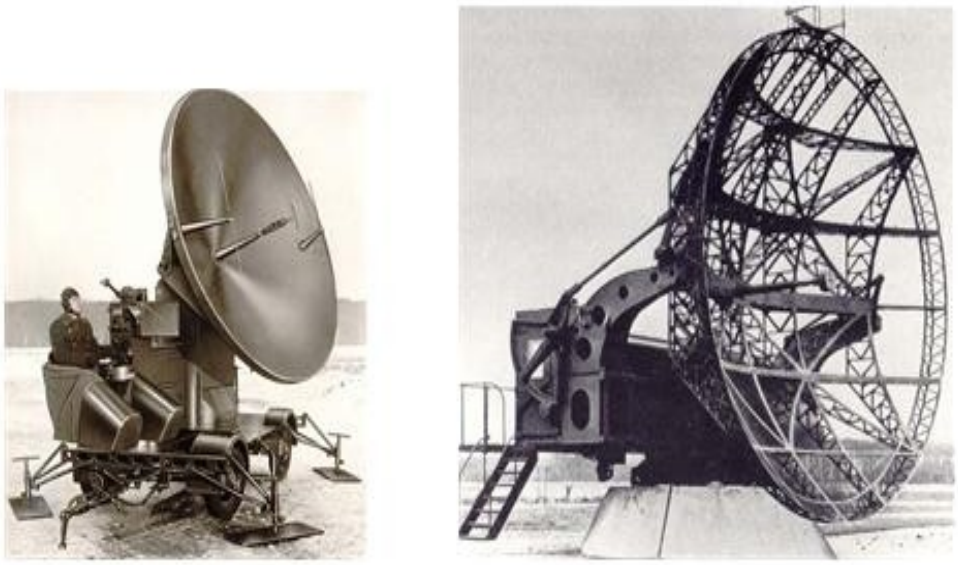

Fig 2.1: Würzburg A and Würzburg-Riese*[111]*

Fig 2.2: A typical air traffic control Radar*[113]*

GRS's successor, SRE-M (Surveillance Radar Equipment-Medium Range), has been operational since 1976 and is still in service today. With the introduction of phased array

radars in 1990, radar technology took a giant step forward (PAR). Due to the lack of any noticeable delay in switching through one angular sector to another, PAR is superior to conventional mechanically moving antenna-based radar systems. It was because of this that mechanically steered antennas were updated to electronic directed antennas. In actual radar systems such as ship and ground-based radars, as well as fighter radars, PAR has a wide range of applications.

Fig 2.3: PAVE PAWS Phased Array Radar*[114]*

2.3 RADAR CLASSIFICATIONS

This segment discusses the many types of radars and how they are classified. Fig.2.4 [11] depicts a straightforward radar categorization hierarchy.

Primary radar, even as name suggests, is radar that transmits high-frequency signals at the target and processes the returning signals in order to extract relevant target information from them. This type of primary radar is further subdivided into CW and pulsed.

CW radars emit and bring higher signals on a continuous basis. It is possible for CW radars to be either bistatic or monostatic. Unmodulated CW radars and modified CW radars may be further divided into two subcategories: The unmodulated CW radar employs waves with a constant magnitude and a constant frequency, which is why it is

called CW radar. It is limited to measuring speed and lacks the capacity to range or classify targets.

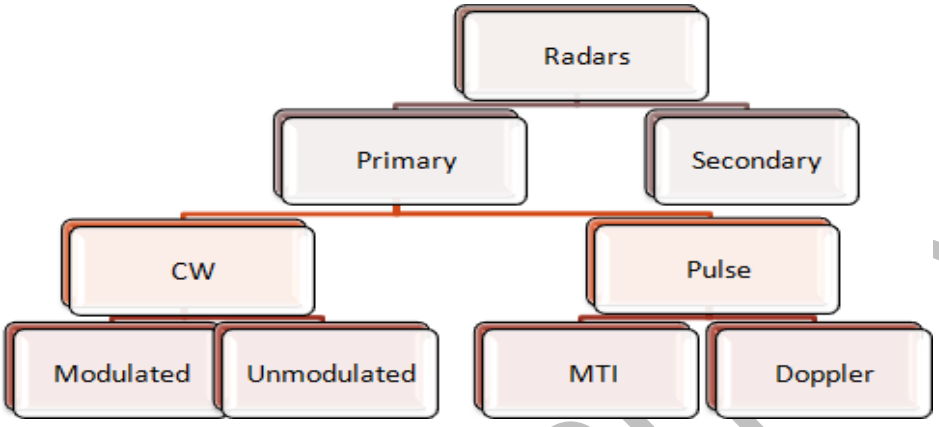

Fig 2.4: Block diagram of radar classification*[11]*

When using moderated CW radar, the frequency is continuously shifted among f1 and f2.' Using the established echoes, we can then figure out how far away we are. Active echoes are used in the secondary radar system. It might be referred to as a questioning device.

2.4 PHASED ARRAY RADAR

As the most prevalent type of radar, phased array radar (PAR) is the most often used. An layout of an array with a relative phase difference here between consecutive members is the simplest version of it. Research on PAR has continued since its inception in the 1930s [12] and has progressed through several stages of maturity and growth since then [13], [14]. Parameter arrays (PARs) can be used in a wide range of applications including military surveillance, aerial synthetic aperture radar (SAR), and connectivity for remotely sensed and radio astronomy as well as in other applications. Each transmit antenna in PAR incorporates a phase shifter, allowing it to electronically guide the beam in the desired direction [17]. The resulting beam is then generated by altering the phase of each radiating element's signal. A straight line in 1-Dimensional or a 2-Dimensional plane can be used to organise the radiating elements, with whichever regular inter-element spacing [19] or non-uniform inter-element spacing [20] in mind.

The array element of an N-element linear array, as presented in Fig. 2.5, can be calculated as follows:

$$AF = \sum_{n=0}^{N-1} W_n^* e^{jnkdsin\theta} \qquad 2.1$$

Where n is the component index, $k = 2\pi/\lambda$

Inter component separation; elevation angle; and complex weight associated with each individual element are all known as wave numbers.

$$AF = W^{H}a(\theta) \qquad 2.2$$

Where w is the N× 1 weight vector.

(θ) is the array steering vector of the form

$$a(\theta) = \left[1\ e^{jkdsin\theta} e^{2kdsin\theta} \ldots\ldots\ldots\ldots e^{(n-1)kdsin\theta}\right]T \qquad 2.3$$

Note that $(.)*$, $(.\ )H$, $(.\ )T$ signify conjugate, hermitian and transpose of a matrix or vector correspondingly.

A desired beampattern may be created by adjusting the weight vector stated above. Linear phased array beampattern, described as the magnitude squared of the array factor, with uniform weights, i.e. $w_n = 1$. is given by

$$B_T(\theta) = \left| \frac{\frac{\sin N\varphi}{2}}{\frac{\sin\varphi}{2}} \right|^2$$

Where w is the N× 1 weight vector.

Beam steering, or traditional beamforming, refers to the ability to aim a beam inside the desired direction. Real-time adaptive beamforming (ABF) is a technique that avoids undesirable sources by directing the pattern's null toward them while keeping the main lobe pointed in the desired direction [18]. When comparing adaptive and traditional beamforming (CBF), the main distinction is that ABF may concentrate null in the wrong

direction, whereas CBF cannot. Weight vector w = (0), where 0 is the intended aspect angle at which the foremost lobe of a pattern is to be focused, is employed in a standard beamformer. Linear Constraint Minimum Variance (LCMV) [22]-[26] and Minimum Variance Distortion-less Response (MVDR) [27]-[31] are two of the most used adaptive beamformer approaches.

[32] When it comes to array geometries: linear phased arrays, square, rectangular and hexagonal phased arrays, components of the array can either be organised linearly or in a plane. Figs. 2.5 and 2.7 illustrate the relative geometries of the corresponding atom. The beampatterns for the rectangular phased array shown in Fig. 2.6 are as follows:

$$B_T(\theta,\varphi) = \left|\left\{\frac{\sin\left(M\Phi_x/2\right)}{\sin\left(\Phi_x/2\right)}\right\} \times \left\{\frac{\sin(N\Phi_y)/2)}{\sin\left(\Phi_y/2\right)}\right\}\right|^2$$

Where

$$\Phi_x = kd_x sin\theta_0 cos\varphi_0$$

$$\Phi_y = kd_y\, sin\theta_0 sin\varphi_0$$

The circular phased array beam patterns are as follows for the Fig. 2.7 geometry:

$$B_T(\theta,\varphi) = \left|\sum_{n=0}^{N-1} \exp\{j2\pi(\, f_0 \frac{a}{c} \sin\theta \cos(\varphi - \varphi_n)\}\right|^2$$

For a normal linear PAR, the beampattern is only dependent on the elevation angle, as

shown in Eq. (2.5), but for a non-linear PAR, the beampattern is dependent on the elevation angle and the azimuth angle. As a result, the planar geometries are able to scan the radar scene in two dimensions (i.e., in two dimensions in elevation and azimuth).

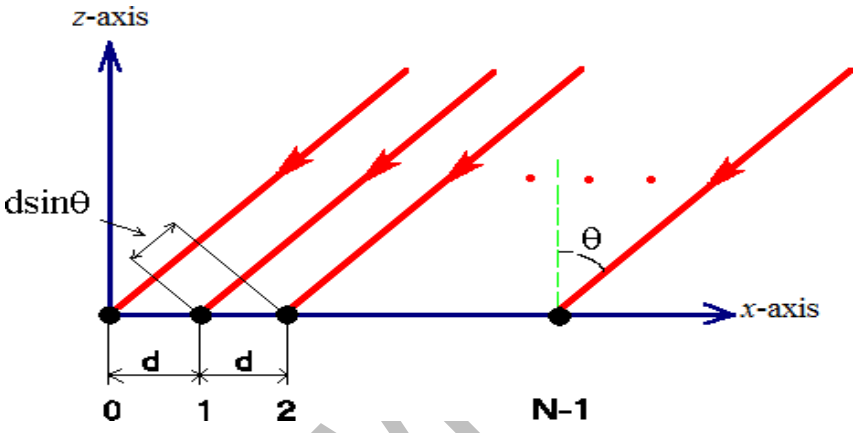

Fig 2.5: Uniform linear array Geometry.

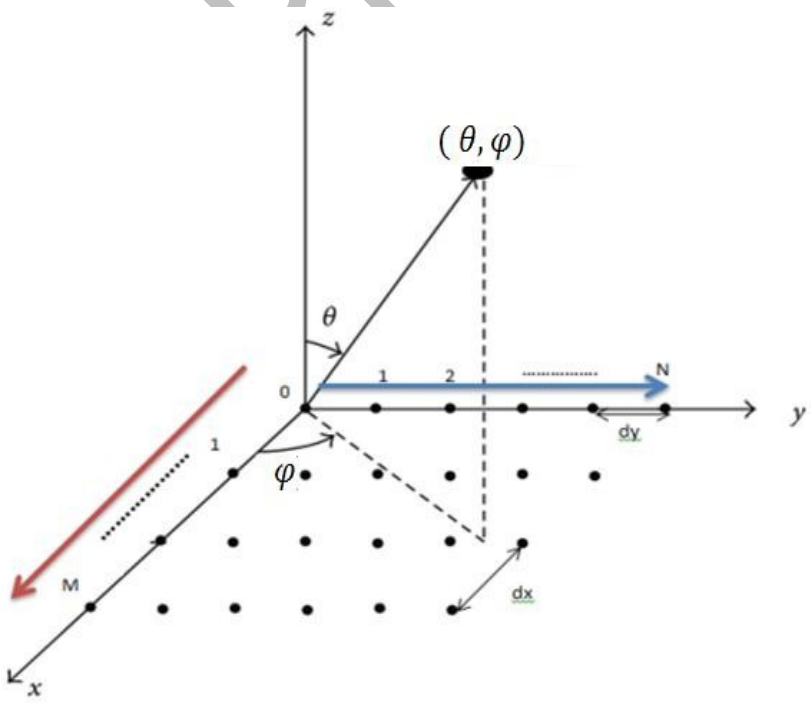

Fig 2.6: Uniform rectangular array Geometry.

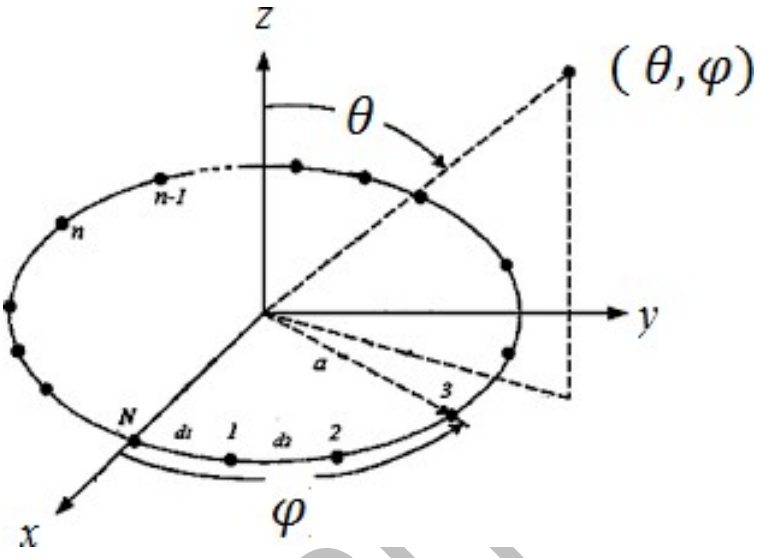

Fig 2.7: Uniform circular array Geometry

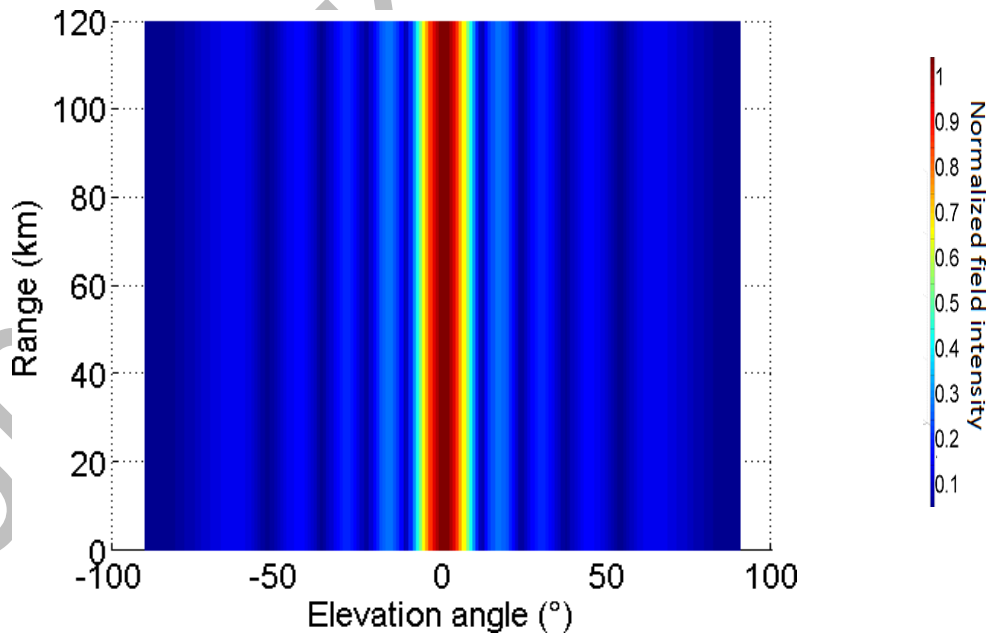

Fig 2.8: Beampattern of linear phased array. (N=10, d=λ/2)

2.5 FREQUENCY DIVERSE ARRAY RADAR

When compared to a conventional phase-locked loop (PLL), a Frequency Diverse Array (FDA) uses a single, uniform frequency for all of its elements to send and receive data. In 2005, Dr. M.C. Wicks, a senior scientist in the Air Force Research Laboratory (AFRL) Rome, New York, introduced the notion of FDA during a keynote lecture. Since then, the FDA has been a popular research destination [34-38]. The array's aperture undergoes a linear, gradual frequency shift in the FDA standard form. A "range-angle-dependent" beampattern is created by the distinct frequencies at every antenna element, unlike PAR, which has simply an angle-dependent beampattern. Additional freedom for system designers may be gained by the use of a time-range and angle modulated beampattern, according to [40]. The radar system may direct the transmitted power to a specific range-angular sector using this time- and range-dependent beampattern [41]. Suppression of range-dependent clutter and interferences [42], improvement of SAR imaging resolution [43], calculation of range angle [44], and imaging [45] all benefit from this characteristic, which in turn improves received SINR. Second, the beam pattern's time dependence allows for an automatic scanning function, in which the beam rotates across all range angle pairings without the usage of phase shifters. [46] on the other hand, proposes a time dependent frequency offset method to generate a time-independent beampattern for a certain range-angle combination. To ensure maximal signal reflection from a given spot, the beampattern is time-independent; the remainder of the beampattern, on the other hand, is time-modulated. Many radar applications have made use of the notion of frequency diversity, including high-resolution target imaging in SAR [47], [48], MIMO systems for multiple target detection [49], [50], and ground motion target indication in the forward radar [51]. [47] In addition to the small and big frequency offsets, there is also a progressive frequency offset (sometimes known as a phase shift). When it comes to beamforming, a small frequency offset has been used [52-54], but a big one has been used to create independent target echoes. Using a linear frequency modulated continuous waveform, FDA radar full-wave modelling and

implementation were described in detail in [57]. With non-uniform or exponentially rising frequency offset recently presented by FDA [58], it is possible to generate a beam pattern with just one maximum at the desired place. The SINR and detectability of the radar system are improved with the single-maximum beampattern rather than the multiple-maximum beampattern. [59] studied and compared the multipath properties of FDA radar more than a ground plane with phased-array. Linear vary regarding continuous waveform (LFCW) radar full-wave modelling and implementation were given in [57]. These lower constraints for predicting direction, range, and velocity have been examined in [61] and [62]. It was developed by Brady [63] and Jones [64] to establish the general ambiguity function of an FDA radar receiver.

Even current research focuses on linear geometries [65]-[69] when discussing FDA in uniform linear arrays (ULA). Other geometries, such rectangular apertures, have received less attention.

2.5.1 LINEAR FREQUENCY DIVERSE ARRAYS

In comparison to a PAR's angle-selective beam pattern, the LFDA's beam pattern is range-angle-selective. In addition, the beam pattern is modified in terms of range, angle, and duration [52]. The array factor of LFDA must be examined in order to understand the angle, range, and timing periodicity of LFDA. In linear FDA, the offset frequency is uniformly applied over the array's whole length. The frequency at the nth element of an N-element array having d inter-element spacing and f0 as the radar working frequency is determined by:

$$f_n = f_0 + n\Delta f \quad (2.8)$$

Path length variation among waves of nth component and zeroth element is demonstrated in Fig.2.5 by using it as an example:

$$R_n = R_0 - n d \sin\theta \qquad (2.9)$$

Let the signal conducted by nth component is conveyed as:

$$S_n(t) = a_v(t)\exp\{-j2\pi f_n t\} \qquad (2.10)$$

Where (t) is a complex weight demonstrating spread and transmission possessions and is ignored here i.e. (t) =1. Complete signal incoming at distant field point (R 0, θ 0) can be stated as:

$$S_T(t) = \sum_{n=0}^{N-1} \exp\left\{-j2\pi f_n (t - \frac{R_n}{c})\right\}$$

Placing in the values of f_n and R_n,

$$S_T(t) = \sum_{n=0}^{N-1} \exp\left\{-j2\pi (f_0 + n\Delta f)(t - \frac{(R_0 - n d \sin\theta_0)}{c})\right\}$$

Creating plane wave supposition: R 0>> (N-1) d and narrow band FDA supposition

$$S_T(t) = \exp\left[j2\pi f_0 (t - \frac{R_0}{c})\right] \sum_{n=0}^{N-1} e^{jn\varphi}$$

Where

$$\varphi = 2\pi\Delta f t + \frac{2\pi f_0}{c} d \sin\theta_0 - \frac{2\pi\Delta f R_0}{c}$$

Incoming at closed method appearance, array influence of the FDA is:

$$AF_n = \frac{|\sin N\varphi/2|}{|\sin \varphi/2|}$$

The array issue will attain a extreme value of N by associating the stage of field to $2m\pi$. where $m = 0,1,2, \ldots$.

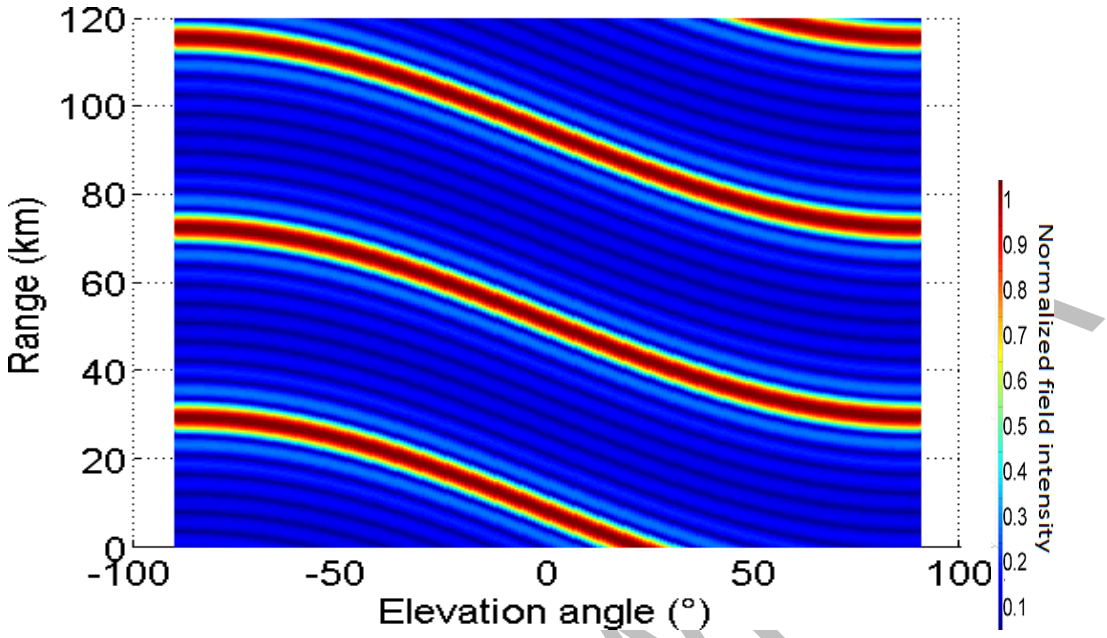

Fig 2.9: Beampattern of linear FDA. (N=10, d=λ/2, Δf=1kHz)

3D beampatterns of the LFDA are depicted in the figure. At each given point in time, there exist infinite (R,) pairs of maximum fields. As a result, Eq. (2.13) shows that the beampattern wanders across time and space, with several maxima in angle, range R, and duration t. An item put at a certain position receives the beampattern's maximums and minimums at different times during the pulse length. In contrast to this, with PAR, a target receives a steady stream of energy from either the radar system.

Keeping the other two constant will allow you to see the modulation in just one of those three parameters. It is possible to see temporal modulation in action by maintaining the

range and angle constant. It is seen in Fig.2.10 that the beam has a periodicity in time.

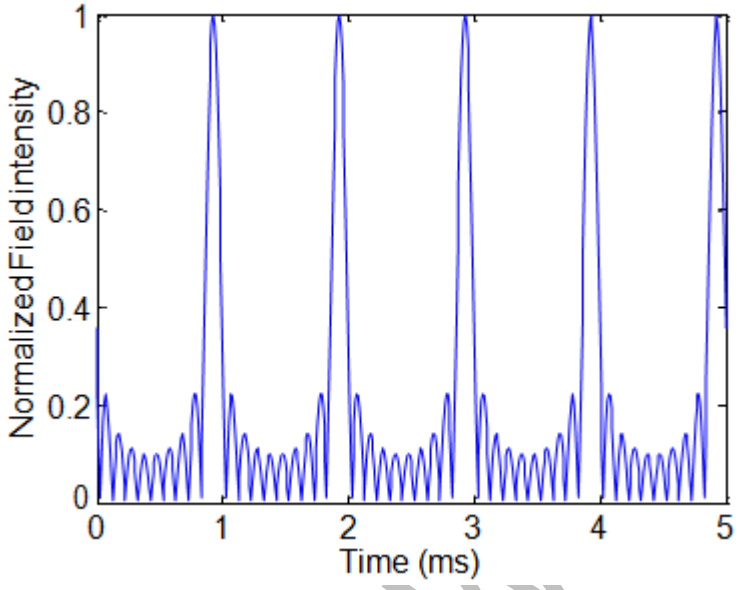

Fig 2.10 Difference of field intensity with admiration to time in LFDA. (N=10, d=λ/2, Δf=1 kHz, R =3km, $\theta = 20^{\circ}$)

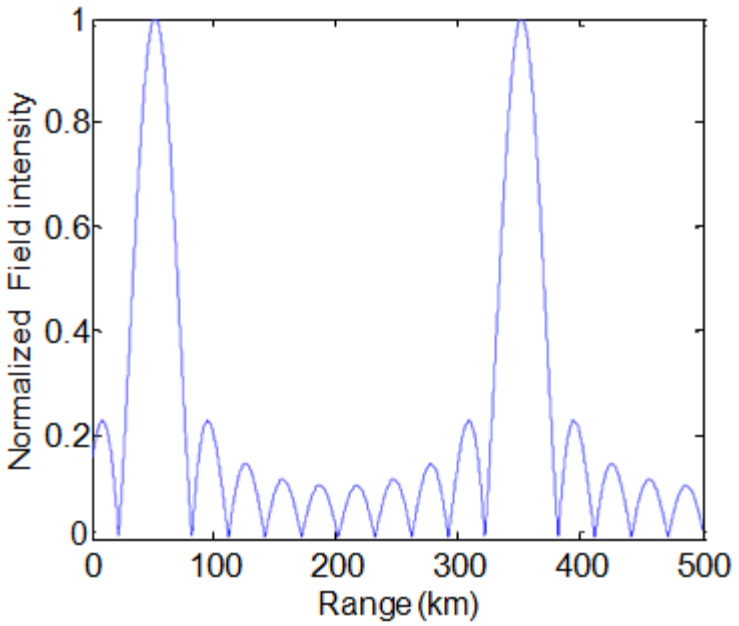

Fig 2.11: Difference of field strength with deference to range in LFDA. (N=10, d=λ/2, Δf=1kHz, t=0.3msec, $\theta = 20^{\circ}$)

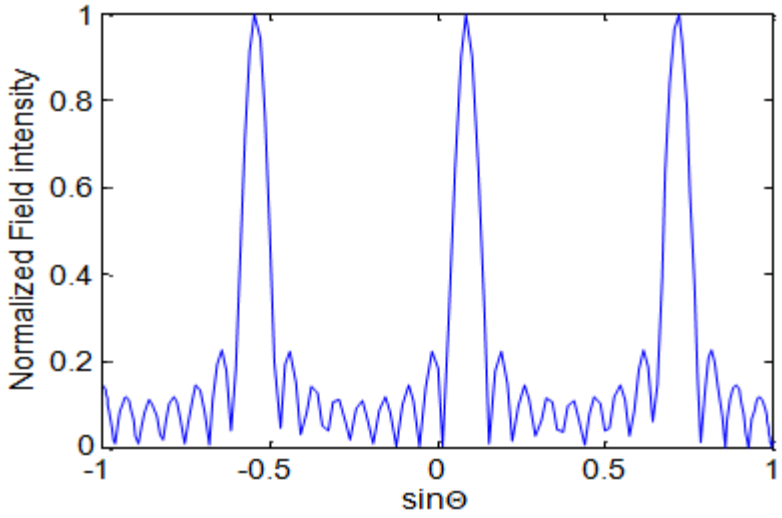

Fig 2.12: Difference of field intensity through respect to $sin\theta$ in LFDA. (N=10, Δf=1kHz, d=λ/2, R =3km, t=0.3 msec)

Periodicity of beampattern in time is $\frac{1}{\Delta f}$., null to null beamwidth $\frac{2}{N\Delta f}$. Similarly, Fig. 2.11 [illegible] choice. Periodicity of beam-pattern in range is $\frac{}{\Delta f}$

null beamwidth is $\frac{2}{N\Delta f}$

of beampattern in position is $\frac{4\pi}{Nkd}$, Zero to Zero beamwidth is $\frac{2\pi}{\kappa}$.

2.5.2 PLANAR FREQUENCY DIVERSE ARRAYS.

The beam pattern of an LFDA radar, which concentrates energy in two dimensions (i.e. range and elevation), does not meet the needs of practical applications [70]. There are numerous benefits to using planar arrays in actual radar applications, the most prevalent of which being higher gain and increased directionality. The array factor and PFDA receiver topologies proposed by [64] were pioneering contributions to PFDA. [70] examined the PFDA beam pattern's auto scanning capability, or the capacity to detect the beam in real time. We'll cover the basics of PFDA in the following section.

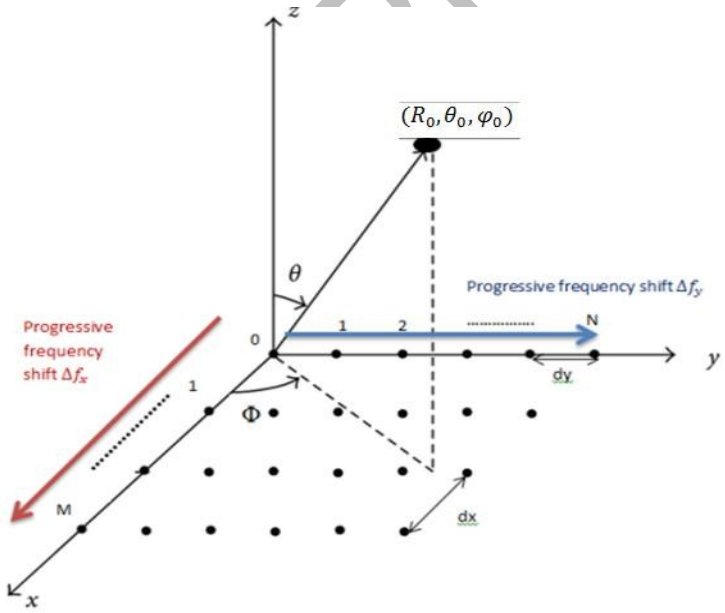

Fig 2.13: Geometry of Planar frequency diverse array.

Chapter 3
Research methodology

3.1 INTRODUCTION

ADMM and adaptive beamforming techniques have been created utilising FDA in this chapter, which is an unique convex optimization alternate direction approach of multipliers A block diagram is used to explain the concept. Detailed descriptions of each block in the flow diagram are provided. Using a phase offset selection formulation; the transmitter processing unit develops null steering. Using the receiver processing unit, not only can the system maintain a null at the interference site, but it can also estimate and anticipate the interference's next likely location. Additionally, the DOA estimator and predictor have been explained in detail. Finally, the results of the simulations confirm the viability of the proposed strategy.

Since the 1970s, scientists have been working on ways to reduce multipath interference in radars and communications systems via 'null steering.' A variety of null steering strategies have been tested in PAR systems in the literature to date [68-[76]. As previously stated, when it relates to signal source localization, PAR systems can only give angle localization. This restricts the PAR system's ability to minimise range-dependent interferences, limiting its effectiveness. A multi beam antenna or Multiple antennas would be used to emphasis the transmit energy in different directions with varied ranges [77]. In addition, the phase shifters required for beam and null steering are quite costly, accounting for over half of the total expenditure. It is possible to reduce clutter and interference by using the 'range-angle' dependent beam-pattern of the frequency diverse array (FDA), which localizes the targets in two sizes, i.e. slant distances and elevation angles.

A radar system's cognition, a phenomenon that goes beyond 'adaptability' [78], has

three main characteristics. Starting with a constant exchange of information with the surrounding environment between the transmitter and receiver. Second, there must be a closed response mechanism among the receiver, transmitter, and surrounding environment. Thirdly, mechanisms for storing the radar return data in a permanent memory.

The suggested system assumes a clutter-free environment with a single point target and one point interference source. Both of the targets and the basis of interference are non-static. It is the primary goal of the cognitively radar system to locate and sustain the deeper null of a pattern at the interference point. The target may be lit with any degree of radiation because of the frequency offset selection-based null steering system (which may or may not be a maximum). Previously, it was thought that the system already knows how to classify a signal source as an interferer. Classification approaches for current targets are discussed in [80, 81]. As a result, the proposed null steering approach outsmarts other current null steering strategies in PAR because it locates the interfering not just in position but also in range. A simple and fast frequency offset selection-based approach has replaced the extensive iterative approach-based procedures like recursive least squares (RLS), LMS, minimal variance distortion-less response (MVDR), etc. The suggested technique is most suitable for practical radar situations since it incorporates cognition to forecast the next position of the sources, which are typically non-stationary. For surveillance radar systems that must make cognitive judgements about potential targets and undesired sources in the future, the suggested approach is well-suited. Both military and civil surveillance radar systems supporting air traffic control can make use of the suggested technology.

3.2 SYSTEM MODEL

The suggested system model is depicted in the block diagram of Fig. 3.1, which includes a detailed flow diagram. The FDA transmitter and the traditional PAR receiver are used in the proposed cognitive radar system. Based on the receiver's response, the transmitter chooses the required frequency offset intellectually, so that the interference

source is located at the pattern's deepest null. Using the (range, elevation angle) tuple (R,) provided by the receiver, the interference source may be located. The MUSIC method, which is noted for its accuracy and high resolution, is used to determine the direction of arrival (DOA). However, the usual propagation delay approach is used to estimate range. Predicting the next position of the interference source (R,) from prior illuminations is done using a 'one-step ahead neural network predictor' Thereafter, the selector unit picks the needed frequency offset and accurately inserts the null at the predicted location of interference source, ensuring successful interference suppression. A deep null at the intended position is maintained in this fashion, since the cognitive loop continues to estimate and forecast the interference source's location. The system's SINR is undoubtedly improved as a result of this interference minimization.

The transmitter processing unit, radar environment, and receiver processing unit are depicted in the block diagram in Fig. 3.1. In the next sections, we'll go through each aspect in great depth.

3.2.1 FDA TRANSMITTER PROCESSING UNIT.

FDA and frequency offset selector are part of the transmitter processing unit.

There is an N-element array through d inter-element spacing in the transmitter, as illustrated in the figure (3.2). Using f0 as the radar's working frequency, a frequency shift of f is applied to each element in the array, resulting in an nth element frequency of provided by:

$$f_n = f_0 + n\,\Delta f \qquad (3.1)$$

As seen in Figure 3.2, the distance among the waves of the nth component and their reference is determined by the path length difference:

$$R_n = R_o - n\,d\,sin\,\theta \qquad (3.2)$$

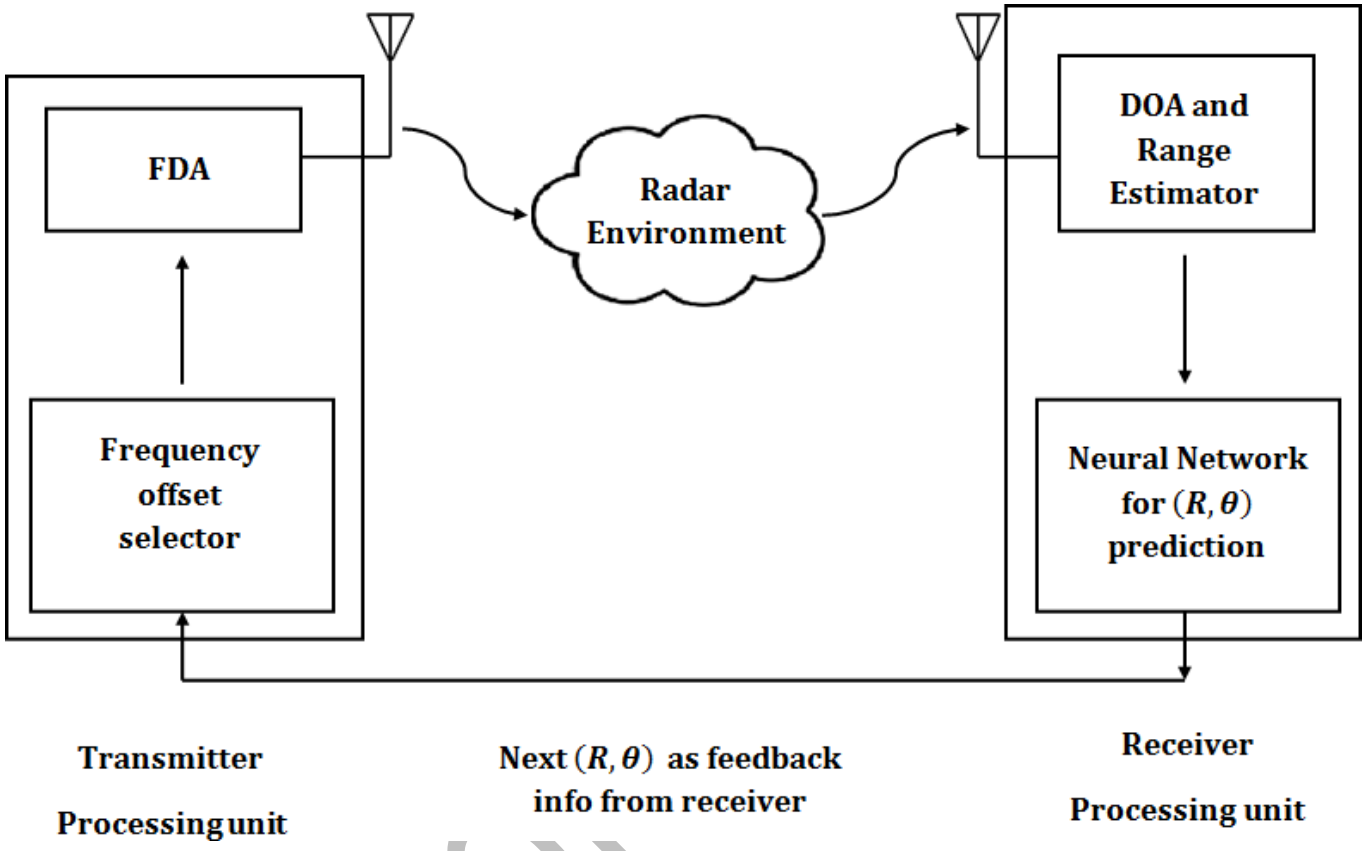

Fig 3.1: FDA radar block diagram for cognitive null steering.

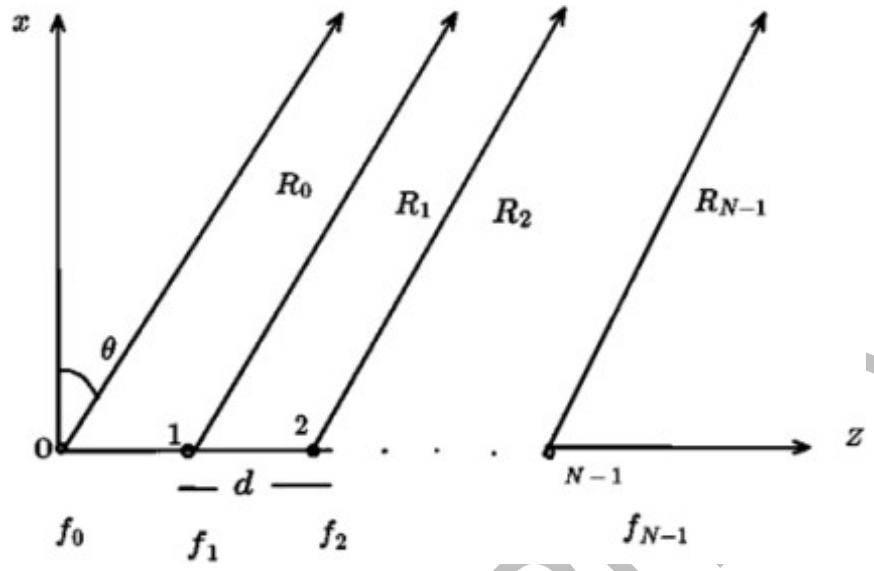

Fig 3.2: FDA transmitter

Let the signal transferred by *n* th component be stated as:

$(t\ ) = (t\ )e\ x\ p\ \{-j\ \ 2\pi f\ _n t\ \}$ for $0 \leq t\ \leq T$ (3.3)

Assuming that ao(t) =1 here, then T is the pulse length and ao(t) represents the complex weight of transmission and broadcast effects. We may represent the whole signal that is received at the far field point ($R\ _0, \theta\ _0$) as:

$$S_T(t) = \sum_{n=0}^{N-1} \exp\left\{-j2\pi f_n\left(t-\frac{R_n}{c}\right)\right\}$$

Placing in the values of $f\ _n$ and $R\ _n$,

$$S_T(t) = \sum_{n=0}^{N-1} \exp\left\{-j2\pi\left(f_0+n\Delta f\right)\left(t-\frac{(R_0-n\,d\sin\theta_0)}{c}\right)\right\}$$

Creating plane wave supposition: $R\ _0$*>> (N-1) d* and narrowband FDA assumption

$(N\ -\ 1)\Delta f\ \ll f\ _o$

Arriving at closed form expression, array factor of the FDA is:

3.2.1.1 Frequency offset selector:

The transmission time of a sharp peaks from a transfer array to a target at a given position is calculated in [52] by comparing the field phase to 2mπ . However, to produce nulls, set AFn = 0 or equivalently

$$\sin\left(\frac{N\psi}{2}\right) = 0$$

This leads to:

Thus, given the position of the interferer at ($R\ i$ −1, −1), Eq. (3.10) may be used to compute the time it takes for the null of the field pattern to propagate from the transmits array to the interferer site:

$$t_{i-1} = \frac{R_i - 1}{c} + \frac{1}{\Delta f_i - 1}\left(\frac{n}{N} - \frac{d}{\lambda_0}\sin\theta_{i-1}\right)$$

Similarly, for the interferer site ($R\ i$,), the time of ground null propagation from either the transmit array towards the interferer position is provided by:

$$t_i = \frac{R_i}{c} + \frac{1}{\Delta f_i}\left(\frac{n}{N} - \frac{d}{\lambda_0}\sin\theta_i\right)$$

It is obvious from the preceding calculations that the time it takes for the null of such field pattern to propagate from the transmits array to the interferer site is proportional to the average offset Δf. So, at instants I and i-1, we may equal the duration of null propagation from the broadcast array to the interferer site.

$$t_i - 1 = t_i$$

Then we can estimate the appropriate frequency offset fi, which, when useful to the FDA in a step-by-step manner, null places at the anticipated location ($R\ i$,)). The following is its worth in terms of prior fi1 and other pertinent constraints:

$$\Delta f_i = \frac{\frac{n}{N}\text{-}\frac{d}{\lambda_0}\sin\theta_i}{\left(\frac{R_{i-1}}{c}\text{-}\frac{R_i}{c}\right)+\frac{1}{\Delta f_{i-1}}\left(\frac{n}{N}\text{-}\frac{d}{\lambda_0}\sin\theta_{i-1}\right)}$$

3.2.2 RADAR ENVIRONMENT.

The estimated interferer trajectory in the distant field is depicted in Fig. 3.3. As previously stated, there is a non-stationary goal and a non-stationary interfering source in the radar environment. Only the interference source's trajectory is considered since the proposed technique calculates, forecasts, and maintains lowest nulls at the interference source.

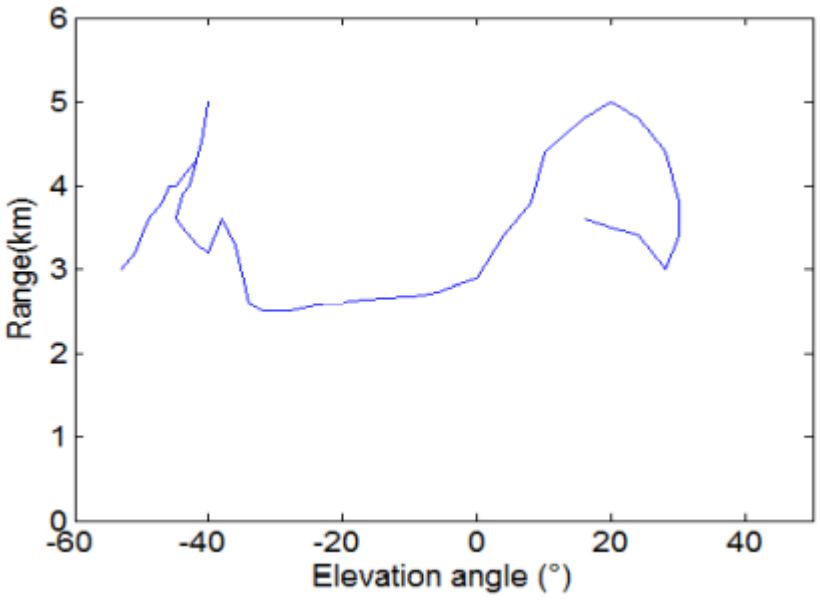

Fig 3.3: Range angle design of the expected trajectory.

3.2.3 RECEIVER PROCESSING UNIT.

The receiver array is a standard phased array with M features (M=N) and d inter-element distance. The processing unit is divided into two halves. For the next position (R , θ) we used a DOA estimator and a neural network prediction.

3.2.3.1 DOA Estimator.

Angle(θ) and Range (R) estimates are included in DOA. For angle of arrival estimate, the MUSIC (Multiple Signal Classification) method was utilised. The MUSIC method is one of the super resolution DOA estimating approaches because it can resolve many signals at once while taking significantly less time to compute [82].

Consider the following configuration of M elements in a uniform linear phased array with d inter component spacing. Let $\theta\, i$ denote the angle of the origin to be identified, with choice Ri, as determined from the reference component, which in our instance is the first element. The signal that the first element receives is:

$$r(t) = S_T(t - \frac{R_i}{c})$$

Similarly, the second element receives a signal.

$$r'(t) = S_T(t - \frac{R_i}{c})\exp \quad (j2\pi\frac{f_0}{c}d\sin\theta_i)$$

Due to the path length discrepancy between the two pieces, an extra phase is added. As a result, the receiver array's input signal vector:

$$x(t) = r(t)a(\phi) + n(t)$$

Where $\boldsymbol{a}(\Phi) = \begin{bmatrix} \exp(-j2\pi \frac{f_0}{c} dsin\theta_i) \\ \vdots \\ \exp(-jM2\pi \frac{f_0}{c} dsin\theta_i) \end{bmatrix}$ is the steering vector and $\boldsymbol{n}(t) = \begin{bmatrix} n_1(t) \\ \vdots \\ n_M(t) \end{bmatrix}$ is white

Gaussian noise vector with n2 variance and zero mean. The linear combination of L incident wavelengths is the array's result for L signals originating at this array.

$$U = Ar(t) + n(t)$$

Where $\boldsymbol{r}\ T\ (t\ )$ = [$r\ 1\ (t\ )\ r\ 2\ (t\ )$ … … … $r\ L\ (t\ )$] and A is M×L array steering matrix of the method

$$\mathbf{A}=\begin{bmatrix} \exp(-j2\pi \frac{f_0}{c} dsin\theta_1) & \exp(-j2\pi \frac{f_0}{c} dsin\theta_2) & \cdots\cdots & \exp(-j2\pi \frac{f_0}{c} dsin\theta_L) \\ \vdots & \vdots & & \vdots \\ \exp(-jM2\pi \frac{f_0}{c} dsin\theta_1) & \exp(-jM2\pi \frac{f_0}{c} dsin\theta_2) & & \exp(-jM2\pi \frac{f_0}{c} dsin\theta_L) \end{bmatrix}$$

Input covariance matrix is assumed as

$$R_u = AR_rA^H + \sigma_n2I$$

If $\lambda\ 1 \geq \lambda\ 2 \geq \lambda\ 3$ … … …. $\lambda\ M$ be eigen values of $\mathbf{R}\ u\ , \boldsymbol{q}\ 1, \boldsymbol{q}\ 2, \boldsymbol{q}\ 3$ … … … . $\boldsymbol{q}\ M$ be eigen vectors of , $v\ 1 \geq v\ 2 \geq v\ 3$ … … … . $v\ L$ be eigen values of $\mathbf{A}\ \mathbf{R}\ r\ \mathbf{A}$ H, then

$$\lambda_i = \begin{cases} v_i + {\sigma_n}^2 & i = 1,2, \ldots \ldots .. L \\ {\sigma_n}^2 & i = L+1, , \ldots \ldots .. M \end{cases}$$

The eigen vector connected with a certain eigen value is just the vector that looks like this:

$$\left(R_u\text{-}\lambda_i I\right) q_i = 0$$

For eigen vectors related with minimum eigen values, we have

$$AR_rA^Hq_i = 0$$

Since A has occupied rank and $\mathbf{R}\ \mathbf{r}$ is non-singular, this illustrations that $\mathbf{A}$ H$q\ i$ = 0 or equivalently

$$a_k{}^H(\Phi)q_i = 0 \qquad i = L+1, \ldots\ldots M \text{ and } k = 1, \ldots\ldots L$$

This indicates that the steering vectors that comprise an orthogonal to the Eigen vectors connected with the M-L lowest Eigen values. One may calculate the steering vectors of signals received by finding steering vectors orthogonal to a Eigen vectors related with the Eigen values of Ru. Estimation within a range. The traditional propagation delay approach is used to compute range. Null takes ti time to achieve the interference source at position (,), as determined in Eq. (3.12). The time required from the interfering source to the receiver is now $T\ i$ i.e. $T\ i$ = $t\ \ i$ + $R\ i\ \ c$, is the total delay between both the wave exit from the transmitter and the arrival at the receiver.

$$T_i = \frac{2R_i}{c} + \frac{1}{\Delta f_i}\left(\frac{n}{N} - \frac{d}{\lambda_0}\mathrm{Sin}\theta_i\right)$$

The range $R\ i$ can be calculated as:

$$R_i = \frac{c}{2}\left(T_i - \frac{1}{\Delta f_i}\left(\frac{n}{N} - \frac{d}{\lambda_0}\mathrm{Sin}\theta_i\right)\right)$$

3.2.3.2 Neural Network Predictor.

The predictor is the following step once the interference source has been located. Prediction is the assertion of a function's future value based on previous values. When dealing with real-time forecasts, it is critical that the approach used to anticipate the future outcome is neither overly complex nor time-consuming to the point that the expected incident happens before the prediction. We used neural networks (NN) as a

time series predictor for the prediction of position (,).

For two reasons, NN are a suitable choice for prediction. They act as a nonlinear and nonparametric technique to accurately estimate any continuous function [83]. Second, when the functional connection between independent and dependent variables is unclear, they are easier to execute and outperform conventional prediction algorithms [84]. NN does not need a model of the system, unlike with the Extended Kalman filters (EKF) implementation [85].

At the start of the setup, each interference source location is written down and organised in a time series order of 'angle' and 'range' separately. This data is sent into NN, which adjusts its weights and trains itself to find the best match till the presentation requirement is reached. The network accepts past input and output values and remains to provide essential step-ahead forecast while preserving the performance criteria as a restraint, readapting its weight as needed in the event of errors among real consequences and its forecasts. We utilised the MATLAB neural network time series toolbox in our scenario. With exogenous inputs, the model used is a non-linear autoregressive model (NARX). The NARX model [86] conveniently depicts any nonlinear model, with nonlinear mapping being approximated by a typical multilayer perceptron (MLP) network [87]. The design and operation of the NARX model are depicted in Figure 3.4.

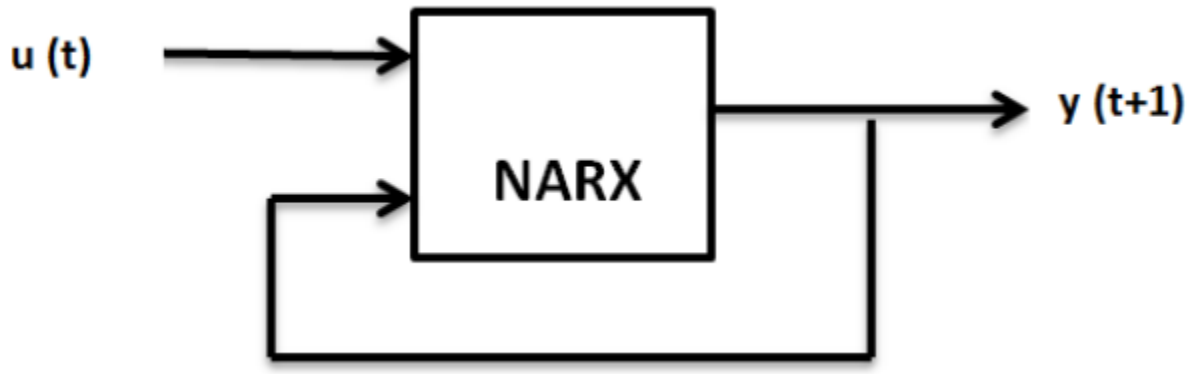

Fig 3.4: Block figure of NARX model.

A two-layer feed forward network is the standard NARX. The sigmoid function is used as the transfer function in the hidden state, whereas the linear transfer function is used in the output layer. y(t+1) is predicted using the NARX time series predictor.

$$y(t+1) = f[u(t), u(t-1), \dots \dots u(t-p_u), y(t), y(t-1), \dots . . y(t-p_y)]$$

Where

u (t) and y(t) are input and output of the structures correspondingly. $p_u \geq 1$ and $p_y \geq 1$ are the output and input instructions. Let x signify the scheme input vector by dimension $p = p_u + p_y$, such that

$$\boldsymbol{x} = [u(t), u(t-1), \dots \dots u(t-p_u), y(t), y(t-1), \dots . . y(t-p_y)]^T$$

f is a nonlinear function approached by the subsequent regression model.

$$y(t+1) = \sum_{i=1}^{p_u} a(i)u(t-i) + \sum_{j=1}^{p_y} b(j)y(t-j) + \sum_{i=1}^{p_u}\sum_{j=i}^{p_u} a(i,j)u(t-i)u(t-j) +$$

$$\sum_{i=1}^{p_y}\sum_{j=i}^{p_y} b(i,j)y(t-i)y(t-j) + \sum_{i=1}^{p_u}\sum_{j=i}^{p_y} c(i,j)u(t-i)y(t-j) \quad (3$$

Where

The exogenous coefficients a(i) and a(i, j) are linear & non-linear, respectively. The linear or non-linear autoregressive coefficients are denoted by b(i) and b(i, j).

The coefficients of nonlinear crossing terms are denoted by c(i, j).

NARX employs tapped delay lines to store previous values of the u(t) and y(t) orders. MSE, which is described as the square difference among the real and predictable result, is a performance criteria. This is the utmost common measure used by estimators, and it is defined as follows:

$$|MSE| = |Actual - Estimated|^2$$

3.3 SIMULATIONS AND RESULTS

The simulation results of the proposed method are reported in this section. The transmit and receive arrays are considered to have ten elements every, with half-wavelength separation. The specified functioning frequency is 10 GHz.

3.3.1 NN PREDICTOR RESULTS:

The NN series data tool in MATLAB is used to import time series orders of sequential angle and range positions of interference sources. The NARX Model has been chosen. The number of unseen neurons is set to eight, while the quantity of tapped suspension lines is set to four. Default The network is trained using the Levenberg-Marquardt back propagation technique. MSE is a system performance criterion. Figures 3.5(a) and 3.5(b) demonstrate the input autocorrelation arcs for angle and range time series forecast, respectively. It is a time-related prediction inaccuracy. The MSE, which is 0.01 and 0.02 for angle and range prediction, is simply represented by the value of the autocorrelation function at zero lag. Second, most other correlations are inside the tolerance threshold, indicating that the method is functioning properly.

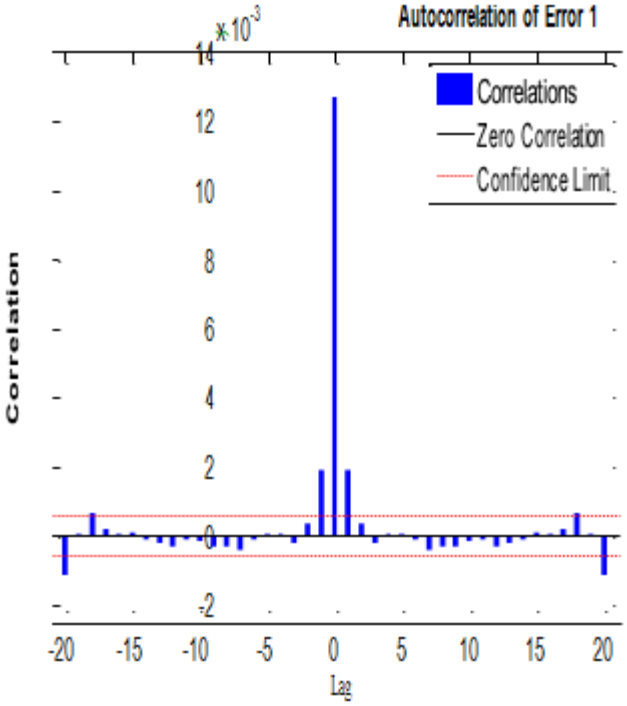
Autocorrelation of Error 1
x 10^-3
Correlations
Zero Correlation
Confidence Limit
Correlation
Lag

(a)

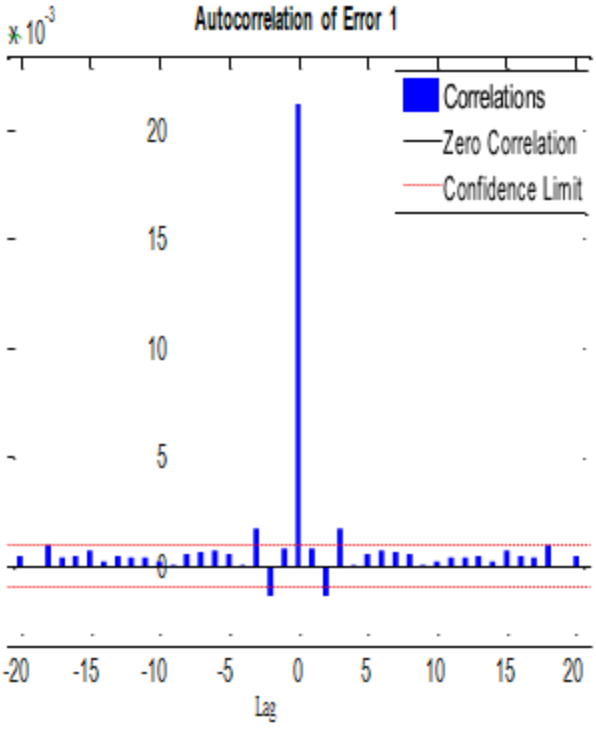
Autocorrelation of Error 1
x 10^-3
Correlations
Zero Correlation
Confidence Limit
Lag

(b)

Fig 3.5: Input autocorrelation curve for (a) Range time sequence prediction. (b) Angle time sequence prediction.

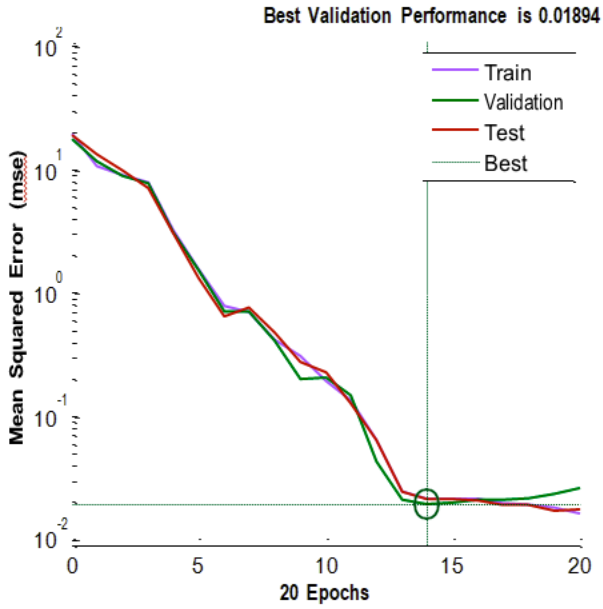

(a)

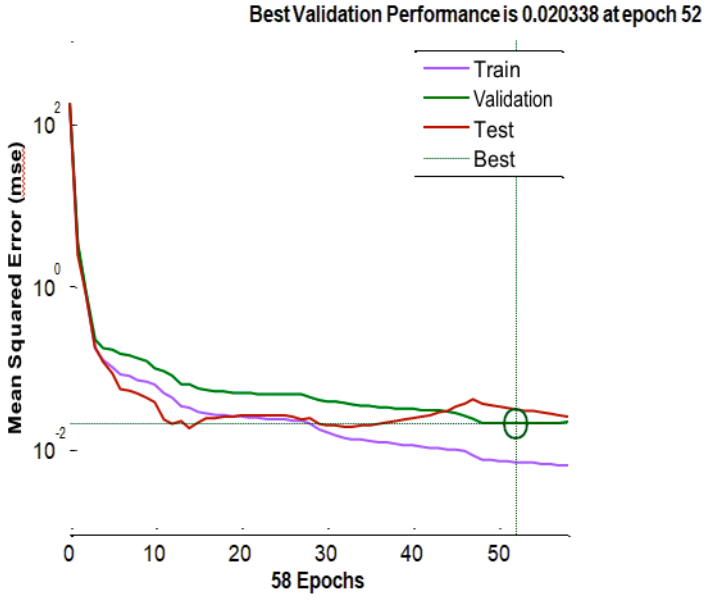

(b)

Fig 3.6: Validation enactment for the prediction of (a) Range time sequence. b) Prediction of angle time sequence

Figures 3.6(a) and 3.6(b) depict performance plots for angle and range time series prediction, accordingly. These graphs illustrate that completely errors (validation, testing, and training) are reducing until the best validation is achieved, indicating that there is no overfitting, i.e. mistakes are continually dropping with each repetition and forecast values are approaching the original values. As a result, the NN is becoming increasingly accurate at forecasting the interferer's future position.

Prediction graphs for angle and range time series are presented in Fig. 3.7(a) and 3.7(b), respectively. The NARX predictor's prediction accuracy is seen in this graph.

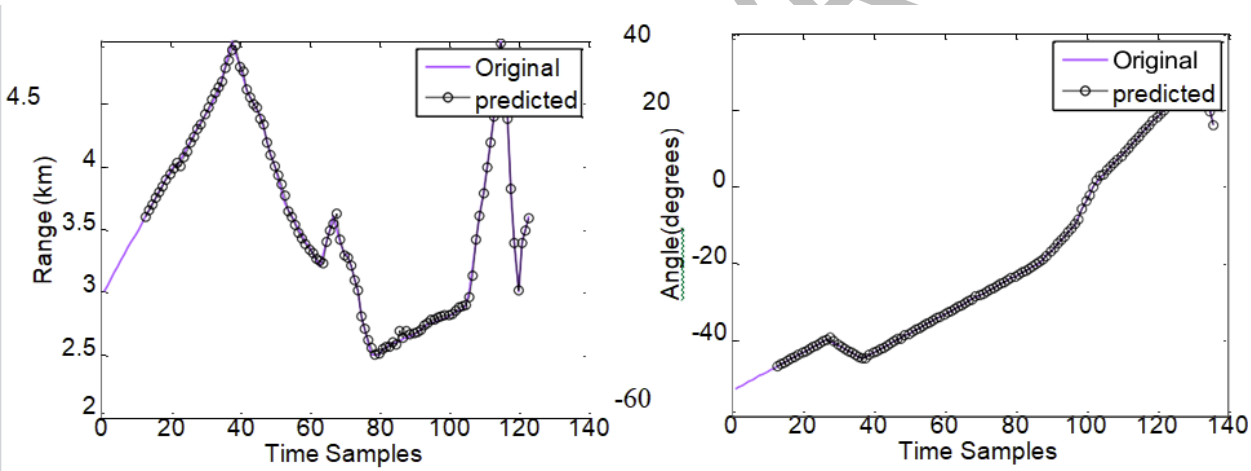

Fig 3.7: Calculation performance plots (a) for range time sequence (b) angle time sequence.

3.3.1 NULL STEERING RESULTS:

For simulation determination, we have measured a 10 GHz FDA, containing of 10

features with $\lambda/2$ 10 kHz starting frequency offset and cross spacing A few sites of the interference source are listed below, as may be seen in Fig. 3.4. The frequency offset calculated from Eq. 3.14 has also been given in Table 3.1 for each site.

Table 3.1: The interference source's position and the frequency offsets established as a result

Location Number	R_i (km)	θ_i (deg)	Δf_i (kHz)
Location 1	3	-48°	10.15
Location 2	4	-41°	10.47
Location 3	2.5	-20°	19.49
Location 4	4.5	10°	-28.82
Location 5	2.8	0°	21.71
Location 6	5	20°	-19.94

Figure 3.8 (a) depicts beampattern nulls in an angle while protection the range constant, whereas Figure 3.8 (b) depicts null settlement in an angle while maintaining the range constant. Sharp nulls on the order of -300 dB are obtained in all cases, demonstrating the adaptability of the projected technology, which may cast nulls at every mixture of (R , θ). Periodic nulls can be seen at various (R , θ) pairings due to the FDA beampattern's periodic character. Deepest nulls, on the other hand, exist exclusively at the interferer's selected places, as determined by the suggested approach.

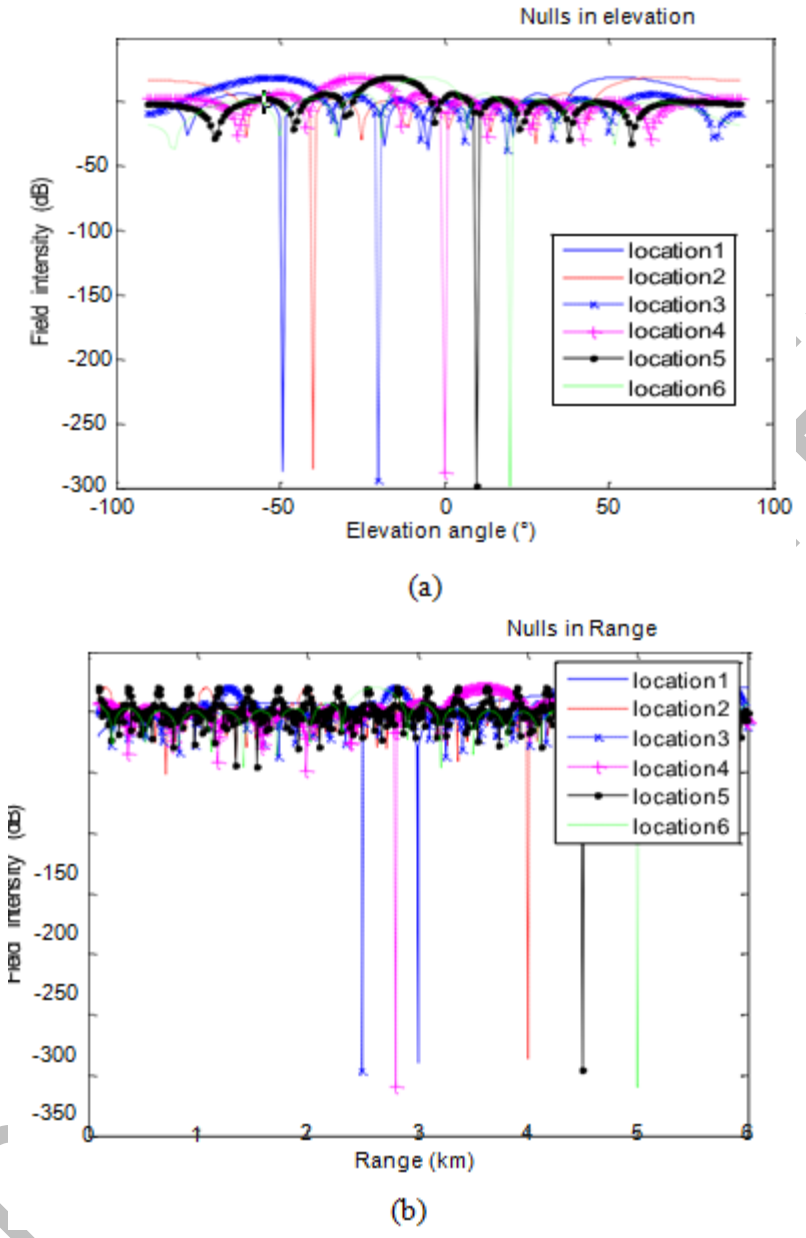

Fig 3.8: (a) Field out between with time and range set for LFDA with N=10, d =0.5. (b) Field vs. range with time and angle held constant

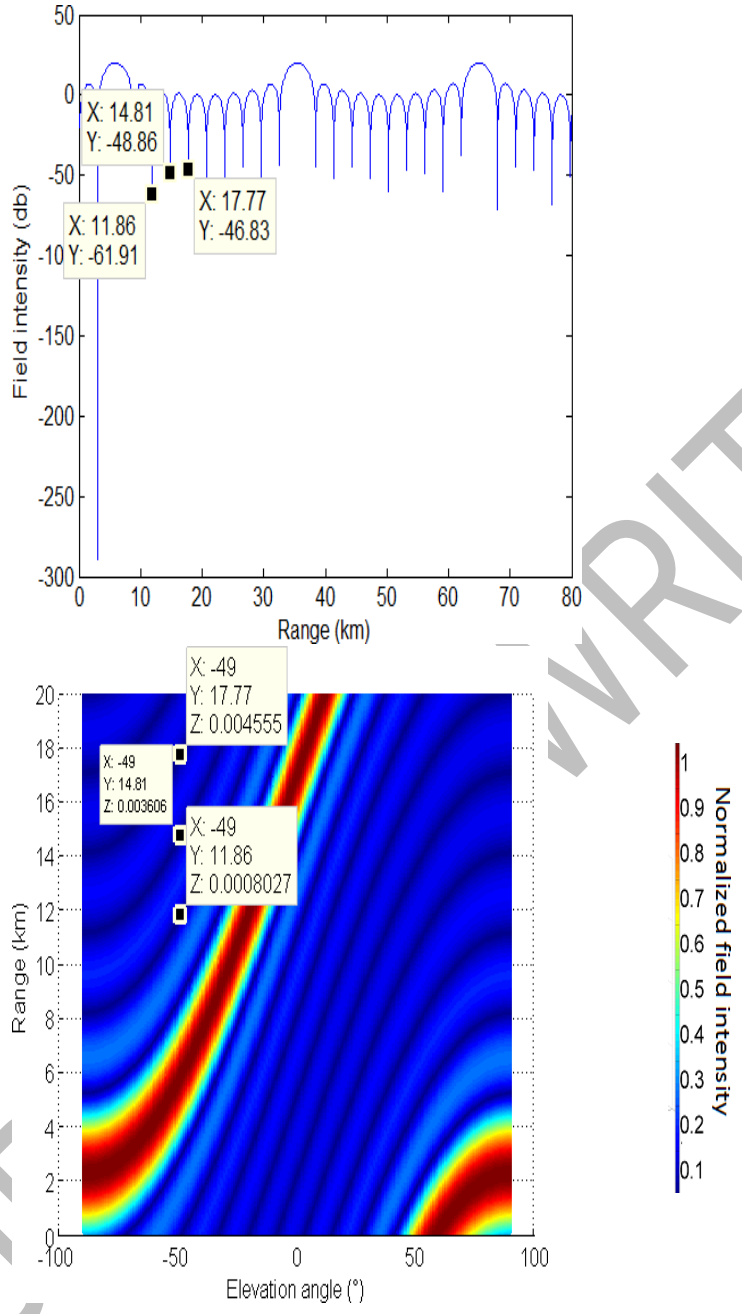

(a) (b)

Fig 3.9: For LFDA with d =0.5λ,N=10, Periodicity of nulls (a) 2D image (b) 3D depiction.

The location of the interferer with dimensions (3km, 49°) is taken into account in order to offer a clear perspective of the nulls. Clear nulls of the order of -40 to -50 dB may be seen in Fig. 3.9(a) in sites other than the planned locations. According to Eq.3.10, the null in the LFDA beampattern has a periodicity of $c \ / N \ \Delta f$. Nulls are repeated every 3km for Δf of 10.15 kHz and a 10 element array. This is supported by Figure 3.9. (a). As a result, not only do other nulls occur, but they also do so on a regular basis. The data points in Fig. 3.9(b) demonstrate how the 3D absolute field depiction validates nulls at additional range-angle pairings.

Figure 3.10 (a-f) depicts 3D range angle based beampatterns for null settlement at each of the six interferer positions. Critical values of the field are shown for clarity, revealing jagged nulls with incredibly low values.

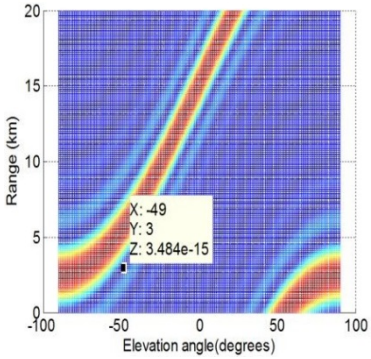

(a

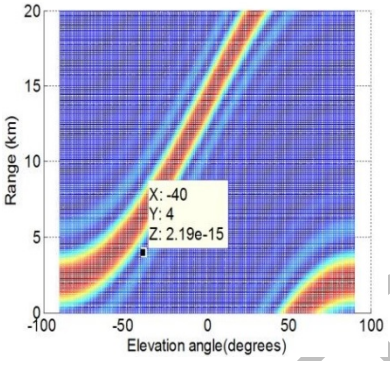

(b

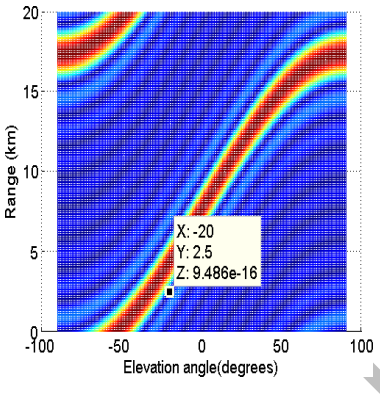

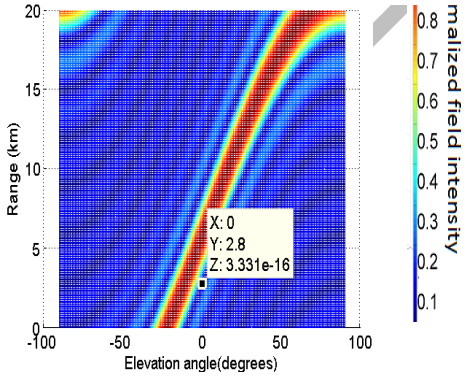

(c)

(d)

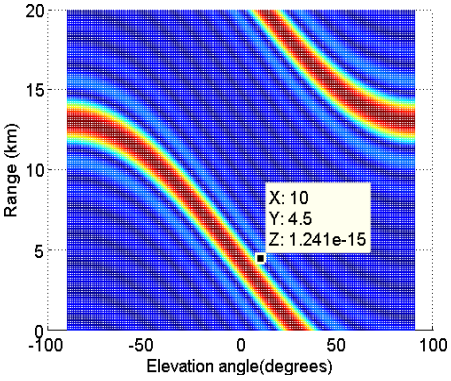

5

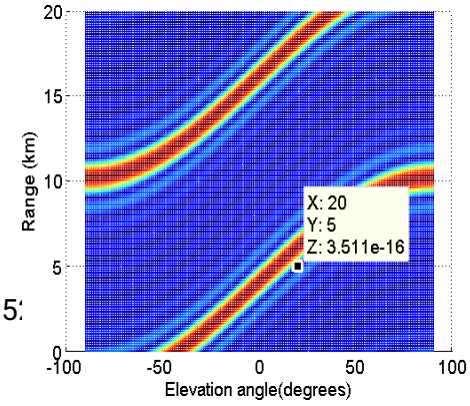

(e) (f)

Fig 3.10: For LFDA with d =0.5λ, N=10, Range angle beampattern with projected offset

CHAPTER 4
RESULTS AND ANALYSIS

4.1 INTRODUCTION

A fresh and easy technique to 3D transmits adaptive beamforming (ABF) in PFDA utilising the frequency offset selection scheme (FOSS) is discussed in this section. In a clutter-free situation with a single target and a single intervention source, the suggested frequency offset selection system beam steers at the aim point while also providing null steering to prevent undesirable interference. As a result, the suggested technique is

stated to be adaptable based on this capacity. The suggested beamformer's array signal processing model is also presented in this chapter, preceded by a SINR analysis. Furthermore, the section compares the suggested method's beamforming capabilities not only with previous PFDA work [64], however also by a robust insignificant variance distortion-less response (MVDR) beamformer methodology in PFDAs (while it has also not been distributed in the works to the preeminent of our information). In positions of null depths, beamforming capabilities, and SINR performance, comparisons are done, providing quantifiable confirmation of the suggested method's superiority.

The existence of undesired interfering signals, radar jammers, clutter returns, and other factors in complicated electromagnetic settings drastically decrease the system's SINR. Adaptive beamforming concentrates maximum gain at the target location while considerably reducing power in undesirable directions to prevent jamming risks or other undesired interferences [8]. The primary distinction among adapted and conventional beamforming (CBF) is that ABF may concentrate null in the interference way, but CBF cannot [21]. There are several adaptive beamforming algorithms for PAR in the research, for both linear and planar geometries [88]. Furthermore, because the PAR beampattern is single angle dependent, it cannot reduce interfering that is range dependent. Although ABF has been suggested for FDA, it has only been studied in linear geometries, i.e. LFDA. Null steering in LFDA depending on frequency offset selection was proposed in the preceding chapter. Similarly, [89] presented frequency offset computation for cognitive beam steering in LFDA. The beam guiding accomplished, meanwhile, is 2D, meaning the target is only localised in range and elevation. As a result, ABF in three dimensions (range R, altitude, and azimuth angle) has yet to be established, particularly in planar frequency varied arrays (PFDA). Planar FDA designs have been examined in [64], which proposes a traditional transmit beamforming method that uses beamforming weights to direct the beam just at the target position. Adaptive beamforming is inadequate without meeting undesirable sources, such as null steering, as scheme anti-jam and interfering cancellation capability has develop an important need for military and great resolution radars. The PFDA outsmarts the LFDA in that it allows for 3D beam steering,

which is impossible with planar PAR. Second, unlike LFDA's's' shaped patterns, which consist of endless (R, θ) points of maximum field, the resultant beampattern consists of a few periodic sharp localised maxima. As a result, PFDA outperforms LFDA in terms of range angle dependent interference suppression.

With exception of MVDR beamformers and conventional, where undesired source reflections are never assured to be negated at the receiver input, the suggested scheme is essentially a transfer beamforming system that ultimately consequences in higher reflections from of the target and repressed reflections from the interferer at the receiver input. As a result, the suggested strategy improves the system's SINR. Furthermore, because it avoids the need of phase shifters and long iterative processes of other ABF systems, where beam-pattern is formed by weights, adaptive techniques, and optimization requirements, the suggested formulation is highly quick and imposes the least amount of compute burden.

4.2 PRELIMINARIES AND GEOMETRY

Study a planar array of M x N equal, isotropic components, all of which are evenly spaced and oriented anywhere beside x and y axes, as shown in Fig. 4.1. The inter component spacing in the x and y directions is represented by dx and dy, respectively. The operating frequency of radar is f0, with incremental occurrence offsets beside the components in the x and y axes being Δfx and Δfy, respectively. The PFDA array factor, as determined by Eq (2.23), is:

$$Af = \left\{\frac{\sin\left(^{m\emptyset x}/_{2}\right)}{\sin\left(^{\emptyset x}/_{2}\right)}\right\} \times \left\{\frac{\sin\left(^{N\emptyset v}/_{2}\right)}{\sin\left(\frac{\emptyset v}{2}\right)}\right\}$$

$$\emptyset x = \Delta wx\left(t-\frac{R}{c}\right) + K_0 d_x Sin\theta Cos\varphi$$

$$\emptyset y = \Delta wy\left(t-\frac{R}{c}\right) + K_0 y\, Sin\theta Sin\varphi$$

$$\frac{\sin\left(M\emptyset x/2\right)}{\sin\left(\omega x/2\right)} = AF_x$$

$$\frac{\sin\left(N\emptyset y/2\right)}{\sin\left(\emptyset v/2\right)} = AF_y$$

Then, the complex array factor is the produce of array influences beside x-axis and alongside y-axis i.e.

$$AF = AF_x \times AF_y .$$

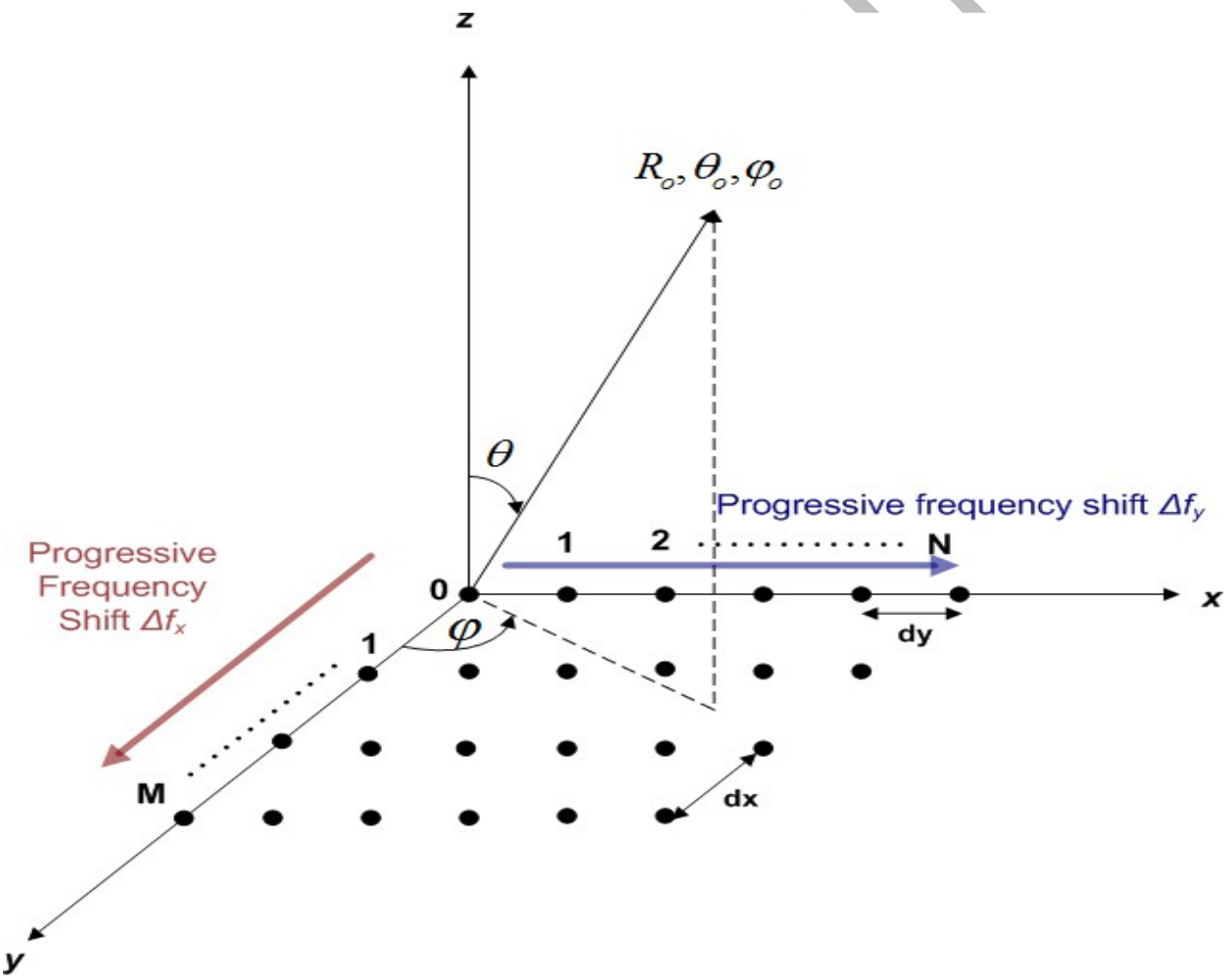

Fig 4.1: Geometry of PFDA

4.3 ARRAY SIGNAL PROCESSING MODEL

The transmit and receive signal arrangement for an MN component PFDA is presently being developed. The receiver and transmitter arrays are presumed to be colocated, and the PFDA receiver design described in [90] is taken into account. Let s(t) be the baseband signal sent by each component of the array. In the case of point sources, let us assume that we have previous information of the target's respective positions at $(R_o, \theta_o, \varphi_o)$, and an interfering source at $(R_i, \theta_i, \varphi_i)$ such that $R_i \neq R_o$ in a clutter permitted environment. At that moment the signal understood at the target location $(R_o, \theta_o, \varphi_o)$ in the distant field is expressedas:

$$(R, \theta, \varphi, \Delta f_x, \Delta f_y) = [\mathbf{w}^H(R_o, \theta_o, \varphi_o, \Delta f_x, \Delta f_y)]s(t) \quad (4.4)$$

Where $\mathbf{w}_t$ is the $MN \times 1$ transmit weight vector and $(R_o, \theta_o, \varphi_o, \Delta f_x, \Delta f_y)$ is the transmitsteering vector of PFDA and is given as:

$$(R_o, \theta_o, \varphi_o, \Delta f_x, \Delta f_y) = v[\boldsymbol{u}(R_o, \theta_o, \varphi_o, \Delta f_x)\boldsymbol{v}^T(R_o, \theta_o, \varphi_o, \Delta f_y)] \quad (4.5)$$

Where:

vec (·) views for the operator that loads the columns of a matrix in one column vector, $(.)^T$ represents the transpose, $\boldsymbol{u}$ & $\boldsymbol{v}$ are vectors of measurement $M\times 1$ and $N\times 1$, correspondingly, that are distinct as follows

$$\boldsymbol{u}(R_o, \theta_o, \varphi_o, \Delta f_x) = [1, \exp 2(_c\ d_x \sin\theta_o cos\ \varphi_o -$$

$_c$), … . , exp2($_c$ $(M-1)$ $d_x \sin\theta_o cos\ \varphi_o$ − $_c$)]

(4.6)

$(R_o, \theta_o, \varphi_o, \Delta f_y) = [1, \exp 2(_c\ d_y \sin\theta_o \frac{\Delta f_y}{s\ i\ n}\ \varphi_o$ − $\frac{R_o}{\ }$ $\frac{\Delta(N-1)}{c}$ ^{T}), … . . , exp2j π ($_c$ $(N-1) d_y \sin\theta_o s\ i\ n\ \varphi_o$ − $_c$)]

(4.7)

Currently let here is an interfering source at $(R_i, \theta_i, \varphi_i)$ in the situation. At receiver cross,received information vector **x** at Time period t is assumed by:

$(t) = \alpha_0 \mathbf{w}_i^H$ (, θ , φ , Δf , Δf) (, θ , φ , Δf , Δf) s (t) +
a R **b** R

$$\alpha_0 \mathbf{w}^H \mathbf{a}(R_0, \theta_0, \varphi_0, \Delta f_x, \Delta f_y)\mathbf{b}(R_0, \theta_0, \varphi_0, \Delta f_x, \Delta f_y)s(t) + \sum_{i=1}^{I} \alpha_i \mathbf{w}^H \mathbf{a}(R_i, \theta_i, \varphi_i, \Delta f_x, \Delta f_y)\mathbf{b}(R_i, \theta_i, \varphi_i, \Delta f_x, \Delta f_y)s(t) + \mathbf{n}(t) \quad (4.8)$$

Where α_0 & α_i are the coefficients reflection of target and the interfering, correspondingly such that $\sigma_o^2 = E|\alpha_o \alpha_o^H|$ is the preferred signal variance and $\sigma_i^2 = E|\alpha_i \alpha_i^H|$ is the variance of Interfering signal. $\mathbf{b}_o$ & $\mathbf{b}_i$ signify receive steering vectors of the target and interferer correspondingly, and have similar form as Eq. (4.5). **n**(t) indicates an additive white Gaussian noise vector through variance σ^2.

After corresponding filtering, the productivity vector **y** is:

$$\mathbf{y} = \alpha_0 \mathbf{g}_0(R_0, \theta_0, \varphi_0, \Delta f_x, \Delta f_y) + \sum_{i=1}^{I} \alpha_i \mathbf{g}_i(R_i, \theta_i, \varphi_i, \Delta f_x, \Delta f_y) + \mathbf{n}$$

(4.9)Where $\mathbf{g}_o$ and $\mathbf{g}_i$ are*MN* x1 vectors, stated as:

$$\mathbf{g}_o(R_0, \theta_0, \varphi_0, \Delta f_x, \Delta f_y) = \mathbf{w}^H \mathbf{a}_o(R_0, \theta_0, \varphi_0, \Delta f_x, \Delta f_y)\mathbf{b}_o$$

$$(R_0, \theta_0, \varphi_0, \Delta f_x, \Delta f_y)$$

$$(R_i, \theta_i, \varphi_i, \Delta f_x, \Delta f_y) = \mathbf{w}^H(R_i, \theta_i, \varphi_i, \Delta f_x, \Delta f_y)\mathbf{b}_i(R_i, \theta_i, \varphi_i, \Delta f_x, \Delta f_y) \quad (4.10)$$

4.4 PROPOSED FREQUENCY OFFSET SELECTION SCHEME(FOSS)

The primary goal of our planar FDA is to adaptively adjust the frequency offset so that the resulting transmit beampattern has a maxima at the target position $(R_0, \theta_0, \varphi_0)$ and a null at the interferer site $(R_i, \theta_i, \varphi_i)$

4.4.1 CONDITION FOR MAXIMUM FIELD

Referring rear to Eq (4.1-4.3), field or the array factor is extreme when

4.12)

4.4.2 CONDITION FOR NULL

Though, field is smallest when:

$$\{\frac{\sin(N\Phi_x/2)}{\sin(\Phi_x/2)}\} = 0 \quad \text{or} \quad \{\frac{\sin(N\Phi_y/2)}{\sin(\Phi_y/2)}\} = 0 \qquad (4.13)$$

For $$\{\frac{\sin(N\Phi_x/2)}{\sin(\Phi_x/2)}\} = 0 \qquad (4.14)$$

$$\Delta\omega_x (t - \frac{R_i}{c_i}) + k_o d_x sin\theta_i cos\varphi_i = \frac{2\pi q}{N}; q = \pm 1, \pm 2; q \neq 0, N, 2N, 3N \ldots. \qquad (4.15)$$

Because the two stages Φ_x and Φ_y in Eqs (4.2) and (4.3) are independent of one another, maxima of either the array factors AF_x and AF_y should be directed concurrently towards $(R_o, \theta_o, \varphi_o)$ in order to position compound maximum at the desired point. Eq (4.11) calculates the time it takes for the maximum of the field pattern AFx to propagate from the transmitting array to the destination position as t_x.

$$= \frac{R_o}{c} + \frac{1}{\Delta f_x} sin\theta_o cos\varphi_o$$

Similarly, Eq (4.12) calculates the time of transmission of the maxima of the field pattern AF_y from the transmission array towards the target position as t_y.

$$= \frac{\nu}{} + \quad ' \qquad n \ \varphi$$

$$y \quad c \quad \frac{}{\Delta} \quad s \ i \ \underline{n} \ \theta$$

$$f \quad \lambda \ o$$

$$y$$

Thus in direction to attain a maxima gain of $M \times N$ at $(R_o, \theta_o, \varphi_o)$: $t_x = t_y =$.
This situation hints to the association among together the frequency offsets, as

$$\Delta f_y = \frac{\Delta f \times [v_x - \frac{d_y}{\lambda_o} sin\theta_o sin\varphi_o]}{[u - \frac{d_x}{\lambda_o} sin\theta_o cos\varphi_o]}$$

Let t_{null} be the time period of transmission of null from the transmission array to the interferer position andis designed by Eq (4.15),

$$t_{null} \quad \frac{R_i}{c} \quad \frac{1}{\Delta f_x} \quad \frac{q}{\lambda_o} \quad sin\theta_i$$

Thus for extreme of the beam-pattern to be retained at $(R_o, \theta_o, \varphi_o)$ and null at $(R_i, \theta_i, \varphi_i)$,at the same time:

$$t_{max} = t_{null} \qquad (4.20)$$

This leads to:

$$\Delta f \quad \frac{+\frac{d_x}{\lambda_o} sin\theta_i cos\varphi_i]}{(M \quad)} \quad for \quad R \neq K \qquad (4.21)$$
$$[_c \times R_i - R_o]$$

.

The values of occurrence offset fx derived from Eq. (4.21), in turn, yield the values of frequency offset fy in Eq. (4.18), ensuring the necessary 3D ABF. As previously stated, the suggested approach is a transmit beamforming technique. On the transmitter side, frequency offsets are chosen, resulting in the positioning of the beam's optimum at the target and blank at the interferer. This consequences in more target reflections and less interferer reflections just at receiver input, eliminating the requirement for any long iterative beamforming system to cancel out the interferer reflections.

4.5 SINR ANALYSIS

The signal-to-noise and signal-to-interference ratios The SINR (signal to noise ratio) is determined as the percentage of desirable to unwanted signal power[91]:

$$\mathrm{SINR} = \frac{\sigma^2 |\mathbf{w}^H \mathbf{g}(R_o, \theta_o, \varphi_o, \Delta f_x, \Delta f_y)|^2}{\mathbf{w}_r^H \mathbf{R}_{\mathbf{I+N}} \mathbf{w}_r}$$

Where $\mathbf{w}_r$ is the collect weight vector while

$\mathbf{R}_{I+N} = |\sigma(R_i, \theta_i, \varphi_i, \Delta f_x, \Delta f_y)\mathbf{g}_i(R_i, \theta_i, \varphi_i, \Delta f_x, \Delta f_y) + \sigma \mathbf{I}|$ is the interference plus noise

covariance matrix. Expanding Eq (4.22)

$$\text{SINR} = \frac{\sigma^2 |\mathbf{w}^H \mathbf{g}_o(R_o,\theta_o,\varphi_o,\Delta f_x,\Delta f_y)|^2}{\mathbf{w}^H [\sigma^2 \mathbf{g}_i(R_i,\theta_i,\varphi_i,\Delta f_x,\Delta f_y)\mathbf{g}_i^H(R_i,\theta_i,\varphi_i,\Delta f_x,\Delta f_y) + \sigma^2 \mathbf{I}]\mathbf{w}} \quad (4.23)$$

$$\text{SINR} = \frac{\frac{\sigma^2}{\sigma_n^2} |\mathbf{w}^H \mathbf{g}_o(R_o,\theta_o,\varphi_o,\Delta f_x,\Delta f_y)|^2}{\mathbf{w}^H [\frac{\sigma_i^2}{\sigma_n^2} \mathbf{g}_i(R_i,\theta_i,\varphi_i,\Delta f_x,\Delta f_y)\mathbf{g}_i^H(R_i,\theta_i,\varphi_i,\Delta f_x,\Delta f_y) + \mathbf{I}]\mathbf{w}} \quad (4.24)$$

Here $\frac{\sigma_o^2}{\sigma_n^2}$ is the input signal to noise proportion (SNR) and $\frac{\sigma_i^2}{\sigma_n^2}$ is the input interference to noise proportion (INR).

4.5.1 MVDR BEAMFORMER FOR PFDA.

One of its most prominent ABF systems is the MVDR beamformer. It reduces the array output power under a linear restriction so that the signal of concern is less distorted; it reduces the array power output. The weighting vector is adaptively chosen to achieve this. In the PFDA,

The MVDR beamformer accomplishes ABF by choosing the receiving weight vector adaptively, while the frequency offsets Δf_x and Δf_y remain constant. The transmit and receive weight vectors for an MVDR beamformer on the reception side are provided by[92]:

$$\mathbf{w}_t = \frac{\mathbf{a}_o(R_o, \theta_o, \varphi_o, \Delta f_x, \Delta f_y)}{\|\mathbf{a}(R, \theta, \varphi, \Delta f_x, \Delta f_y)\|} \tag{4.25}$$

$$\mathbf{w}_{DR} = \mathbf{w}_{MV} \frac{\mathbf{R}^{-1}\mathbf{g}_o(R_o, \theta_o, \varphi_o, \Delta f_x, \Delta f_y)}{\mathbf{g}_o^H(R_o, \theta_o, \varphi_o, \Delta f_x, \Delta f_y)\mathbf{R}^{-1}\mathbf{g}_o(R_o, \theta_o, \varphi_o, \Delta f_x, \Delta f_y)} \tag{4.26}$$

Thus the SINR for PFDA consuming MVDR beam former weights is attained as:

$$\text{SINR} = \sigma^2 \mathbf{g}_o^H(R_o, \theta_o, \varphi_o, \Delta f_x, \Delta f_y)[\mathbf{R}^{-1}\mathbf{g}_o(R_o, \theta_o, \varphi_o, \Delta f_x, \Delta f_y)] \tag{4.27}$$

4.5.2 CONVENTIONAL BEAMFORMER FOR PFDA

For a predictable beamformer, the spread weight vector is similar as Eq (4.25). However the obtain weight vector is assumed by:

$$W_{r,CB} = \frac{g_0(R_{0,}\theta_0,\varphi_{0,}\Delta f_x,\Delta f_y)}{\left|g_0\left(R_{0,}\theta_0,\varphi_{0,}\Delta f_y\right)\ g_0(R_0,\theta_{0,}\varphi_0,\Delta f_y)\right|}^H \frac{1}{2}$$

$$SINR_{CB} = \frac{\sigma_S^2|\mathbf{g_o}\ (R_o,\theta_o,\varphi_{o},\Delta f_x,\Delta f_y)|^4}{\sigma_i^2|\mathbf{g}(R_0,\theta_0,\varphi_0,\Delta f_x,\Delta f_y)^H \mathbf{g}_i(R_i,\theta_i,\varphi_i,\Delta f_x,\Delta f_y)|^2 + \sigma_n^2|\mathbf{g_0}(R_0,\theta_0,\varphi_0,\Delta f_x,\Delta f_y)|^2} \quad (4.29)$$

4.5.3 FOSS BEAMFORMER FOR PFDA:

FOSS beamformer is a frequency offset selection process that includes Eqs 4.18 and 4.21 to pick offsets Δf_y and Δf_x. It does, however, use unit weighting for both transmission and receiving weight vectors, ensuring that

$$\mathbf{w}_t = \mathbf{w}_r = \mathbf{w}_{FOSS} = [1]_{MN\times 1} \quad (4.30)$$

Finally, the SINR comes out to be;

$$SINR_{FOSS} = \frac{\sigma_s^2|\sum_{k=0}^{MN-1} \sigma_k (R_o,\theta_o,\varphi_o,\Delta f_x,\Delta f_y)|}{\sigma_i^2[\sum_{m=0}^{MN-1}\sum_{n=0}^{MN-1} g_{im}(R_i,\theta_i,\varphi_i,\Delta f_x,\Delta f_y) g_{in}(R_i,\theta_i,\varphi_i,\Delta f_x,\Delta f_y)|+MN\sigma_n^2} \quad (4.31)$$

where $g_{o\,k}(R_o, \theta_o, \varphi_o, \Delta f_x, \Delta f_y)$ is the kth component of the steering vector of preferred signal source. $g(R_i, \theta_i, \varphi_i, \Delta f_x, \Delta f_y)$ and $g_{i\,n}(R_i, \theta_i, \varphi_i, \Delta f_x, \Delta f_y)$ is the is the mth component and nth component of the steering vector of interfering source correspondingly.

4.6 SIMULATION RESULTS AND DISCUSSION

In order to compare the adaptive beampatterns of MVDR and proposed FOSS beamformer, we assume PFDA radar, in a clutter free environment, at 3GHz frequency, with 8 elements along x axis and y axis each; inter element spacing of half wavelength. Noise is modeled as white Gaussian. Let the respective location (R, θ, φ) of target be (7km, 50^o, 60^o) and that of interferer be (20km,-20^o, 80^o). Frequency offset for MVDR beam former is taken as $\Delta f_x = 10$ kHz, $\Delta f_y = 1$ kHz. However, for proposed FOSS, frequency offsets calculated are $\Delta f_x = 9$ kHz and $\Delta f_y = -6.4$ kHz. 4D, sliced visualization of field obtained using proposed FOSS beamformer are presented in Fig. 4.2. The three axes indicate spherical coordinates (R, θ, φ), whereas the colours in the beampattern denote field strength. The segments of the range–elevation beampattern for fixed azimuth angle of target (60^o) and interference (80^o) are shown in Fig. 4.2(a).

Similarly, sliced 4D field visualisation for $\theta_0 = 50^o$, $\theta_i = -20^o$ has been displayed in Fig. 4.2(b), while sliced 4D field visualisation for R_0 = 7 km, R_i = 20 km has been plotted in Fig. 4.2(c).

According to Fig. 4.2, extremely localised maxima and nulls are produced at specific target and interferer locations. The MVDR beamformer's as beampatterns are shown in Fig. 4.3. Even though MVDR produces precise beamforming, the maxima are slightly dispersed in range and angular axis, as can be observed. Broad maxima, on the other hand, are regarded a danger in radar applications because they might expose the antenna to noise and interference signals originating from directions other than the

desired frequency direction. Any unwanted signal source in close proximity to the desirable signal source is equally highlighted by the array. As a result, as compared to the MVDR beamformer in PFDA, FOSS-based PFDA produces considerably sharper and directed maxima.

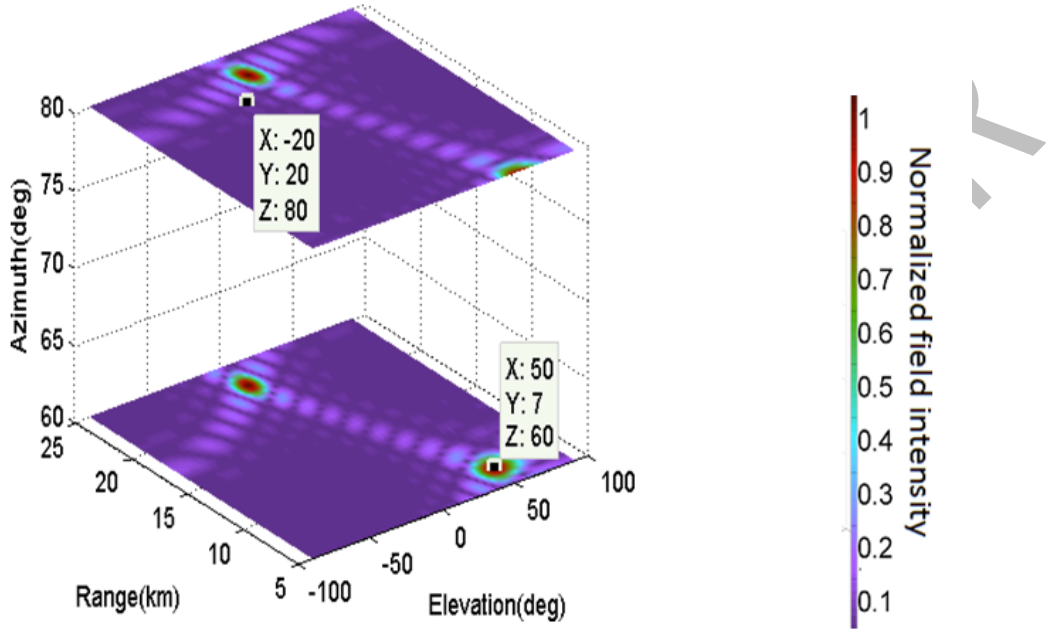

(a)

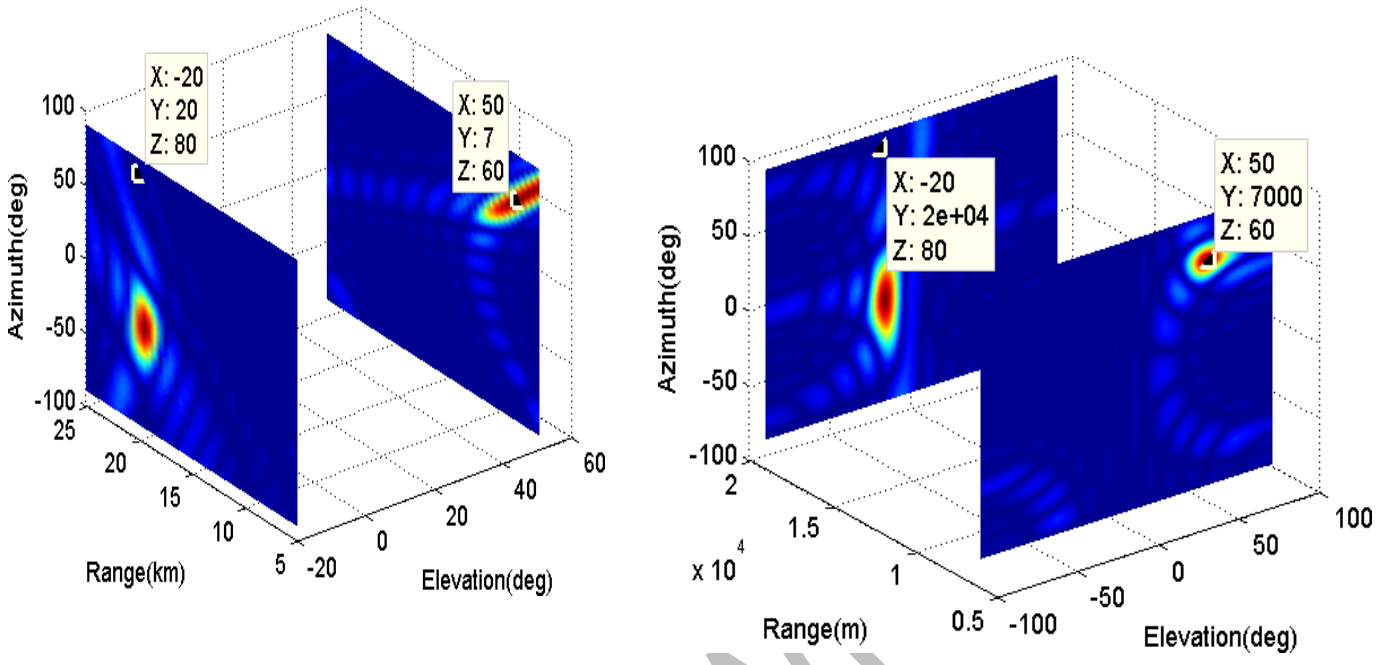

Fig 4.2: 4D sliced visualization of field attained by FOSS beamformer (M=8, N=8, $d_x = d_y = \lambda$, $\Delta f_x = 2.9k\ Hz$ and $\Delta f_y = -6.4k\ Hz$

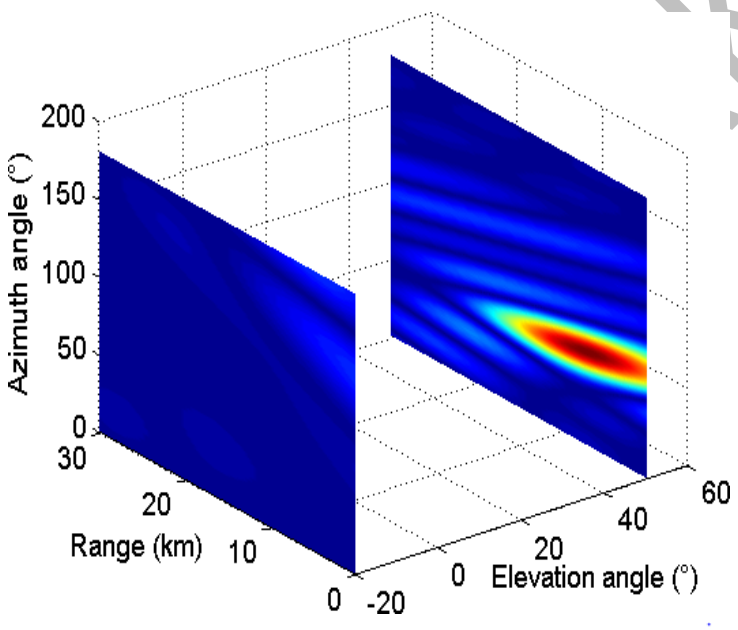
Azimuth angle (°)
200
150
100
50
0
30
20
Range (km)
10
0
-20
0
20
40
60
Elevation angle (°)

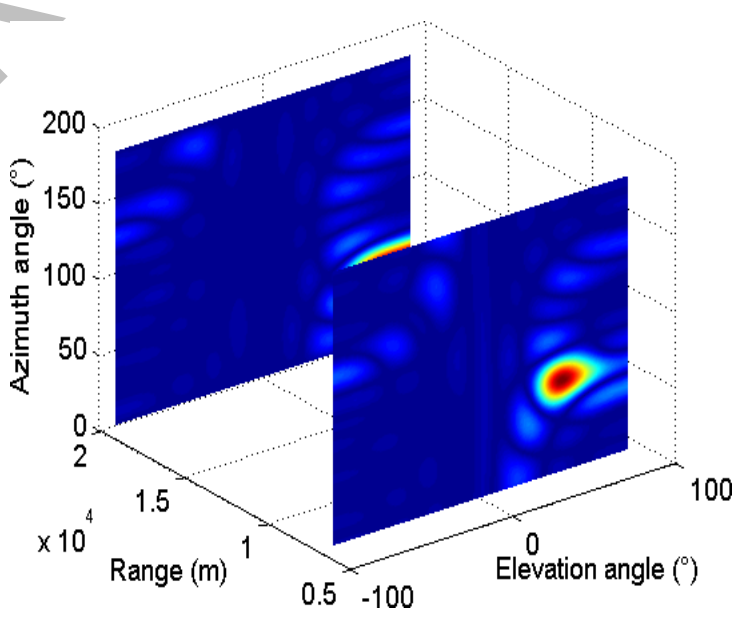
Azimuth angle (°)
200
150
100
50
0
2
1.5
x 10^4
Range (m)
1
0.5
-100
0
100
Elevation angle (°)

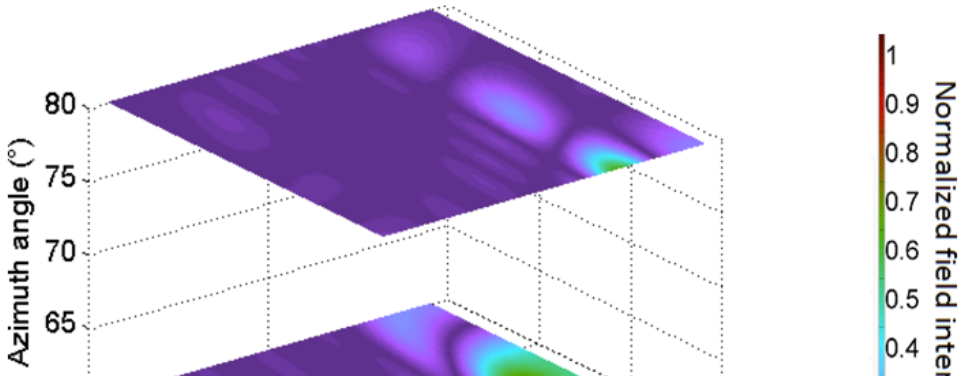
Azimuth angle (°)
80
75
70
65
1
0.9
0.8
0.7
0.6
0.5
0.4
Normalized field inte

Fig 4.3: 4D sliced visualization of field obtained by MVDR beamformer (M=8, N=8, $d_x = d_y = \lambda/2$, $\Delta f_x = 10kHz$, $\Delta f_y = 1kHz$)

Range –height beampattern at fixed azimuth angle of target and interfering, Range azimuth field pattern at fixed target and interferer elevation angles, and Field pattern at fixed target and interferer ranges are all depicted in this diagram. To compare the beamforming performance of the CB and MVDR beamformers to that of the FOSS beamformer, Fig. 4.4 displays the null placement capabilities and null depths of the three beamformers. The 3D adaptive radiation pattern showed field strength in decibels as a function of range and elevation angle while maintaining the azimuth angle constant. The 3D radiation patterns of the CB, MVDR beamformer, and FOSS beamformers are depicted in Fig. 4.4(a, b, c). As previously stated, CB fails to guide nulls. Nulls in Fig. 4.4(a) are not only shallower, but also misaligned. The MVDR beamformer is a very resilient adaptive beamformer that puts nulls precisely where they are needed. However, the null depth of the suggested FOSS in Fig. 4.4(c) is considerably greater than that of the MVDR beamformer in Fig. 4.4. (b). The suggested FOSS nulls are substantially deeper than the nulls of the MVDR beamformer. As a result, when contrasted to CB and MVDR beamformers, FOSS is better at reducing interfering and clutter.

Finally, for the CB, MVDR beamformer, and suggested FOSS, Fig. 4.5 shows output SINR vs input SNR. The FOSS has a 20dB greater SINR gain than the MVDR beamformer and a roughly 30dB greater SINR increase than the CB. SINR gains are due to deeper nulls and greater interference reduction than the other two strategies.

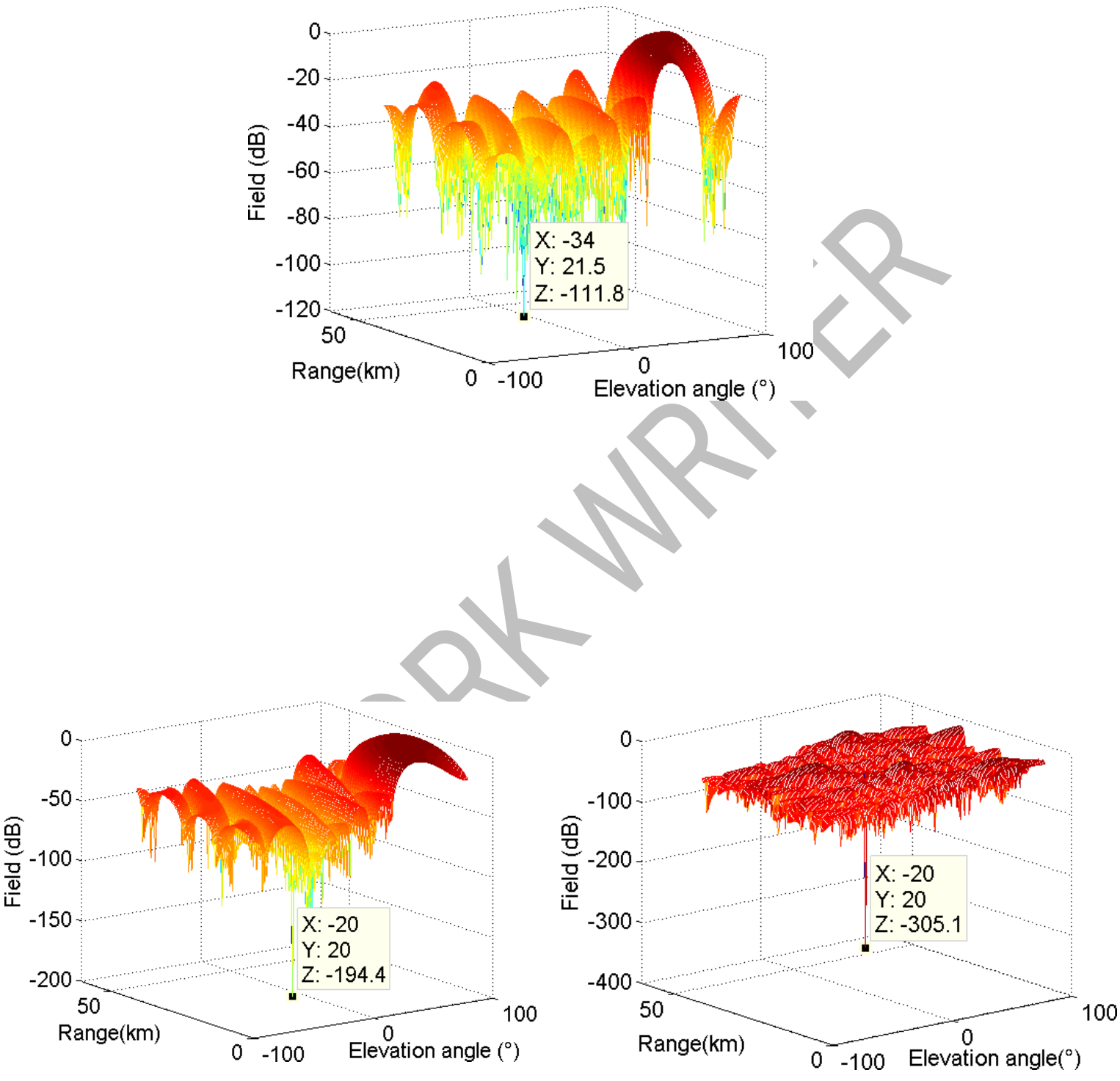

Fig 4.4: Null depth evaluation (M=8, N=8, $d_x = d_y = \lambda/2$) (a) CB ($\Delta f_x = 10kHz$, $\Delta f_y = 1kHz$) (b) Beamformer of MVDR ($\Delta f_x = 10kHz$, $\Delta f_y = 1kHz$) (c) Beamformer

of FOSS ($\Delta f_x = 9kHz$ and $\Delta f_y = -6.4$)

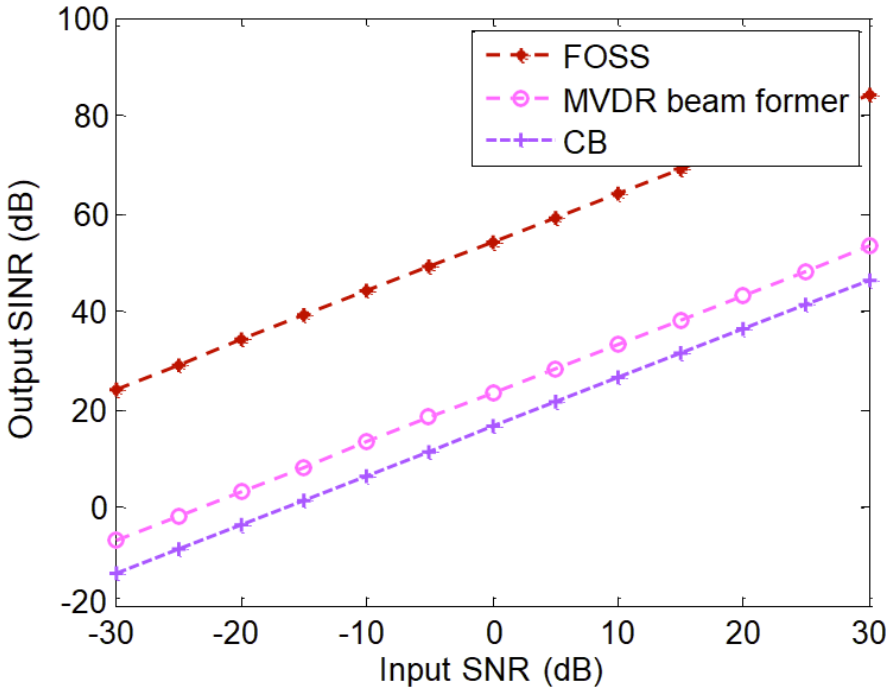

Fig 4.5: Output SINR vs input SNR of CB ($\Delta f_x = 10kHz$, $\Delta f_y = 1kHz$), MVDR ($\Delta f_x = 10kHz$, $\Delta f_y = 1kHz$) beamformer, and FOSS beamformer ($\Delta f_x = 9kHz$ and $\Delta f_y = -6.4$) for PFDA with (M=8, N=8, $d_x = d_y = \lambda$, INR =30dB).

4.7 INTRODUCTION UNIFORM CIRCULAR FREQUENCY DIVERSE ARRAYS.

For the very first time, circular arrays have been studied theoretically and statistically in the domain of frequency diversity in this section. Uniform circular frequency diversity

arrays is the name given to the suggested geometry (UCFDA). First and foremost, the UCFDA array factor has been calculated. Existing LFDA and PFDA spatial beampatterns are contrasted to the 3D spatial beampatterns. The 2D patterns compare beam widths, side lobe levels, directivities, and null depths of the three geometries for a more thorough analysis. In addition to looking at periodicities in range, time, and angle, the effect of changing various parameters on the beampattern has been explored. Finally, the chapter compares the results of UCFDA with LFDA, ULPA, and PFDA using ABF and SINR analysis. The MVDR beamformer was selected and implemented.

FDA has previously been primarily focused on linear geometries (LFDA) and planar geometries (PFDA). Although circular arrays are a frequent and simple geometry in radars, they have yet to be examined by the FDA. As a result, further research into the range-angle-dependent FDA beampattern in circular geometries is still required. Uniform circular arrays (UCA) have been studied extensively in PAR systems to date. CDMA methods [93], smart antenna networks, and wideband applications have all been examined using adaptive beamforming in UCA [94]. Various evolutionary algorithms, such as genetic algorithm and particle swarm optimization [96], have been used to improve UCA overall performance of beam forming, beam widths, energy consumption, and ambiguity resolutions by varying the number of components [95], component locations [7], and complex excitations. Other circular designs, such as concentric circular arrays and planar circular arrays [32], have been extensively investigated in terms of ABF capacity, directivity, side lobe levels, null gain margins, and residual powers, among other things. However, in all of these experiments, UCA has come up with a standard range independent beampattern restriction. As a result, UCA in the FDA might be a feasible option for 3D steeribility. The benefits of UCA, such as beam scanning azimuthally through 360o, greater spatial resolution [18] than ULA and URA, and more directed beams [33], are driving this research.

Simulations show that UCFDA has better performance characteristics than LFDA and PFDA. The range and height of targets are localised in two dimensions in LFDA,

whereas the range, height, and azimuthal angle are localised in three dimensions in UCFDA. The maximum field pairings in LFDA's's' shaped patterns are infinite (R,). Few narrow maxima in UCFDA, on the other hand, offer improved source localisation. As a result, UCFDA might provide significantly better interfering reduction and noise rejection than LFDA. Though PFDA offers 3D scanning, it does so at the expense of a greater number of antennas.

4.7.1 TRANSMIT SPATIAL BEAMPATTERN.

The form of the main beam is graphically depicted in this part, which examines the presentation of broadcast spatial pattern in UCFDA and then discusses the representation of transmit spatial pattern in UCFDA. As illustrated in Fig. 5.1, a circular array of N antenna components is equally distributed on a circle of radius a. With f0 as the frequency response of the radar, a progressive frequency shift of f is used throughout the width of the array, resulting in the frequency at the nth element being provided by:

$$f_n = f_0 + n\ \Delta f \quad (5.1)$$

If R is the length between the centre of the circle and the observation place, then the distance among the nth component and the point of view is defined by:

$$R_n = R - a\ \sin\theta\ \cos(\varphi - \varphi_n) \quad (5.2)$$

Where θ is the elevation angle of the observation point with position to z axis, φ is the azimuth angle of the observation point with reference to x-axis $= \frac{2\pi n}{N}$. Let the signal transmitted and φ_n by n th element at time t is expressed as:

$$(t\ ) = \alpha_n \exp\{-j2\pi f_n t\ \} \quad \text{for} \quad 0 \le t\ \le T \quad (5.3)$$

Where T is the pulse period and α_n is a composite excitation for each component n.

Complete signalincoming at distant field point (R, θ, φ) can be stated as:

$$S_T(t) = \sum^{N-1} \exp\{-j2\pi \quad (5.4)$$

Where c is the light speed. Placing in the values of f_n and R_n

$$S_T(t) = \sum^{N-1} \exp \quad (5.5)$$

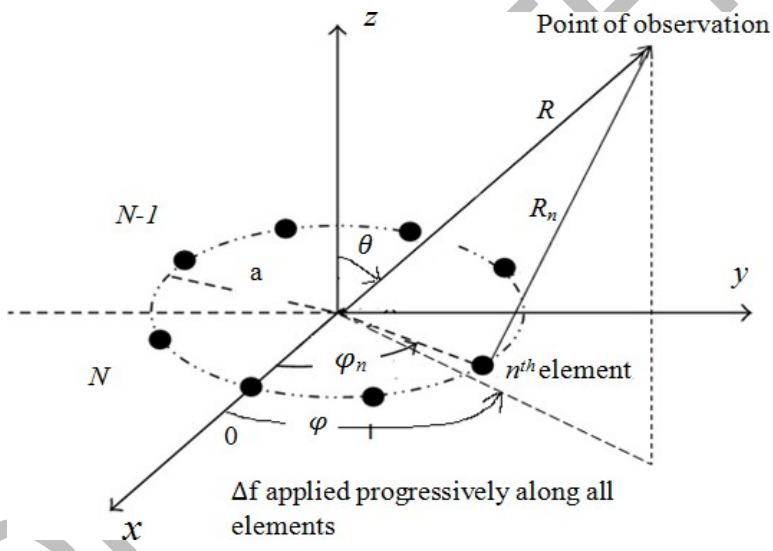

Fig 5.1: Geometry of UCFDA.

Creation plane wave supposition i.e. $R \gg (N-1)$ and narrow and FDA assumption i.e. $(N-1)\Delta f \ll f_0$ the appearance decreases to:

$1)\Delta f \ll f_0$ the expression reduces to:

$$S_T(t) = \exp \quad (5.6)$$

$$|S_T| = |\sum_{n=0}^{N-1} \alpha \quad (5.7)$$

4.7.2 BEAM STEERING

Currently to direct the extreme radiation near a point target in distant-field through coordinates ($R_o, \theta_o,$), the composite excitation α_n for every component is assumed by

$$\alpha_n(R_o, \theta_o, \varphi_o) = \exp(j2\pi[f_0 \frac{a}{c} \sin\theta_o \cos(\varphi_o - \varphi_n) + n\Delta f \frac{R_0}{c}]) \quad (5.8)$$

Re-writing Eq (5.6) with further phase period gives the whole array factor for the communicate beamforming in the way (R_o, θ_o, φ_o) is:

$$AF = |\sum_{n=0}^{N-1} \exp[j2\pi\{f_0 \frac{a}{c}(\sin\theta \cos(\varphi - \varphi_n) - \sin\theta_o \cos(\varphi_{0-} - \varphi_n)) + n\Delta f(t - \frac{R-R_o}{c})\}]| \quad (5.9)$$

Taking absolute square of the array factor provides spread beampattern B(t, R, θ, φ) of the projected UCFDA.

$$(t, R, \theta, \varphi) = |\sum_{n=0}^{N-1} \exp[j2\pi\{f_0 \frac{a}{c}(\sin\theta \cos(\varphi - \varphi_n) - \sin\theta_o \cos(\varphi_{0-} - \varphi_n)) + n\Delta f(t - \frac{R-R_o}{c})\}]|^2 \quad (5.10)$$

Let's set our goal at (30°, 4km, 60°). Figure 5.2(a, b, c) depicts the beampattern in four dimensions, with the primary beam guided to the required point. The three axes indicate spherical coordinates (R,,), whereas the colours in the beampattern represent the normalised field intensity |ST|N. To expose the field beampattern in the regions of interest, the field slices are positioned at planes with defined azimuth, height, and range values. The range-elevation beampattern is shown in Fig. 5.2(a) with a fixed azimuth angle of 60o. At the target position, a localised maximum may be seen precisely. The resulting beampattern is sliced at fixed θ = 30° in Fig. 5.2(b), while the elevation-azimuth pattern at a fixed target range of 4km is displayed in Fig. 5.2(c). At the required areas, sharp and 3D localised maxima may be seen.

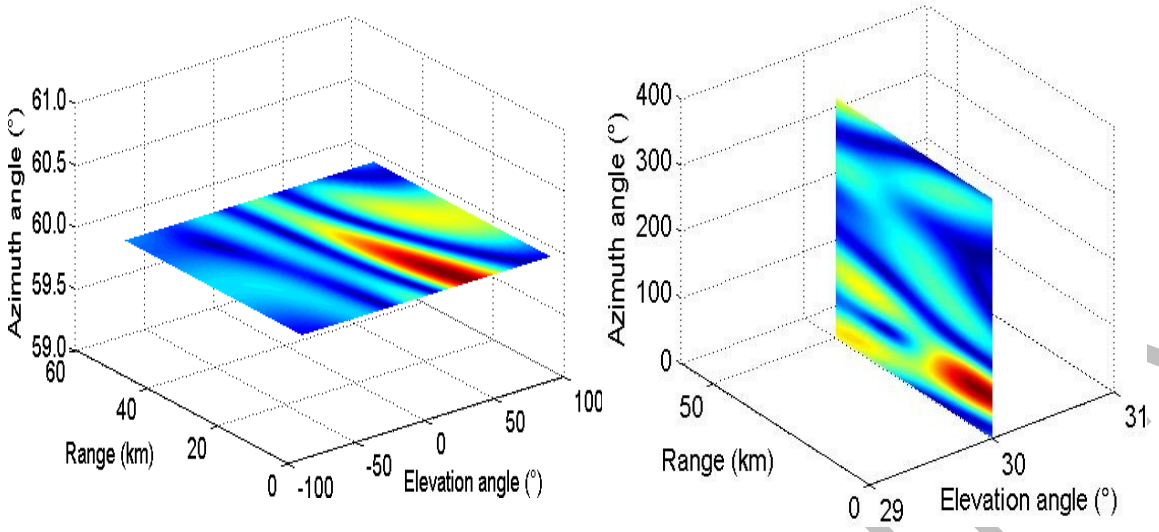
Azimuth angle (°)
61.0
60.5
60.0
59.5
59.0
60
40
20
0
Range (km)
-100
-50
0
50
100
Elevation angle (°)
Azimuth angle (°)
400
300
200
100
0
50
0
Range (km)
29
30
31
Elevation angle (°)

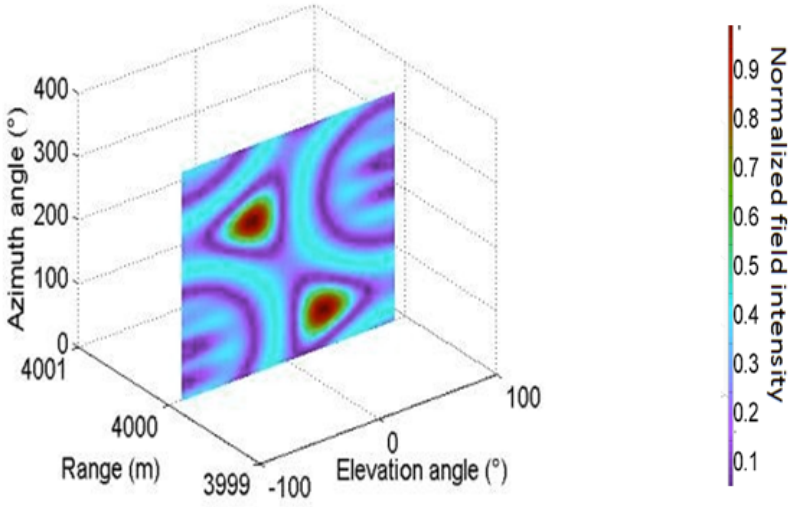
Azimuth angle (°)
400
300
200
100
0
4001
4000
3999
Range (m)
-100
0
100
Elevation angle (°)
Normalized field intensity
0.9
0.8
0.7
0.6
0.5
0.4
0.3
0.2
0.1

(c)

Fig 5.2: 4D beampattern of UCFDA (N=9, d =0.5λ, Δf =2kHz) at (30°, 60°, 4k m). (a) at fixed target azimuthal 60° angle. (b) at fixed target elevation 30° angle. (c) at fixed target range of 4km.

4.7.3 BEAMPATTERN COMPARISON OF UCFDA WITH LFDAAND PFDA.

The transmission spatial beampattern of UCFDA is clearly influenced by a number of parameters, including time, range, elevation, and azimuth angle. The characteristics for the transmission spatial beampattern of UCFDA, as well as comparison beampatterns of LFDA and PFDA, are now listed in Table 5.1. The transmit spatial beampattern generated by Eq (5.6) is shown in Fig. 3.

The range-elevation pattern of UCFDA for fixed azimuth values is shown in Fig. 5.3(a). Unlike LFDA, where the design is just range-angle (R,) dependent and widely dispersed in the angular axis as illustrated in Fig. 5.4, very directed maxima are precisely put at the appropriate location (R„). The maximum field has an endless number of (R,) pairings. Only just few periodic maxima emerge along the range axis in Fig. 5.3(a). As a result, UCFDA outperforms LFDA in terms of clutter rejection and interference reduction of 'range and angle dependent sources.' Furthermore, UCFDA outperforms LFDA in terms of beam scanning for applications requiring a 3D field of view.

When compared the UCFDA beampattern to the PFDA range-elevation beampattern in Fig. 5.4(b), it becomes obvious that, while maxima are 3D localised, the localisation is not as strong as in UCFDA. The maxima in PFDA are relatively large. To attain a beam width equivalent to that of UCFDA, PFDA requires a greater multiple antennas, which takes more space and costs more money.

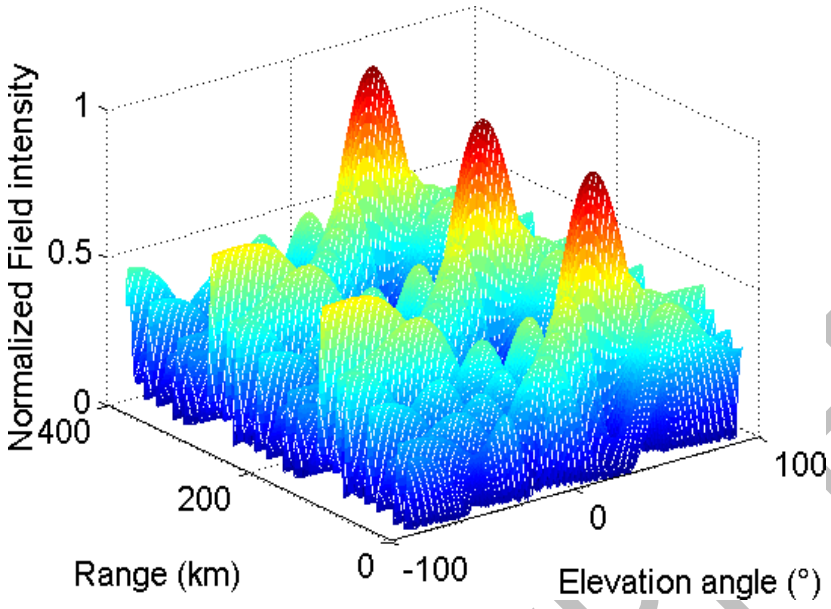

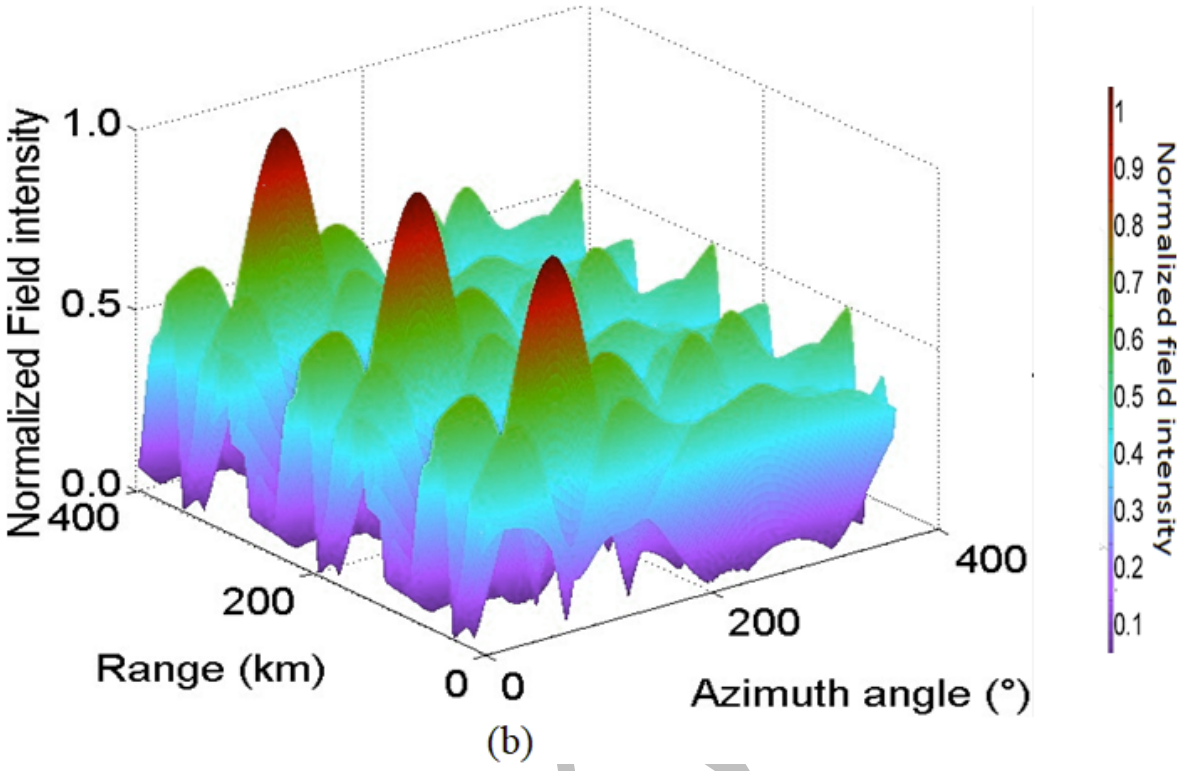

(b)

Fig 5.3: 3D Transmit spatial beampattern of UCFDA (N =9, Δf =1kHz, d =0.5λ). (a) Range -elevation outline for fixed φ = 60°. (b) Range-azimuth pattern for fixed θ = 30°.

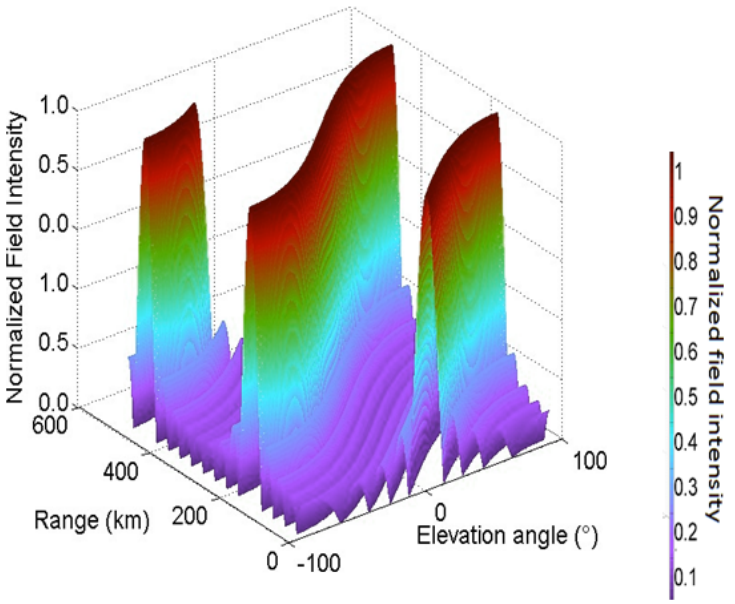

(a)

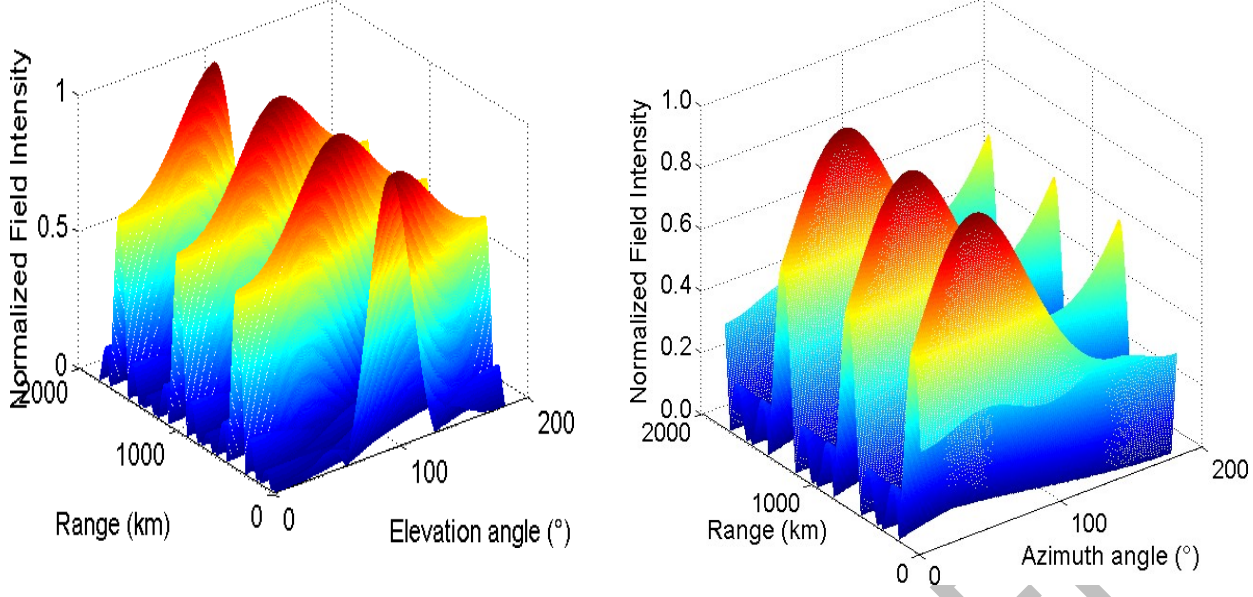

Fig 5.4: (a) Range-elevation pattern of LFDA (N =9, d =0.5λ, Δf =1kHz). (b) Range-elevation profile of PFDA ($\Delta f_x = 1kHz$, $\Delta f_y = 1kHz$ (M=3, N=3, $d_x = d_y = \lambda$) at $\varphi = 60°$. (c) Range-2 azimuth profile of PFDA at $\theta = 30°$.

Table 5.1 Simulation Parameters: (a and d stated in wavelength λ)

Parameters	**UCFDA**	**LFDA**	**PFDA**
Quantity of antennas	9	9	9 (i.e. 3×3)
Radius of circle, a	0.9λ	-	-
Carrier frequency	3GHz	3GHz	3GHz
Inter-element spacing, d	-	0.5λ	0.5λ beside every x and y axis.
Frequency offset	1kHz	1kHz	1kHz beside x- axis, 1kHz beside y-axis

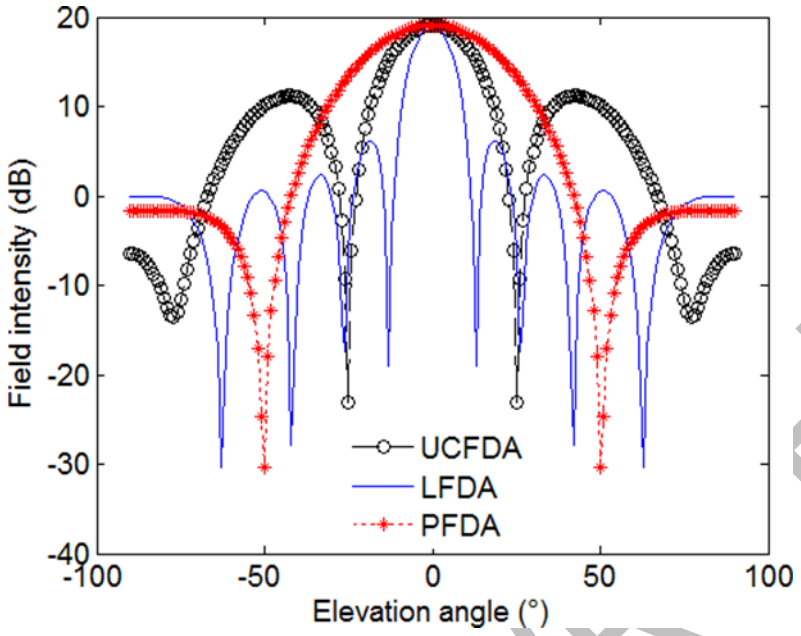

Fig 5.5: 2D beampattern of UCFDA, LFDA, and PFDA for Δf= 1kHz, and N=9.

Figure 5.5 shows 2D patterns of UCFDA, PFDA, and LFDA for a more in-depth analysis of beampattern features. The patterns are displayed for fixed values of azimuth angle and target range, i.e. 4 km and 60°. UCFDA, PFDA, and LFDA have 50°, 25°, and 14° beam widths, correspondingly. As a result, the UCFDA inserts sharper maxima at the goal point than the PFDA. UCFDA, PFDA, and LFDA have directivity values of 18.8dBi (gain in dB with regard to isotropic antenna), 12dBi, and 23dBi, correspondingly. As a result, when it relates to 3D target tracking, UCFDA outperforms PFDA in terms of directional accuracy. Furthermore, while being the most directed of the 3 geometries, LFDA's 2D steering capacity limits it. Considering the null depths, the initial null depths of LFDA, UCFDA, and PFDA are -23.07dB, -17.4dB and 30dB correspondingly. This

suggests that UCFDA achieves 6dB deeper nulls as opposed to LFDA; nonetheless, PFDA reaches deepest nulls. Because the LFDA pattern is regular in angle, somewhat deeper nulls are obtained at alternate angles.

4.8 ANALYSIS

There is a variation in time, range, and angle according to the beampattern defined in Eq (5.6). The sum of the magnitudes of such N complex exponentials gives ST(t) its maximum value. As a result, the maximum radiation direction (R_o, θ_o, φ_o) is reached when:

$$2\pi[f_0 \frac{\text{“}}{c} \sin\theta_0 \cos(\varphi_0 - \varphi_n) + n\Delta f(t - \frac{\text{“}}{c})] = \pm 2m\pi \qquad (5.11)$$

Where m = 0, 1, 2, 3….

An in-depth examination of the UCFDA beampattern indicates that the pattern's recurrence in duration and range is identical to that of the LFDA. In terms of time, the periodicity of the beampattern is $1/\Delta f$. Figure 5.6(a) shows the pattern repeating every 1ms for Δf = 1 kHz, while Figure 5.6(b) shows the pattern repeating every 0.5ms for Δf = 2 kHz. Similarly, the periodicity of range maxima is $c/\Delta f$. This is seen in Fig. 5.7(a), where the peak repeats every 300 kilometres for Δf = 1 kHz, and every 150 kilometres forΔf = 2 kHz. When it comes to frequency in angles, though, the situation is different. Periodicity in angle is defined by in LFDA for wavelength and inter-element spacing d [97], $\lambda/d = sin\theta 1 - sin\theta 2$ (5.12

In UCFDA, meanwhile, no periodicity of pattern in elevation or azimuth has been identified.

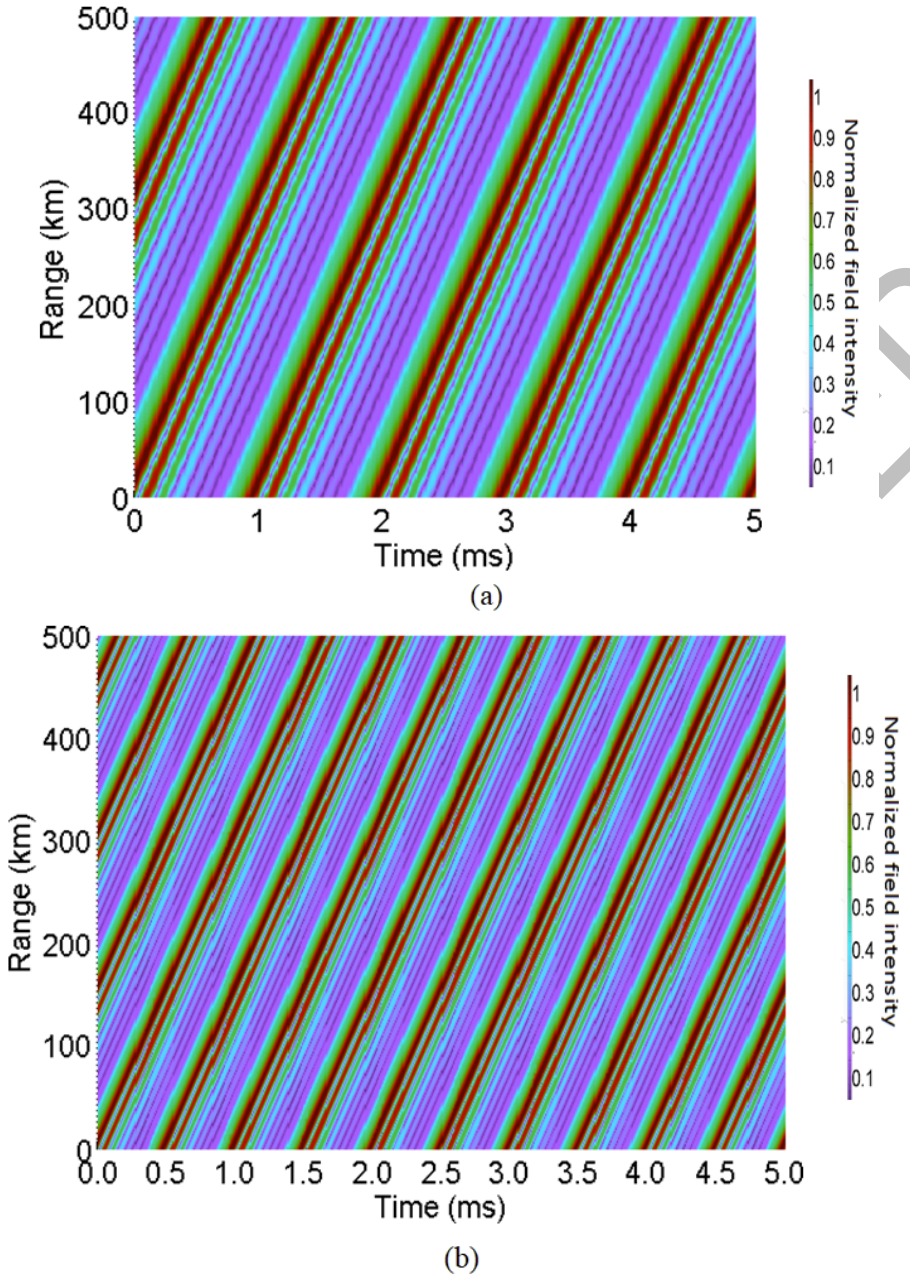

Fig 5.6: Periodic pattern of time period in UCFDA with (a) Δf = 1kHz (b) Δf = 2kHz

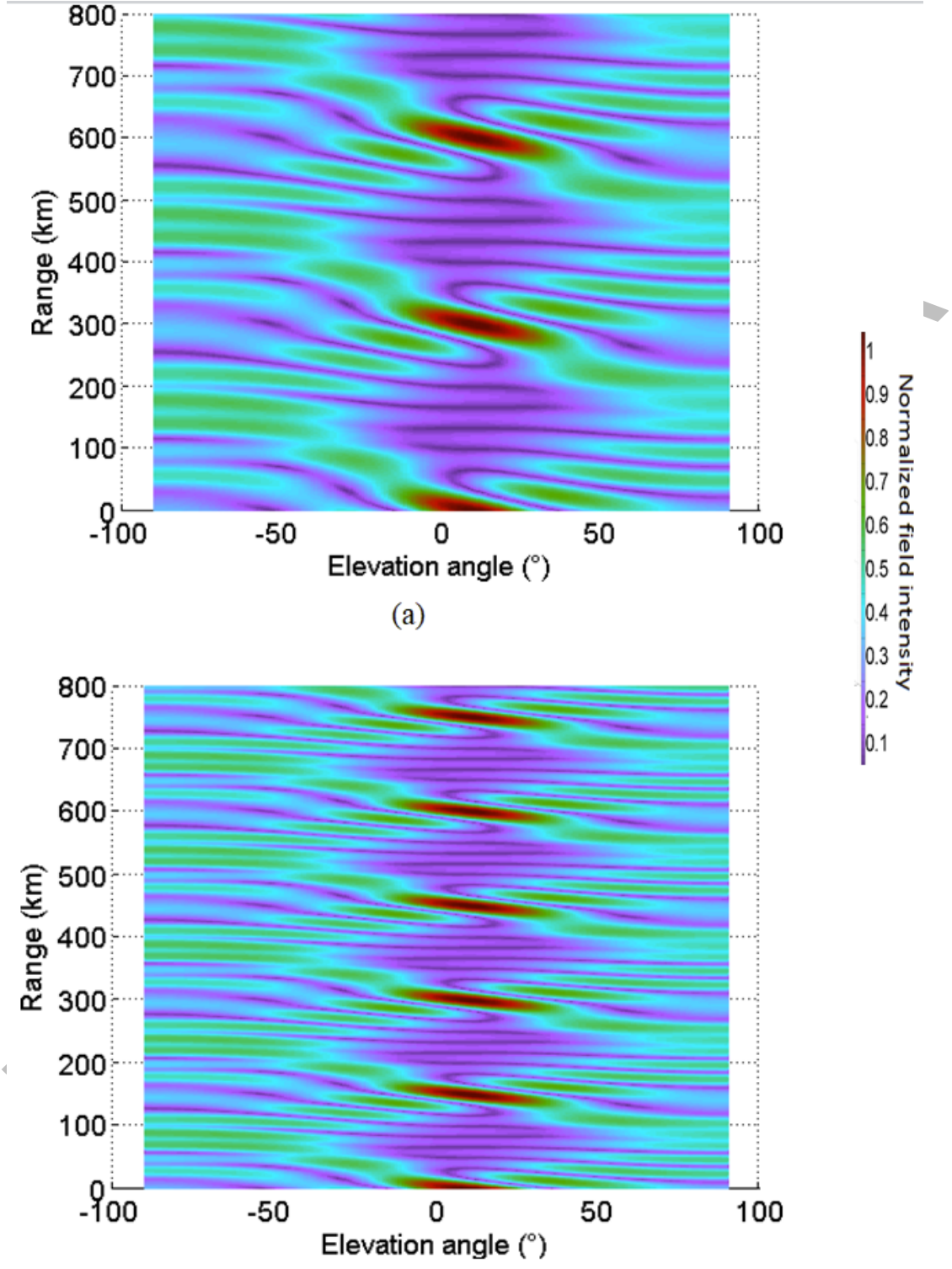

Fig 5.7: Periodic design of range in UCFDA with (a) Δf = 1kHz (b) Δf = 2kHz

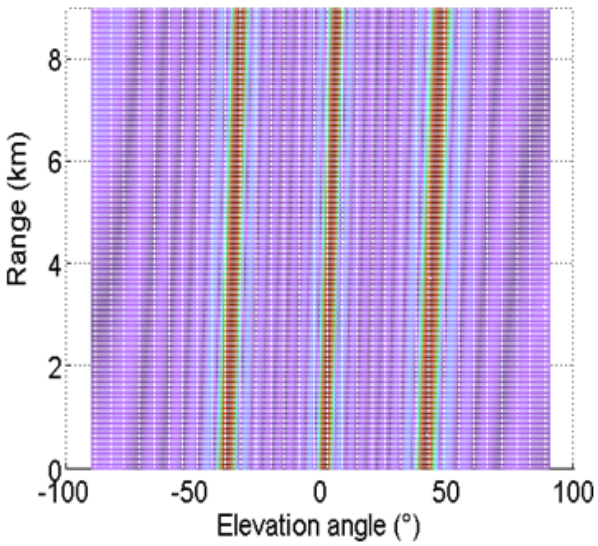

(a)

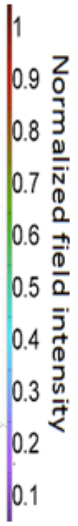

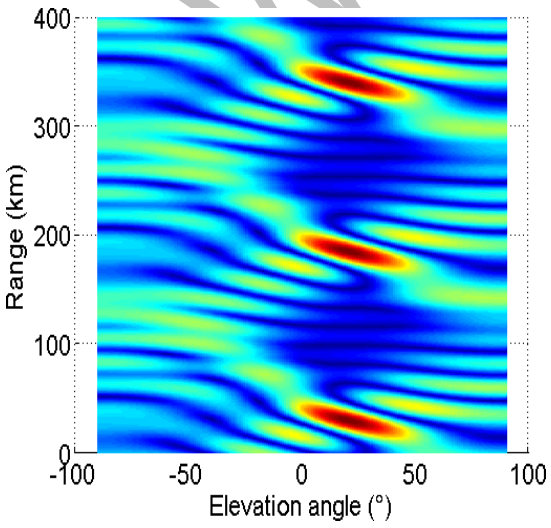

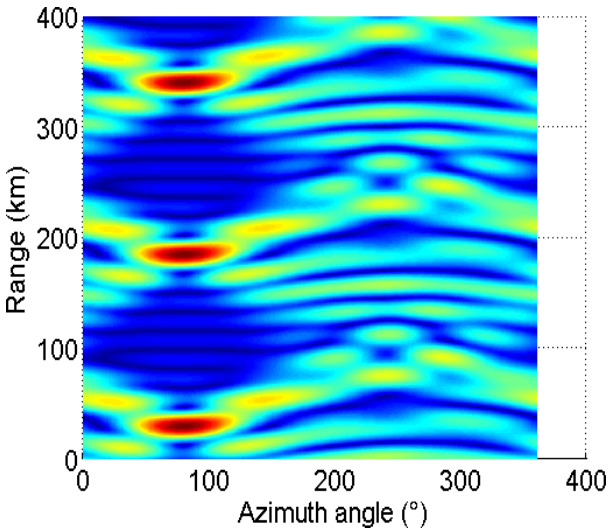

Fig 5.8: (a) Range-angle beampattern in LFDA. (b) Range elevation outline for fixed azimuth angle in UCFDA. (c) In UCFDA, the range –azimuth profile for a fixed elevation angle.

The range and angle beampattern in LFDA with a 2 kHz offset is shown in Fig. 5.8(a). Along the angular axis, the pattern repeats. Figures 5.8(b) and 5.8(c) in UCFDA, on the other hand, illustrate that the periodicity does not occur along the elevation or azimuthal axes. Because there is no enforced repetition of beampattern at normal angular intervals, this characteristic of UCFDA can help with adaptive multi-target recognition and numerous null steering.

4.8.1 EFFECT OF VARIATION OF DIFFERENT PARAMETERS ON BEAMPATTERN.

The effect of increasing various factors such as the number of elements N, inter-element spacing d, and circle radius an is now explored. These variables are linked by means of; $N\,d = 2\pi a$

Figure 5.9 (a-c) shows beampatterns created by UCFDA with f= 2kHz for various circle radii (given in wavelength), namely 1, 3, and 5. As seen in Fig. 5.9, increasing the circle width while maintaining the number of items constant increases the inter element separation, resulting in high amplitude side lobes.

When the radius of the circle is increased by raising the number of components while maintaining the inter element spacing constant, HPBW decreases while peak 2 to side lobe ratios improve considerably, as seen in Fig 5.10 (a-c).

However, in this example, the radius of the circular arrays remains constant at 5, while the inter element spacing decreases as the number of elements increases. This is seen in Figure 5.11 (a-c), where a rise in the number of components leads to greater directivities and lower side lobe levels. The radiation pattern suffers from severe side lobe levels as the inter-element distance grows, as seen in the previous discussion. This

is in line with the situation that $d \leq \frac{\lambda}{2}$ in order to avoid side lobes at all frequencies [16].

Table 5.2 shows HPBW and peak to side lobe ratios (PSR) for all the three cases. Table 5.2: HPBW and PSR for all the three cases.

	N	***d(λ)***	***a (λ)***	**HPBW** (°)	**PSR** (dB)
Case 1	10	0.66	1	20	4.29
	10	1.8	3	11	3.22
	10	3.1416	5	07	3.46
Case 2	10	0.5	0.5	44	4.5
	20	0.5	1.59	21	4.4
	30	0.5	2.3	11	4.6
Case 3	10	1.0	5	05	3.7
	20	1.6	5	05	4.3
	30	0.7	5	05	3.9

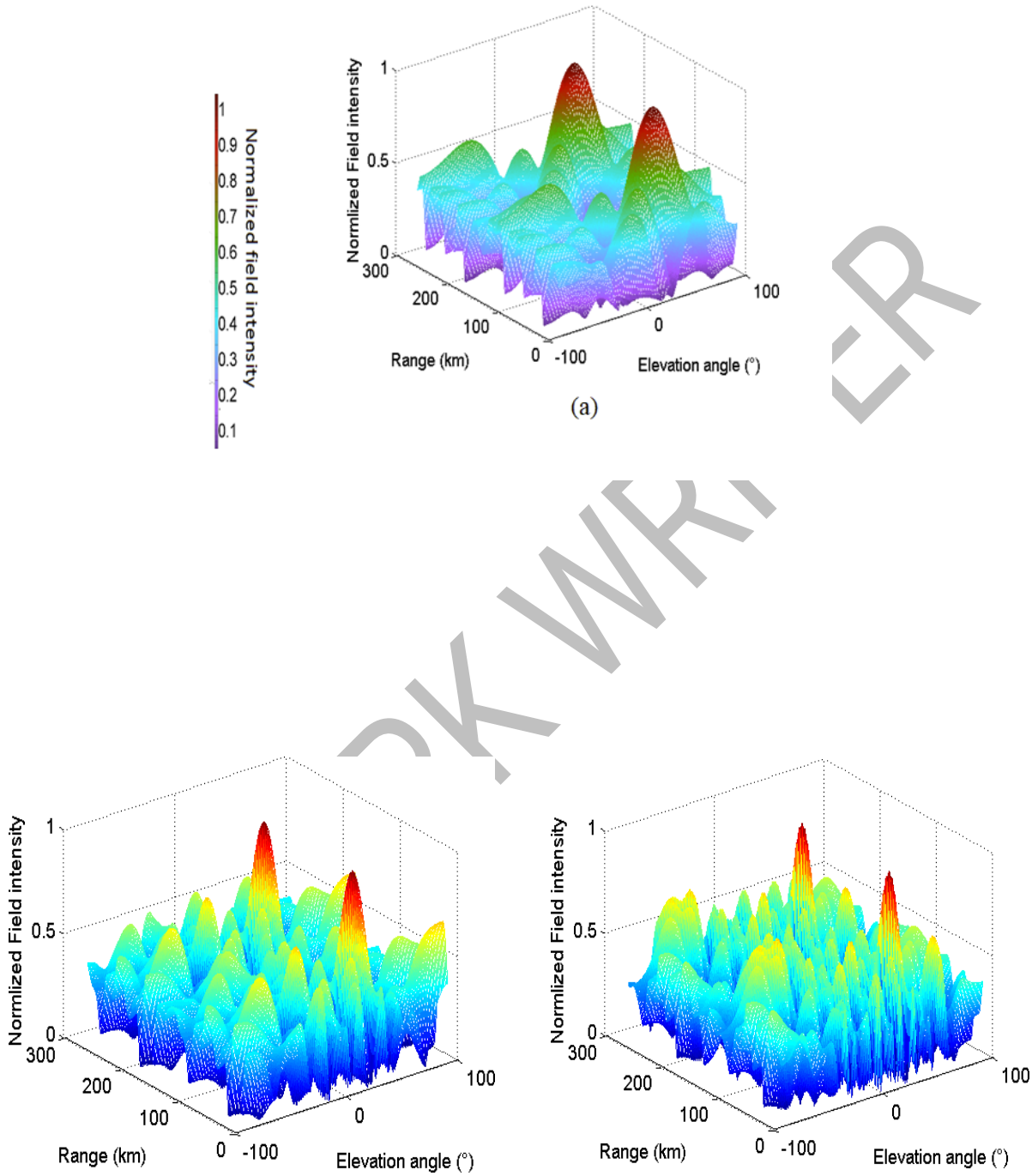

Fig 5.9: Beampattern of UCFDA for Case 1 through N=10, Δf= 2kHz and (a) a=1λ (b) a=3λ, (c) a=5λ

4.8.2 SIMULATION RESULTS:

A single target and two interfering sources are assumed in a clutter-free environment. ULPLFDA, A, PFDA (3 3), UCFDA arrays of 3GHz, 9 components, and 0.5 inter-element spacing are used as a comparative. Table 5.3 lists additional simulation settings as well as source locations.

The case analysed is such that one of the interferers has the same elevation and azimuth angle with the target in order to underline the advantages of UCFDA over LFDA, PFDA, and ULPA in respect of 3D beam scanning. ULPA, LFDA, PFDA, and UCFDA adaptive beampatterns are compared in Figures 5.12 and 5.15.

ULPA fails to find a minimum at the interferer site with the same elevation angle as the target in Fig. 5.12. Consequently, the LFDA only delivers 2D beam scanning regardless of azimuth angle in Fig. 5.13. In the maximum field region, endless (R , θ) maxima pairings may be seen.

However, as seen by the sliced 4D beampattern in Fig. 5.14, PFDA does enable 3D beam scanning. The nulls are positioned precisely at their designated places, however the maximum is extra broad. Broad maximum is an unwelcome characteristic in radar communications because one of the interferers with the same angles as the target receives a high quantity of radiation as a result of the wide maximum.

The UCFDA, on the other hand, provides significantly sharper maxima and minima at the appropriate places than the PFDA in Fig. 5.15. All interferers are securely hidden in the shadows. As a result, UCFDA delivers adaptive beampattern in the scenario when the interferer and target have the same angle, which is a rare occurrence in radar systems [98] using ULPA and LFDA. As a result, UCFDA is expected to outperform its linear and planar equivalents in terms of interference reduction and clutter rejection.

In the SINR comparison shown in Fig. 5.16, UCFDA clearly outperforms ULPA, LFDA, and

PFDA. In comparison to ULPA, LFDA, and PFDA, this result shows that UCFDA offers clearer maxima and prevents interfering signals from degrading the smart antenna array's efficiency.

Parameters	UCFDA	LFDA	ULPA	PFDA
Radius of circle, *a inwavelengths λ*	$\frac{5}{2\pi}\lambda$ (for d=0.5λ)	-	-	-
Frequency offset	2kHz	2kHz	0	2kHz
Target location	$(7k\ m, 10^0, 80^o)$			
Interferer 1	$(20k\ m, 10^0, 80^o)$			
Interferer 2	$(12k\ m, -90^0, 200^o)$			

Table 5.3: Simulation parameters for adaptive beamforming and SINR analysis.

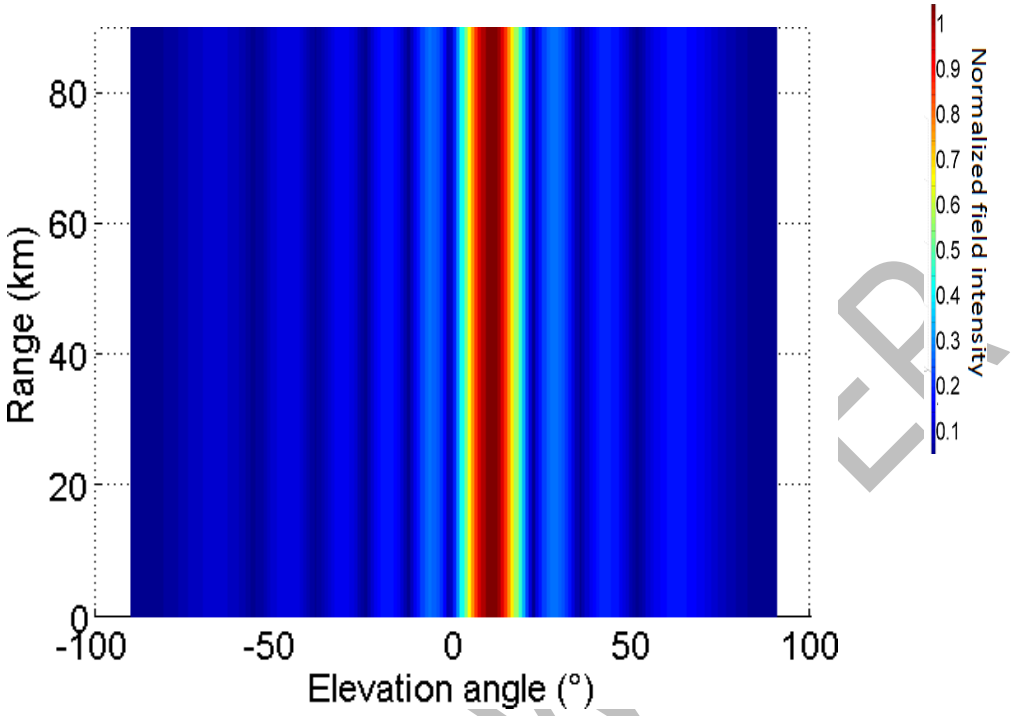

Fig 5.12 Adaptive beampattern for ULPA (N =9, Δf =0, d =0.5λ)

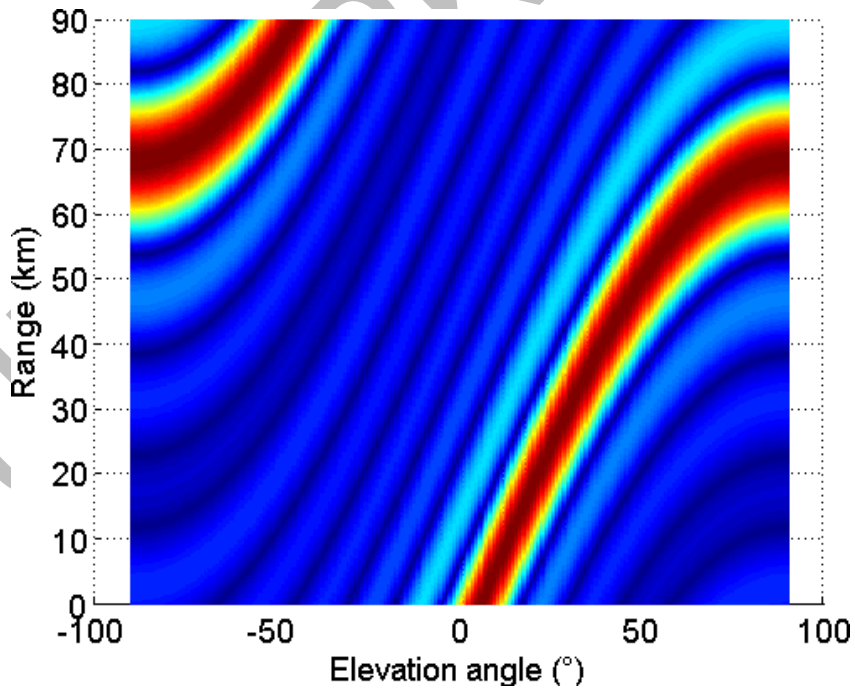

Fig 5.13 Adaptive beampattern for LFDA (N =9, Δf =2kHz, d =0.5λ)

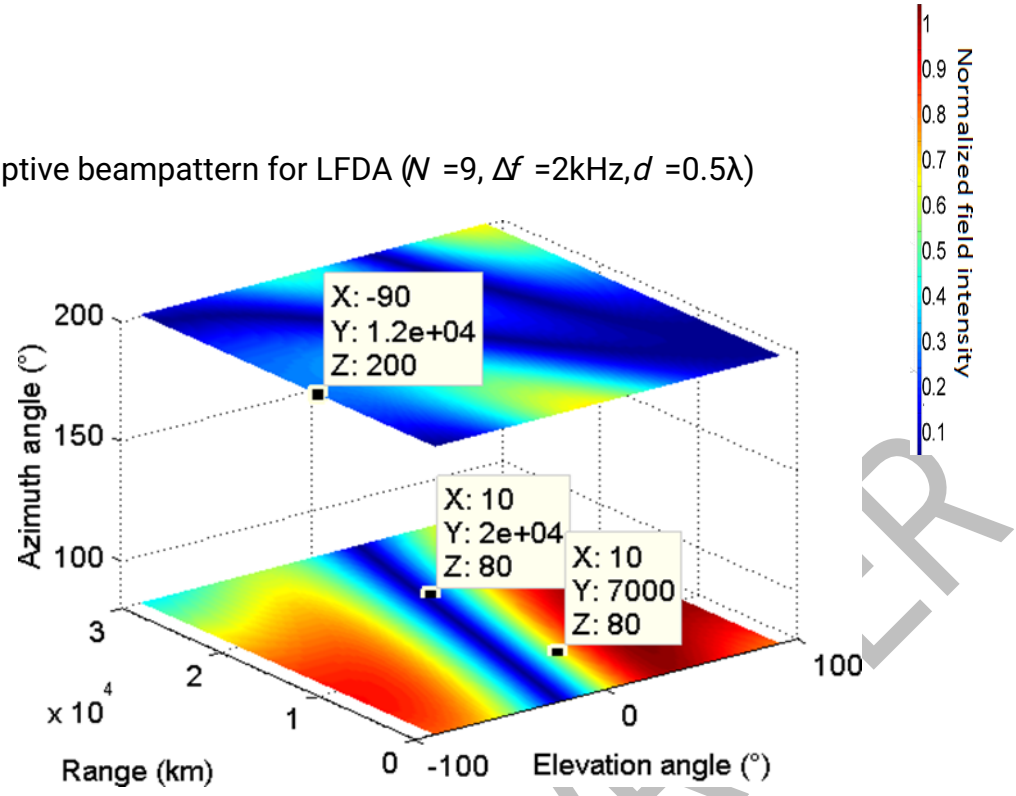

Fig 5.13: ABF pattern of PFDA ($\Delta f_x = 2kHz$, $\Delta f_y = 2kHz$ M=3, N=3, $d_x = d_y = \lambda$)

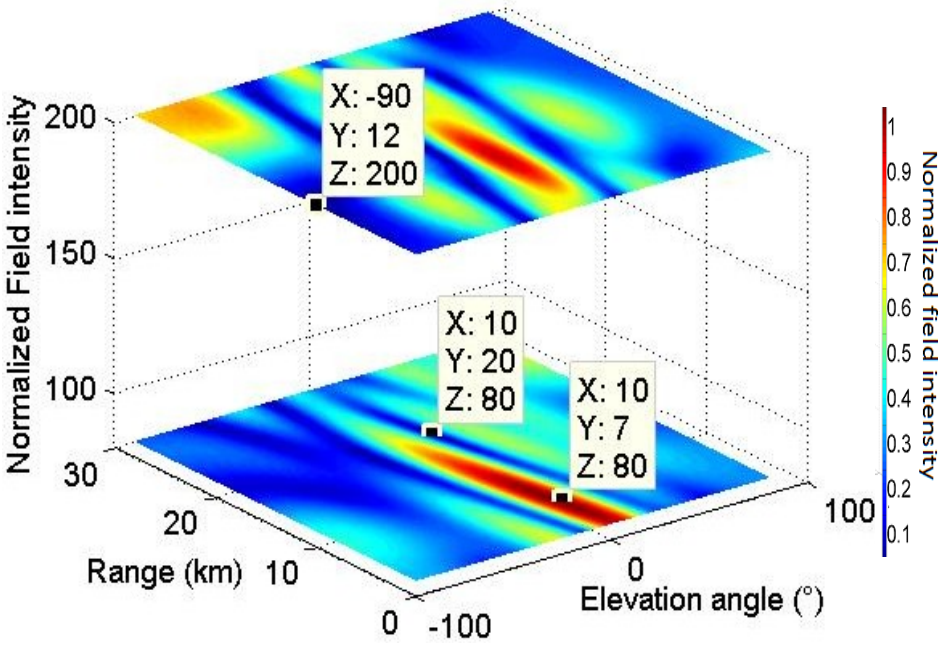

Fig 5.15: ABF pattern of UCFDA (N =9, Δf =2kHz, d =0.5λ)

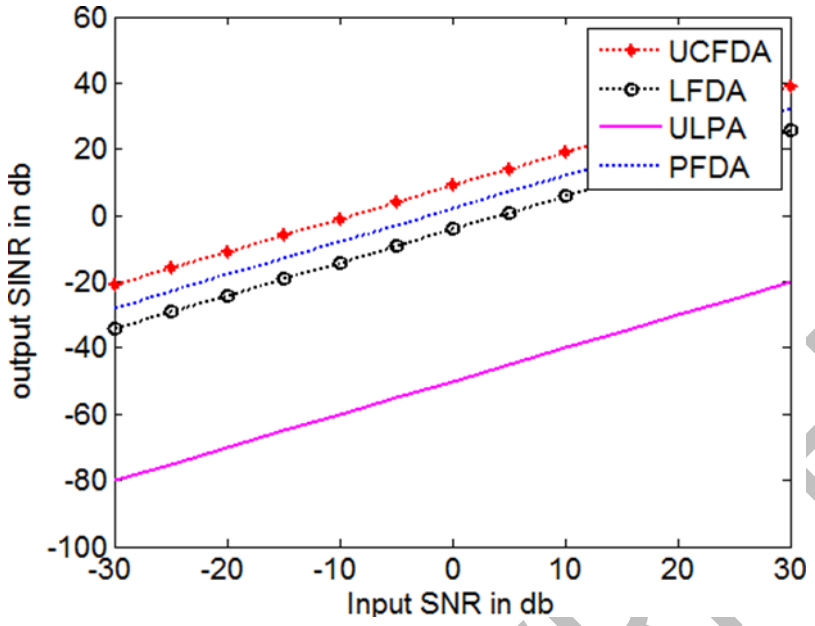

Fig 5.14: Comparative curve of input SNR versus output SINR, with input INR=30dB (Simulation parameters of Table 5.3).

Chapter 5

CONCLUSIONS AND FUTURE WORK

5.1 CONCLUSIONS

We created novel and easy ways to beamforming in the already established geometries in FDA, i.e. LFDA and rectangular arrays often referred to as PFDA, in this dissertation. The dissertation, on the other hand, looks at novel geometries such elliptical and circular geometries that aren't covered in FDAs.

We designed an implementable cognitive null steering technique for LFDA radars. Precision null insertion in angle and range has been obtained, which is not feasible with PAR systems, because to the greater mobility and higher degree of freedom provided by frequency diversity. The proposed scheme's key characteristics are DOA estimation, next location prediction, and accurate and lowest nulls placement at the expected next places of the interference source. As a result, undesirable interferer returns are reduced, and improved system performance in terms of SINR can be expected.

We suggested a 3D adaptive transmission beamforming approach in PFDA radars as a solution to traditional 2D localization challenges in PAR and LFDA. Because of their increased range and angle selectivity, 3D localised maxima and nulls offer a higher system SINR, greater interference suppression, and improved clutter rejection. The aforementioned ABF approach is extremely quick and computationally simple, outperforming other strategies in terms of sharp localised high output maxima, deeper nulls, and clearly improved SINR.

For the first time, the research introduces "Uniform circular frequency diverse arrays (UCFDA)." In comparison to LFDA and PFDA, the analysis finds distinct patterns that demonstrate that UCFDA has a far better capability of target localisation. Range

dependent clutter and interferences can be reduced better in UCFDA with this feature, potentially boosting received SINR. As a result, UCFDA appears to be a preferable alternative in all cases where pin point targets must be localised. PFDAs with 2D rectangular geometry and a larger number of antennas are often used to accomplish 3D target localisation. This disadvantage is overcome by UCFDA, which achieves finer localization, better peak to side-lobe ratio, enhanced directivity, and better SINR with a basic 1D circular shape and fewer antennas (equivalent to LFDA), thereby saving space and money.

Apart from constant frequency offset, the dissertation also looks at tangent hyperbolic circular frequency varied array, which is a variety of UCFDA (TH-CFDA). The suggested TH-CFDA radar shows to be a highly customizable and simple radar system, allowing three alternative CFDA configurations to be produced by modifying a single system parameter. The suggested approach's adaptability allows it to be used in a variety of practical radar applications. In order to show the usefulness of the suggested approach, two such situations are explored.

Last but not distant, the thesis investigates another feasible geometry in the realm of frequency diversity, namely the elliptical array. The most notable aspect of EFDA (where it beats all other kinds of FDA) is its extremely range selective beampatterns with the lowest side lobe levels, according to research. TH-EFDA, a non-uniform frequency offset design based on the tangent hyperbolic function, has also been presented. This TH-EFDA provides a single maximum beampattern that efficiently suppresses any interferer situated other than the target position. In terms of dramatically lowered side lobe levels and very range selective beampatterns, TH-EFDA outsmarts other known non-uniform frequency offset techniques.

5.2 FUTURE WORK

Several aspects of radar ABF difficulties remain undiscovered in FDA radars for a wide

range of challenges.

• For 3D numerous null steering, the frequency offset selection approach may be expanded.

• In order to learn more about the UCFDA's capabilities, researchers might look into null steering and multi-target tracking.

• Another option to consider is circular frequency varied array radars with a temporal independency feature.

• Multi-ring structures with circular geometry can be investigated for improved array system performance, particularly in terms of peak to side lobe ratio.

• To handle multi target beam steering concerns, machine learning approaches can be used in combination with a frequency offset selection system.

• Even though only single signal sources are investigated in this study, future research might include multi-target identification.

• One of the next directions in EFDA is to minimise SLL utilising different global evolutionary optimization methods with an added fitness function eccentricity 'e'.

• Because PFDA has an extra degree of freedom in respect of frequency offset along the x and y axes, a more reliable frequency offset selection technique to create numerous beams aiming in diverse spatial areas may be designed.

Other EFDA designs, such as multiple ellipses along the horizontal axis or multiple ellipses along the vertical axis (cylinder-like structure), can be investigated for improved array performance outcomes, such as directivity and SLL.

• A 3D time independent beampattern might be created using a planar FDA with a time dependent frequency offset. As a result, clutter reduction based on range angle may be accomplished more effectively.

• Combining the ideas of waveform diversity and FDA in planar and circular geometries might lead to new research areas in planar and circular frequency diverse MIMO.

• A study of planar frequency varied MIMO with time-dependent frequency offsets is required.

• Binomial function as a non-uniform frequency offset function can be examined in non-uniform frequency offset FDA.

• Non-uniform frequency offsets may also be reconstructed from various quadratic, sinusoidal, and exponential functions.

• In the realm of frequency diversity, a variety of additional geometries, such as parabolic geometries, can be investigated.

References

[1] M.I.Skolnik, Introduction to Radar Systems, 3rd ed., Singapore: Mc Graw Hill, 2001.

[2] B.R.Mahafza, Radar Systems Analysis and Design Using MATLAB, Third Edition, Boca Raton,FL: CRC Press, 2013.

[3] "http://www.nps.navy.mil/faculty/jenn".

[4] "http://www.navsys.com/papers/07-11-002.pdf".

[5] "https://en.wikipedia.org/wiki/Beamforming".

[6] T.Haynes, "A Primer on Digital Beamforming," Spectrum Signal Processing, 1998.

[7] K. R. Mahmoud, M. El-Adawy, S. M. M. Ibrahem, R. Bansal and K. R. Mahmoud, "A comparison between circular and hexagonal array geometries for smart antenna systems using particle swarm optimization algorithm," PIER, no. 72, pp. 75-90, 2007.

[8] C.A.Balanis and P.Ioannides, "Uniform Circular and Rectangular Arrays for Adaptive Beamforming Applications," IEEE Antennas and wireless propagation letters, vol. 4, pp. 351-354, 2005.

[9] C.A.Balanis and P. and, "Uniform circular arrays for smart antennas," IEEE Transactions on Antennas and Propagation, vol. 47, no. 4, pp. 192-206, 2005. [10] "http://www.100-jahre-radar.fraunhofer.de/vortraege/Holpp-The_Century_of_Radar.pdf". 127

[11] "http://www.engineersgarage.com/articles/types-of-radars(classification)".

[12] K.Milne, "Phased Arrays in radar," in IEEE Tutorial Meeting on Phased Array Radar, London, 1989. [13] Z. Spasojevic, S. Dedeo and R. Jensen, "Dwell Scheduling Algorithms for Phased Array Antenna," IEEE Trans. Aerospace and Electronic Systems, vol. 49, no. 1, pp. 42-54, 2013.

[14] E. Yoshikawa, T. Ushio, Z. Kawasaki, S. Yoshida, T. Morimoto, F. Mizutani and M. Wada, "MMSE Beamforminf on fast scanning phased array weather radar," IEEE Trans. Geoscience and Remote sensing, vol. 51, no. 5, pp. 3077-3088, 2013. [15] A. Fenn, D. Temme, W. Delaney and W. Courtney, "The Development of Phased Array rechnology," Lincoln Lab journal, vol. 12, no. 2, pp. 321-340, 2000.

[16] P.Patel, "Fundamentals of phased arrays," Astron, Netherlands Organization of Scientific Research, Netherlands, 2007.

[17] "www.radartutorial.eu/06.antennas/Phased%20Array%20Antenna.en.html".

[18] P.Ioannides and C. Balanis, "Uniform Circular and Rectangular Arrays for Adaptive Beamforming Applications," IEEE Antennas and Wireless Propagation Letters, vol. 4, pp. 351-354, 2005.

[19] H.Unz, "Linear arrays with arbitrarily distributed elements," IRE Trans Antennas and propagation, Vols. AP-8, pp. 222-223, 1960.

[20] D. D. King, R. F. Packard and R. K. Thomas, "Unequally spaced broad band antenna arrays," IRE Trans Antennas and propagation, Vols. AP-8, pp. 380-385, 1960.

[21] C.Baixiao and W.Jianqi, Synthetic Impulse and Aperture Radar (SIAR): A Novel Multi-128 Frequency MIMO Radar, 1st ed., Singapore: Wiley and Sons, 2014.

[22] A.Hakam, R.Shubair, S.Jimaa and E.Salahat, "Robust interference suppression using a new LMS-based adaptive beamforming algorithm," in IEEE Mediterrranian Electrotechnical Conference, Beirut, 2014.

[23] R.M.Shubair and A.Hakam, "Adaptive beamforming using variable step-size LMS algorithm with novel ULA array configuration," in IEEE International Conference on Communication Technology, Guilin, 2013.

[24] J.A.Srar, K.S.Cheng and A.Mansour, "Adaptive Array Beamforming Using a Combined LMS-LMS Algorithm," IEEE Transactions on Antennas and Propagation, vol. 58, no. 11, pp. 3545-3554, 2010.

[25] W.Shao, Y.Yu and Z.Qian, "An effective variable step size CS-LMS algorithm for adaptive beamforming," in International conference on Signal processing Systems, Dalian, 2010.

[26] A.Senapati, K.Ghatak and J. Roy, "A Comparative Study of Adaptive Beamforming Techniques in Smart Antenna Using LMS Algorithm and Its Variants," in IEEE International conference on Computational Intelligence and Networks, Bhubaneswar, 2015.

[27] G.Lin, Y.Li and B.Jin, "Research on the algorithms of robust adaptive beamforming," in International Conference on Mechtronics and Automation, Xi'an, 2010.

[28] R.Qian, M.Sellathurai and D.Wilcox, "A Study on MVDR Beamforming Applied to an ESPAR Antenna," IEEE Signal Processing Letters, vol. 22, no. 1, pp. 67-70, 2015.

[29] S. Salem, T.S.Kiong, J.K.S.Paw and G.C.Hock, "Artificial immune system assisted Minimum Variance Distortionless Response beamforming technique for adaptive

antenna 129 system," in IEEE International Conference on Convergence, Jeju, 2013.

[30] Y.Wang and A.Tennant, "MVDR beamforming applied to a time-modulated reflectorarray," in Loughborough Antennas and Propagation Conference, Loughborough, 2013.

[31] M.Sharma and K.K.Sharma, "GA-aided MVDR beamforming in wide band MISO wireless channel," in IEEE International conference on Signal processing and Integrated Metworks, Noida, 2014.

[32] N.Noordin, V.Zuniga, A.El-rayis, N.Haridas, Ahmet.Erdogan and T.Arslan, "Uniform circular arrays for phased array antenna," in Loughborough Antennas and Propagation Conference, Loughborough, 2011. [33] C.A.Balanis, Antenna Theory,Analysis and Design, 2005.

[34] P.Antonik and M. C. Wicks, "Frequency diverse array with independent modulation of frequency, amplitude and phase," U.S. Patent 7319427, 15 Jan 2008.

[35] P. Antonik, M. C. Wicks, H. Griffiths and C. J. Baker, "Frequency Diverse Array Radars," in IEEE Radar Conference, Verona, NY, 2006.

[36] P. Antonik, M. Wicks, H. Griffiths and C. Baker, "Range Dependent Beamforming Using Element Level Waveform Diversity," in International Waveform Diversity and Design Conference, 2006.

[37] P.Antonik and M. C.Wicks, "Method and apparatus for simultaneous synthetic aperture and moving target indication," U.S.Patent 0129584, June 2008.

[38] M. C. Wicks and P. Antonik, "Method and apparatus for a frequency diverse array," U.S.Patent 7511665B2, 31 March 2009. 130

[39] A.Aytun, "Frequency Diverse Array Radars," Master's thesis, Naval Postgraduate School, 2010.

[40] P. Antonik, M. C. Wicks, H. Griffiths and C. J. Baker, "Multi-mission multi mode waveform diversity," in IEEE Radar Conference, Verona, Italy, 2006.

[41] J. Huang, K. F. Tong, K. Woodbridge and C. Baker, "Frequency diverse Array: Simulation and Design," in IEEE Radar Conference, Pasadena, USA, 2009.

[42] W. Q. Wang, "—Range-Angle Dependent Transmit Beampattern Synthesis for linear frequency diverse arrays," IEEE Trans. Antennas and Propagation, vol. 61, no. 08, pp. 4073-4081, 2013.

[43] J. Farooq, M. A. Temple and M. A. Saville, "Exploiting frequency diverse array processing to improve SAR imaging resolution," in IEEE radar Conf, Rome, Italy, 2008.

[44] W.Q.Wang, "Transmit subaperturing for range and angle estimation in frequency diverse array radar," IEEE Transactions on Signal Processing, vol. 62, no. 8, pp. 2000-1011, 2014.

[45] W.Wang, "Non-uniform Frequency Diverse Array for Range-Angle Imaging of Targets," IEEE Sensors Journal, vol. 14, no. 8, pp. 2469-2476, 2014.

[46] W.Khan and I.M.Qureshi, "Frequency Diverse Array Radar With Time-Dependent Frequency Offset," IEEE Antennas and Wireless Propagation Letters, vol. 13, pp. 758-761, 2014.

[47] J.Farooq, "Frequency diversity for improving synthetic aperture radar imaging," PhD Dissertation, OH,USA, 2009.

[48] J. Farooq, M. A. Temple and M. A. Saville, "Application of frequency diverse arrays

to synthetic aperture radar imaging," in International conference on Electromagnetics, 131 Torino,Italy, 2007.

[49] X.He, B. Liu and D. Wang, "Sparcity-driven frequency diverse MIMO radar imaging for moving targets," International Journal of Information and Electronics Engineering, vol. 3, no. 4, pp. 409-413, 2013.

[50] P.F.Sammartino, C.J.Baker and H.D.Griffiths, "Frequency diverse MIMO techniques for radar," IEEE Trans. Aerospace and Electronic Systems, vol. 49, no. 1, pp. 201-222, 2013.

[51] P.Baizert, T.B.Hale, M.A.Temple and M.C.Wicks, "Forward-looking radar GMTI benefits using a linear frequency diverse array," IET Electronics Letters, vol. 42, no. 22, pp. 1311- 1312, 2006.

[52] M. Secmen, S. Demir, A. Hizal and T. Eker, "Frequency diverse array antenna with periodic time modulated pattern in range and angle," in IEEE Radar Conf., 2007.

[53] X.Z.Liu and L. Zhuang, "Precisely beam steering for frequency diverse arrays based on frequency offset selection," in Proc Int. Radar Conf, 2009.

[54] J. Huang, K.-F. Tong and C.Baker, "Frequency diverse arrays with beam scanning feature," in IEEE Int. Symposium on Antennas and Propagation, San Diego, USA, 2008.

[55] C.Yong-guang, L. Yun-tao, W. Yan-hong and C. Hong, "Research on the Linear Frequency Diverse Array Performance," in IEEE 10Th Int Conf on Signal Processing, Beijing, 2010.

[56] K. Shanbhag, D.Deb and M.Kulkarni, "MIMO radar with spatial frequency diversity for improved detection performance," in IEEE Int. Communication, Control

Computation,Technology Conf, 2010.

[57] J.Shin, J.H.Choi, J.Kim, J.Yang, W.Lee, J.So and C.Cheon, "Full-wave simulation of 132 frequency diverse array antenna using the FDTD method," in Asia Pacific Microwave Conference, Seoul, 2013.

[58] W.Khan, I.M.Qureshi and S.Saeed, "Frequency diverse array radar with logarithmically increasing frequency offset," IEEE Antennas and Wireless Propagation Letters, vol. 14, 2015.

[59] C. a. S.Demir, "Multipath characteristics of frequency diverse arrays over a ground plane," IEEE Transactiona on Antennas and propagation, vol. 62, no. 7, pp. 3567-3574, 2014.

[60] T.Eker, S.Demir and A.Hizal, "Exploitation of linear frequency modulation continuous waveform (LFMCW) for frequency diverse arrays," IEEE Transactions on Antennas and Propagation, vol. 61, no. 7, pp. 3546-3553, 2013.

[61] Y.B.Wang, W.Q.Wang and H.Z.Shao, "Frequency diverse array radar Cram´er-Rao lower bounds for estimating direction, range and velocity.," Internal Journal of Antennas and Propagation, pp. 1-15, 2014.

[62] W.Q.Wang, "Frequency diverse array antenna: New opportunites.," IEEE Antennas and Propagation Magazine, vol. 57, no. 2, pp. 145-152, 2015.

[63] S.Brady, "Frequency Diverse Array Radar: Signal Characterization and Measurement Accuracy," MS Thesis, Air Force Institute of Technology, Air University, USA, 2010.

[64] A.M.Jones, "Frequency diverse array receiver architectures," MS thesis, Department of Electrical Engineeringt and Computer Science, Wright Dtate University, 2011.

[65] W.Q.Wang, "Overview of frequency diverse array in radar and navigation applications," IET Radar, Sonar and Navigation, vol. 10, no. 6, pp. 1001-1012, 2016.

[66] J.Xiong, W. Wang, H.shao and H. Chen, "Frequency diverse array transmit beampattern 133 optimization with genetic algoritm," IEEE Antennas and Wireless Propagation Letters, no. 99, p. 1, 2016.

[67] K.Gao, W.Wang and a. J. X. J.Cai, "Decoupled frequency diverse array range–angledependent beampattern synthesis using non-linearly increasing frequency offsets," IET Microwave Antennas and Propagation, vol. 10, no. 8, pp. 880-884, 2016.

[68] H. Shao, X. Li, W. Wang, J. Xiong and H. Chen, "Time invarant transmit beampattern synthesis via weight designfor FDA radar," in IEEE Radar Conference 2016, 2016.

[69] S. Qin, Y. D. Zhang and M. G. Amin, "Multi- target Localization using frequency diverse coprime arrats with coprime frequency offsets," in IEEE Radar Conference 2016, 2016.

[70] Y. Xu, X.Shi, J.Xu and W. Li, "Beampattern analysis of planar frequency diverse array.," International Journal of RF and Microwave Computer aided Engineering, vol. 25, no. 5, pp. 436-444, 2015.

[71] H.Steyskal, "Synthesis of antenna pattern with prescribed nulls," IEEE Transactions on antennas and Propagation, vol. 30, no. 2, pp. 273-279, 1982.

[72] S.Irteza, E. Schafer, R.Stephan and A. Hornbostel, "Compact antenna array receiver for robust satellite navigation system," Int.J.Microw. Wirel.Technol., pp. 1-11, 2014.

[73] S.Mehmood, Z.Khan, F.Zaman and B. Shoaib, "Performance analysis of the different null steering techniques in the field of adaptive beamforming," Research Journal of

applied Siciences, Engineering and Technology, vol. 5, no. 15, pp. 4006-4012, 2013.

[74] D.Baird and G.Rassweiler, "Adaptive sidelobe nulling using digitally controlled phase shifters," IEEE Transactions on Antennas and Propagaion, vol. 24, no. 5, pp. 638-649, 1976. 134

[75] R.Vescovo, "Null synthesis by phase control for antenna array," IET Electronics Letters, vol. 36, no. 3, pp. 198-199, 2000.

[76] N.Karaboga, K. Gü ney and A. Akdagli, "Null steering of linear antenna arrays with use of modified touring Ant Colony optimization algorithm," Intl. Journal of Microwaves and Wireless Technologies, vol. 12, no. 4, pp. 4006-4012, 2013.

[77] W.Q.Wang, H.Shao and J.Cai, "Range-angle dependent beamforming by frequency diverse array antenna," International Journal of Antennas and Propagation, vol. 2012, pp. 1-10, 2012.

[78] S.Haykin, "Cognitive radar, a way of the future," IEEE Signal Processing magazine, vol. 23, no. 1, pp. 30-40, 2006.

[79] X.Zhang and C.Cui, "Range-spread target detecting for cognitive radar based on trackbefore-detect.," TnF International Journal of Electronics, vol. 101, no. 1, pp. 74-87, 2014.

[80] N. Ince, E. E. Topuz, E. E. Panayirci and C. C. Isik, Principles of integrated Maritime Surveillance Systems, Massachusetts,USA: Kluwer Academic Publishers., 2000.

[81] G.Kouemou, Radar Technology, Croatia: InTech Publishers, 2010.

[82] L.Osman, I. Sfar and A. Gharsallah, "The application of high-resolution methods for DOA estimation using a linear antenna array," International Journal of Microwaves and

Wireless Technologies, vol. 7, no. 1, pp. 1-8, 2014.

[83] B.Islam, "Comparison of Conventional and Modern Load Forecasting Techniques Based on Artificial Intelligence and Expert Systems.," International Journal of Computer Science Issues, vol. 8, no. 5, pp. 504-513, 2011.

[84] M.A.Raji and K.Athappilly, "A comparative predictive analysis of neural networks (NNs), 135 nonlinear regression and classification and regression tree (CART) models.," Expert Systems with Applications, vol. 29, no. 1, pp. 65-74, 2005.

[85] A.S.Bashi and E.J.Kaminsky, "Comparison of Neural Network and Extended Kalman Filter Determination of Kinematics from Impact Acceleration Tests," in IEEE International conference on Computational Cybernetics and Simulation., Orlanado,FL, 1997.

[86] F. Awadz, I. Yassin, M. Rahiman, M. Taib and A. Zabidi., "System Identification of Essential Oil Extraction System Using Non-Linear Autoregressive Model with Exogenous Inputs (NARX)," in IEEE Control and System Graduate Research Colloquium, Shah Alam, 2010.

[87] H.Xie, H.Tang and Y.H.Liao, "Time series prediction based on NARX neural networks: An advanced approach.," in IEEE 8th International conference on Machine learning and Cybernetics, Boading, 2009.

[88] P.J.Bevelacqua and C. Balanis., "Optimizing antenna geometry for interference suppression," IEEE Trans. Antennas and Propagation, vol. 55, no. 3, pp. 637-641, 2007.

[89] A.Basit, I.M.Qureshi, W.Khan and S.U.Khan, "Cognitive frequency offset calculation for frequency diverse array radar," in IEEE International conference on Applied Sciences

and Technology, Bhurban, 2015.

[90] A. M. Jones and B.D.Rigling, "Planar frequency diverse array receiver architecture," in IEEE Radar Conf, 2012.

[91] A. B. Gershman, E. Németh and J. F. Böhme, "Experimental Performance of Adaptive Beamforming in a Sonar Environment with a Towed Array," IEEE Transactions on SIgnal Processing, vol. 48, no. 1, pp. 246-250, 2000. 136

[92] H.Shao, J. Li, H.Chen and W. Wang, "Adaptive frequency offset selection in FDA radar," IEEE antennas and wireless propagation letters, vol. 13, pp. 1405-1408, 2014.

[93] J.A.Tsai and B. Woerner, "Adaptive beamforming of uniform circular arrays (UCA) for wireless CDMA system," in IEEE Signals, Systems and Computer Conference, Pacific Grove, CA, USA, 2001.

[94] W.Lei, "Blind adaptive beamforming for wideband circular arrays," in IEEE International Conference on Acoustics, Speech and Signal Processing, Taipei, 2009.

[95] A.R.Khulaib, R.M.Shubair, M.A.Al-Qutayri and N.G.JWP, "Performance evaluation of linear and circular arrays in wireless sensor localization," in IEEE International Conference on Electronics, Circuits and Systems, Beirut, 2011.

[96] T.B.Chen, Y.L.Dong, Y. Jiao and F.S.Zhang, "Synthesis of circular antenna array using partcle swarm optimization algorithm," Journal of Electromagnetic Waves and Applications, vol. 20, no. 13, pp. 1785-1795, 2006.

[97] P.Antonik, "An Investigation of a Frequency Diverse Array," PhD Thesis, London, 2009.

[98] M.Feldmann, U.Nickel and W.Koch, "Adaptive air to air target tracking in severe

jamming environment," in 14th International Conference on information fusion, 2011.

[99] S.Saeed, I.M.Qureshi, W.Khan and A.Salman, "An investigation into uniform circular frequency diverse array (UCFDA) radars.," Remote Sensing Letters, vol. 6, no. 9, pp. 707-714, 2015.

[100] W.Q.Wang and H.Shao, "Range-angle localization of targets by a double pulse frequency diverse array radar," IEEE Journal of selected topics in signal processing, vol. 8, no. 1, pp. 106-114, 2014. 137

[101] B.R. Jackson, S. Rajan, B.J. Liao and S. Wang, "Direction of arrival estimation using directive antennas in uniform circular arrays," Ieee Transactions on Antennas and Propagation, vol. 63, no. 2, pp. 736-747, 2015.

[102] S.Astapov, J. Berdnikova and J.S. Preden, "A two stage approach to 2D DOA estimation for a compact circular microphone array," in International Conference on Informatics, Electronics and Vision, 2015.

[103] M.I. AlHajri, R.M. Shubair, L. Weruaga, A.R. Kulaib, A. Goian, M. Darweesh and R. AlMemari, "Hybrid method for enhanced detection of coherent signals using circular antenna arrays," in IEEE National Symposium on Antennas and Propagation & USNC/URSI, 2015.

[104] R.Bera and J.S.Roy, "Optimization of thinned elliptical antenna arrays using Particle Swarm Optimization," in International Conference on Communications, Devices and Intelligent systems, Kolkata, 2012.

[105] Z. G, "Gain enhancement of printed log-periodic dipole array antenna using an elliptical patch," in IEEE 4th Asia Pacific Conference on Antennas and Propagation, 2015.

[106] M.A.baumgartner, M.T.Ghasr and R.Zoughi, "Wideband Imaging Array Using Orthogonally Fed Dual Varactor-Loaded Elliptical Slots," IEEE Transactions on Instrumentation and Measurement, vol. 64, no. 3, pp. 740-749, 2015.

[107] A.Sharaqa and N.Dib, "Position-Only Side Lobe Reduction Of A Uniformly Excited Elliptical Antenna Array Using Evolutionary Algorithms," IET Microwaves ,Antennas and Propagation, vol. 7, no. 6, pp. 452-457, 2013.

[108] B. L, N. Carvalho and P. P, "Circular Polarized Planar Elliptical Array," in European Conference on Antennas and Propagation, 2013. 138

[109] R. A.Sadeghzadeh, A. A. L. Neyestanak, Naser-Moghadasi and Ghiamy, "A Comparison of Various Hybrid Elliptical Antenna Arrays," Iranian Journal of Electrical and Computer Engineering, vol. 7, no. 2, 2008.

[110] J.D.Kraus, R.J.Marhefka and A.S.Khan., Antennas for all applications, New York: Mc Graw Hill Companies ,Inc., 2002.

[111] W. Muller, Ground Radar Systems of the German Luftwaffe to 1945, Atglen, PA: Schiffer Publishing Ltd., 1998.

[112] H.Steyskal, "Simple method for pattern nulling by phase perturbation.," IEEE Transactions in Antennas and propagation, vol. 31, no. 1, pp. 163-166, 1983.

[113] "http://www.radartutorial.eu/19.kartei/pic/img2061.jpg(ATC".

[114] "http://mostlymissiledefense.com/2012/04/12/pave-paws-and-bmews-radars-april-12- 2012".

[115] "http://wtlab.iis.u-tokyo.ac.jp/~wataru/lecture/rsgis/rsnote/cp3/cp3-7.htm".